1 OF 2
AD
A070 740

MICROCOPY RESOLUTION TEST CHART

AFML-TR-76-125

LEVEL II

EXPLORATORY DEVELOPMENT ON SILICON MATERIAL FOR LADIR

ROCKWELL INTERNATIONAL
3370 MIRALOMA AVE
ANAHEIM, CA 92803

NOVEMBER 1978

TECHNICAL REPORT AFML-TR-76-125

FINAL TECHNICAL REPORT FOR PERIOD 1 AUGUST 1975 — 30 SEPTEMBER 1977
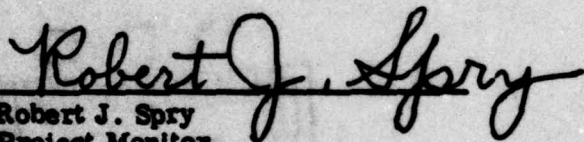
AIR FORCE MATERIALS LABORATORY
AIR FORCE WRIGHT AERONAUTICAL LABORATORIES
Air Force Systems Command
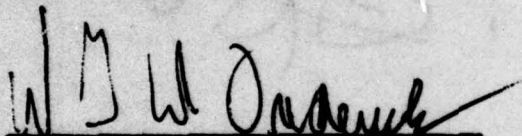Wright-Patterson Air Force Base, Ohio 45433

79 07 02 048

NOTICE

When Government drawings, specifications, or other data are used for any purpose other than in connection with a definitely related Government procurement operation, the United States Government thereby incurs no responsibility nor any obligation whatsoever; and the fact that the government may have formulated, furnished, or in any way supplied the said drawings, specifications, or other data, is not to be regarded by implication or otherwise as in any manner licensing the holder or any other person or corporation, or conveying any rights or permission to manufacture, use, or sell any patented invention that may in any way be related thereto.

This technical report has been reviewed and is approved for publication.

Robert J. Spry
Project Monitor

FOR THE COMMANDER

WILLIAM G.D. FREDERICK, Chief
Laser and Optical Materials Branch
Electromagnetic Materials Division
Air Force Materials Laboratory

REPORT DOCUMENTATION PAGE	READ INSTRUCTIONS BEFORE COMPLETING FORM

1. REPORT NUMBER	2. GOVT ACCESSION NO.	3. RECIPIENT'S CATALOG NUMBER
AFML-TR-76-125		

4. TITLE (and Subtitle)	5. TYPE OF REPORT & PERIOD COVERED
EXPLORATORY DEVELOPMENT ON SILICON MATERIAL FOR LADIR.	Final rept. 1 Aug 1975 – 30 Sep 1977
	6. PERFORMING ORG. REPORT NUMBER
	C77-239/034A

7. AUTHOR(s)	8. CONTRACT OR GRANT NUMBER(s)
Dr. M. C. Arst, et al.	F33615-76-C-5024

9. PERFORMING ORGANIZATION NAME AND ADDRESS	10. PROGRAM ELEMENT, PROJECT, TASK AREA & WORK UNIT NUMBERS
Rockwell International 3370 Miraloma Ave. Anaheim, CA 92803	P. E. 62102F W. U. 73710234

11. CONTROLLING OFFICE NAME AND ADDRESS	12. REPORT DATE
Air Force Materials Laboratory Electromagnetic Materials Division (AFML/LPO) Wright-Patterson Air Force Base, Ohio 45433	September 1977
	13. NUMBER OF PAGES
	134 p.

14. MONITORING AGENCY NAME & ADDRESS(if different from Controlling Office)	15. SECURITY CLASS. (of this report)
	Unclassified
	15a. DECLASSIFICATION/DOWNGRADING SCHEDULE

16. DISTRIBUTION STATEMENT (of this Report)

Approved for public release; distribution unlimited.

17. DISTRIBUTION STATEMENT (of the abstract entered in Block 20, if different from Report)

18. SUPPLEMENTARY NOTES

19. KEY WORDS (Continue on reverse side if necessary and identify by block number)

silicon, infrared detectors, float zoning, purification, compensation, impurity concentration, dopant, material evaluation, extrinsic detector performance, FLIR.

20. ABSTRACT (Continue on reverse side if necessary and identify by block number)

This report discusses the problems and significant results achieved on Contract F33615-76-C-5024, "Exploratory Development on Silicon Material for LADIR" during the period from 1 August 1975 to 30 September 1977. The Principal Investigator and Project Engineer was Dr. M. C. Arst. The goal of the program was to develop advanced purification procedures for starting materials and to prepare single crystal detector grade gallium-doped silicon with optimum properties compatible with the fabrication processes used to prepare detectors integrated with on-chip electronics.

DD FORM 1473 1 JAN 73   EDITION OF 1 NOV 65 IS OBSOLETE

389 126

20. ABSTRACT (Cont)

The significant results achieved during the contract were as follows:

1. Vacuum float zone refining procedures for polysilicon were developed which significantly reduced the concentration of all measurable impurities except boron.

2. While not removed during the purification and the growth, the concentration of boron was not increased when adding the compensating donor and the extrinsic impurity.

3. The residual boron concentration of 1 to 2×10^{12} cm^{-3} can be rendered electrically inactive by exact compensation with a donor impurity. To accomplish this, it was first necessary to develop a highly sensitive technique to determine quantitatively the low residual concentration of boron. The new technique is based on high resolution IR impurity absorption in the 30 to 40 micrometer band. It will also allow the measurement of residual concentrations of phosphorus. The Far IR absorption technique was repeatable and correlatable with other measurements such as Hall Effect, 4-point probe resistivity measurements, and spectral response. Using infrared techniques, it was also verified that the float zoning procedures did not add oxygen or carbon. Ingots were grown that were closely compensated.

4. Three experimental approaches to compensating the residual boron in gallium doped silicon were studied: (1) compensation by the chemical addition of interstitial and substitutional impurities, (2) compensation by nuclear transmutation doping, and (3) compensation by phosphorus which was not completely removed during zone refining of the polysilicon starting material.

5. Material from the experimental crystals was fabricated into detectors and evaluated under high and low background flux conditions. The resulting performance measurements were then compared for the various detector materials. Test results indicate that at a boron concentration of about 2×10^{12} cm^{-3} detectors showed good signal responsivity and specific detectivity (D*), and an acceptable operating temperature at the gallium concentration of 4×10^{16} cm^3. Responsivity and detectivity of detectors with residual boron concentrations in the 10^{12} cm^{-3} range show little dependence on the concentration of the compensating donor.

6. The compensating impurity, antimony, is the best of those studied for compensating residual boron in gallium-doped silicon.

PREFACE

Significant advances made under the program were: development of vacuum float zone refining procedures which reduced residual impurity content to of order 10^{12}cm^{-3} of boron; evaluation and development of several techniques of donor compensation of boron; establishment of procedure for reproducible gallium doping of float zoned crystals; fabrication of gallium doped silicon detectors whose performance was insensitive to compensating donor concentration.

iii

CONTENTS

v

CONTENTS (Cont)

ILLUSTRATIONS

TABLES

SECTION I

INTRODUCTION

This report presents the status of work accomplished on contract F33615-76-C-5024, "Exploratory Development on Silicon Material for LADIR," during the period of 1 August 1975 to 30 September 1977. This report contains a background description of the program, an evaluation of test approaches, test results, and a description of the process which has been developed to produce silicon material which meets the requirements of the contract. Where applicable, these subjects are discussed under the following tasks:

Task I, Purification of Intrinsic Silicon

Task II, Growth of Doped Silicon Crystals

Task III, Crystal Material Evaluation

Task IV, Definition of Growth Process

A major conclusion of the program is that the most suitable counter dopant for the residual boron concentration is antimony (Sb). This impurity has characteristics that are compatible with the other impurities in the material and remains stable during the on-chip microelectronics processing. In addition, it is easy to introduce into the silicon ingot during the doping process and distributes evenly over the bulk.

Advanced test methods utilizing infrared measurement techniques were developed and used to determine the residual boron content and the effectiveness of the accomplished compensation of the silicon crystal material. The most critical steps of the material growth process were the initial materials purification and the accurate evaluation of the residual boron concentration in order to closely compensate it by counter doping.

1.1 BACKGROUND AND DISCUSSION

The main objective of the LADIR program is the development of low cost arrays for the detection of infrared radiation in the 8 to 14 μm wavelength band. A further objective is the achievement of batch processing of the detectors, signal processing electronics, and interconnects between the detectors and the electronics. Lower array costs, increased array performance, and significant reductions in size and power will also be realized. Further, by eliminating the manual process for making electrical connections and by using redundant signal flow paths, permitted by the adoption of integrated circuitry techniques, greater array reliability is predicted.

Silicon doped detectors have been fabricated and used at Autonetics for both high and low background applications. Systematic studies carried out with a variety of dopants have revealed no preferred crystal orientation which optimizes detector performance. However, MOSFET devices and CCD's (charge coupled devices) are influenced by the orientation of the silicon substrate on which they are formed.

1

Their best performance is obtained when they are fabricated on ⟨100⟩ oriented substrates. This orientation provides the minimum concentration of surface states and thereby minimum threshold voltages and reduced noise associated with surface state transitions. Since LADIR will utilize detectors in conjunction with MOSFET and/or CCD components, the preferred wafer orientation is in the <100> direction.

Gallium is a leading candidate for providing the required infrared sensitivity in the 8 to 14 μm band. Accordingly, the development of controlled growth of gallium doped silicon provides the best potential as starting material for use on the LADIR program.

1.2 PROBLEM AREAS

There are three main problems inherent in producing high quality gallium doped silicon crystals for the 8 to 14 μm wavelength band. These problems are: (1) minimizing the residual boron, (2) achieving optimum compensation of residual boron, and (3) controlling the doping of the single crystal to the desired gallium concentration. These problems must be solved consistent with a full integrated device fabrication process.

1.3 PROPERTIES OF EXTRINSIC DETECTORS AND THEIR EFFECT UPON MATERIAL CHARACTERISTICS

Photoconductivity processes involve the transition of electrons between different energy states in the crystal. They involve the absorption of energy from photons which excite charge carriers from a non-conducting ground state to a higher energy conducting state, thereby contributing to the electrical conductivity.

Intrinsic photoconduction occurs when electron-hole pairs are generated by photoexciting carriers across the intrinsic band gap, i.e., from the valence to the conduction band.

Extrinsic photoconduction occurs when carriers are optically excited from energy sites within the forbidden band to either the conduction or the valence band. Impurity atoms, added to the host material, introduce the required donor or acceptor sites for extrinsic photoconduction. In an n-type extrinsic photoconductor, electrons are photo-excited from donor atoms to the conduction band. In a p-type extrinsic photoconductor, holes are photo-excited from the acceptor atoms to the valence band. Extrinsic photoconductivity results only in majority carrier conduction; the opposite charge is fixed at the ionized donor or acceptor sites. This is contrasted to intrinsic photoconductivity where the photo-excited electron and hole are both free to conduct.

The host material in this program is silicon. The dopant for the LADIR material is gallium, an acceptor with an ionization energy of about 0.07 eV. The ionization energy is the characteristic energy which determines the minimum energy a photon must have to generate photoconductivity. This threshold energy determines the long wavelength cutoff as:

$$\lambda_c = \frac{1.24}{E_a} \tag{1}$$

2

where

> λ_c is the long wavelength cutoff (micrometers)
>
> E_a is the ionization energy (electron volts).

The characteristics of extrinsic detectors are determined by the types and concentrations of impurities in the detector material. Controlled impurities are added to tailor the characteristics of the detector to meet specific objectives. In addition to the impurity (also called dopant) added in a controlled manner, a residual impurity (boron) remains in the silicon, even after multiple vacuum zone passing. This vacuum zone passing process, which precedes the doping process, is performed to purify the silicon. In this process, most impurities are swept to the upper end of the crystal, thus purifying the bulk of the crystal. The only remaining impurity resisting this purification process is boron.

The maximum operating temperature of an extrinsic detector is determined by its impurity content. If the temperature is too high, thermal ionization of the impurities results in an excessive dark current, rendering the material useless as an optical detector. Boron has a lower ionization energy than gallium; therefore, if boron is present, the detector cooling requirements can be more severe than would otherwise be the case. Although boron atoms cannot be completely removed, they can be rendered inactive by the addition of an n-type compensating impurity in a concentration equal to N_B. This leaves the boron impurities in an ionized state without introducing free carriers (holes). Thus, for a fully compensated material, $N_C = N_B$, where N_C is the concentration of compensating impurities and N_B is the boron concentration.

A brief theoretical treatment of a detector is given here and illustrates the requirement for residual impurity control. The input to an extrinsic detector is radiant power; the output is an electrical current. The ratio between output and input is the responsivity. For more detailed discussions of the extrinsic detector response models, see Ref. 1 through 5.

The responsivity of a photoconductor at wavelength, λ, is:

$$R_\lambda = \frac{q}{hc} \eta G \lambda$$

$$= 0.806 \, \eta G \lambda \text{ amp/watt} \tag{2}$$

1. Breckenridge, R.G., Russell, B.R., and Hahn, E.E., Photoconductivity Conference, (John Wiley & Sons, Inc., N.Y., N.Y., 1956).
2. Burstein, E., Picus, G., and Sclar, N., "Optical Photoconductivity Properties of Silicon and Germanium", Reference 1, pp 353-413.
3. Hudson, R.D., Jr., and Hudson, J.W., Infrared Detectors, (John Wiley & Sons, Inc., N.Y., N.Y., 1975).
4. Bube, B.M., Photoconductivity in Solids, (John Wiley & Sons, Inc., N.Y., N.Y., 1960).
5. Moss, G.S., Burrell, G.J., Ellis, B., Semiconductor Opto-Electronics, (John Wiley & Sons, Inc., N.Y., N.Y., 1973).

where

    q   is the electron charge

    hc is the product of Planck's constant and the velocity of light

    η is the detector quantum efficiency

    λ is the wavelength in micrometers

    G   is the photoconductive gain.

The photoconductive gain is given by:

$$G = \frac{\mu \tau E}{L} \qquad (3)$$

where

    μ is the mobility of the free carriers

    τ is the lifetime of the photo–excited carriers

    E is the applied electric field

    L is the interelectrode spacing.

For simplicity consider the case of a crystal containing gallium dopant at concentration N, residual boron at concentration N_B, and compensating donor at concentration N_D. The boron is assumed fully compensated so that $N \gg N_D > N_B$. Very low photon flux levels and temperatures below those for significant ionization are also assumed.

The quantum efficiency for a detector with parallel front and rear surfaces separated by a distance, d, along the path of the incident radiation is given by:

$$\eta = \frac{(1 - R)\ [1 - \exp(-2\alpha d)]}{1 - R \exp(-2\alpha d)} \qquad (4)$$

where

    R is the front surface reflectance of silicon equal to 0.31; the back surface reflectance is assumed large $\simeq 1$

    α is the absorption coefficient associated with photoconductivity.

The absorption coefficient is given by:

$$\alpha = \sigma_A \left(N - N_C \right)\ cm^{-1} \qquad (5)$$

4

where

σ_A is the cross section for photoconductive absorption

$N_C = N_D - N_B$ is the concentration of gallium which is compensated.

The lifetime of the photo-excited carriers in a photo conductor with one excitable impurity is given by:

$$\tau = 1/\left(B \, N_C\right) \sec \tag{6}$$

where B is the recombination coefficient.

The recombination coefficient is given by:

$$B = <\sigma_R \cdot v> cm^3 \, sec^{-1} \tag{7}$$

where

σ_R is the recombination cross-section

v is the velocity of the free carrier

< > denotes an average over velocity.

If σ_R is independent of velocity and the velocity distribution is Maxwellian, then:

$$B = \left(\frac{8kT}{m^*}\right)^{1/2} \sigma_R \, cm^3 \, sec^{-1} \tag{8}$$

where

m* is the effective mass of the charge carriers

k   is the Boltzmann's constant

T   is the absolute temperature.

Finally, if the mobility of the charge carriers is limited by scattering by ionized impurity centers, which in the photoconductive temperature domain is frequently the case, the mobility is given by:

$$\mu \cong \frac{KT^{3/2}}{2N_D} \, cm^2 \, volt^{-1} \, sec^{-1} \tag{9}$$

where K is a constant of proportionality.

5

Equations (6) and (9) show reciprocal dependence of both mobility and lifetime on the concentration of compensating impurities. Since the concentration of the residual p-type impurities (boron in this case) determines the requirements for compensation, it can be seen that the control of these residual impurities is important if the responsivity which depends on mobility and lifetime [see Eq (2) and (3)] is to be made large.

As the detector responsivity is increased, the detector signal and noise will rise. When the responsivity is sufficiently high, the detectivity of the system will become limited by the detector self-noise rather than by load resistors, preamplifiers, or spurious noise sources. The detectivity at peak wavelength under this circumstance for a well behaved semiconductor detector is given by:

$$D^*_{pk} = \frac{2.52 \times 10^{18} \lambda_{pk} \sqrt{\eta}}{\left[\left\{ \frac{4.84 \times 10^{30} \, a(\eta) B (m^*/m)^{3/2} T^{3/2}}{\sigma_{pk} g} \exp -\left(\frac{\Delta E}{kT} \right) \right\} + Q_B \right]^{1/2}} \, cm \, Hz^{1/2} \, w^{-1}$$

(10)

where, in addition to previously defined quantities,

σ_{pk} is the photoconductive absorption cross-section at peak wavelength in units of 10^{-15} cm^2

(m^*/m) is the density of state effective mass ratio of the free charge carriers

$a(\eta)$ is a function defined by $a(\eta) = \alpha d/\eta$ which is a property of the host silicon material and is of the order of unity

g   is the degeneracy of the ground state of the impurity and is also of the order of unity

(ΔE) is the extrinsic impurity (dopant) activation energy

Q_B is the background radiation flux density.

If the detector temperature is low enough and the background high enough, Q_B is the dominant term in the denominator of Eq (10). Under these conditions, Eq (10) reduces to the well known expression for background limited detectivity (the BLIP condition):

$$D^*_{pk(BLIP)} = 2.52 \times 10^{18} \lambda_{pk} \left[\frac{\eta}{Q_B} \right]^{1/2} cm \, Hz^{1/2} \, w^{-1}$$

(11)

This applies to all extrinsic detectors and has been found to agree closely with experimental data obtained on extrinsic germanium detectors as well as on extrinsic silicon detectors, such as Si:In, Si:Ga, Si:S, Si:As, Si:Bi, and Si:Aℓ.

6

It is useful to determine the temperature at which a detector goes from a background limited detectivity condition to one limited by temperature. This temperature can be obtained approximately by setting equal the two terms in the denominator of Eq (10) and solving. This yields:

$$T = \frac{5.037 \times 10^3 \, (\Delta E)}{\log \, (A/Q_B) + 1.50 \log T} \, °K \tag{12}$$

where

$$A = \frac{2.36 \times 10^{30} \, a(\eta)B(m*/m)^{3/2}}{\sigma_{pk}g}.$$

The background radiation flux density is given approximately by

$$Q_B = \sin^2 \, (\theta/2) \int_0^{\lambda_{1/2}} Q_T(\lambda) \, d\lambda \, (\text{ph cm}^{-2} \, \text{sec}^{-1}) \tag{13}$$

where

θ is the angle subtended by a circular field-of-view of the background at the detector

$Q_T(\lambda)$ is the Planck's blackbody photon spectral density function

$\lambda_{1/2}$ is the cutoff wavelength of the detector.

Appendix A contains a detailed theoretical analysis showing the relations between detector temperature, flux level, and compensating impurity concentration. Figures 1 and 2 summarize the results obtained from the analysis. From Figure 1, it can be seen that for high background conditions ($\phi \sim 10^{17}$ ph/cm^2 sec), the donor concentration level, N_D, is not important. Detectivity D*, at high background is independent of detector temperature ($T < 30°$ K) for values of N_D up to 10^{14} cm^{-3}. For low background conditions ($\phi \sim 10^8$ ph/cm^2 sec), D* is strongly temperature dependent at low donor concentrations and less temperature sensitive for $N_D \gtrsim 10^{13}$ cm^{-3}.

In comparing theoretical D* values with practical measurements it should be kept in mind that limits are set on the maximum value of D* by both material purity and other sources of system noise (e.g., amplifier noise). The shaded area of Figure 1 marks the region of donor concentration that is accessible to detectors at the present state of the art. The optimum choice for N_D would involve a tradeoff study among responsivity, operating temperature, amplifier noise and other systems parameters.

7
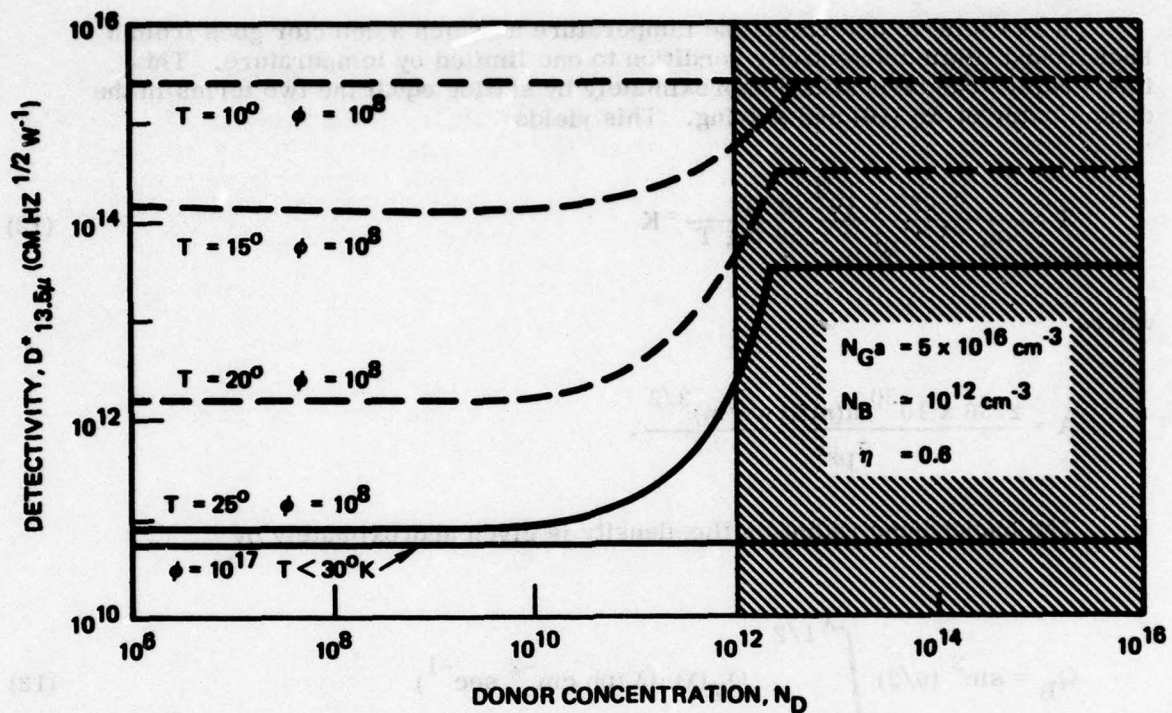
Figure 1. Detectivity vs Donor Concentration
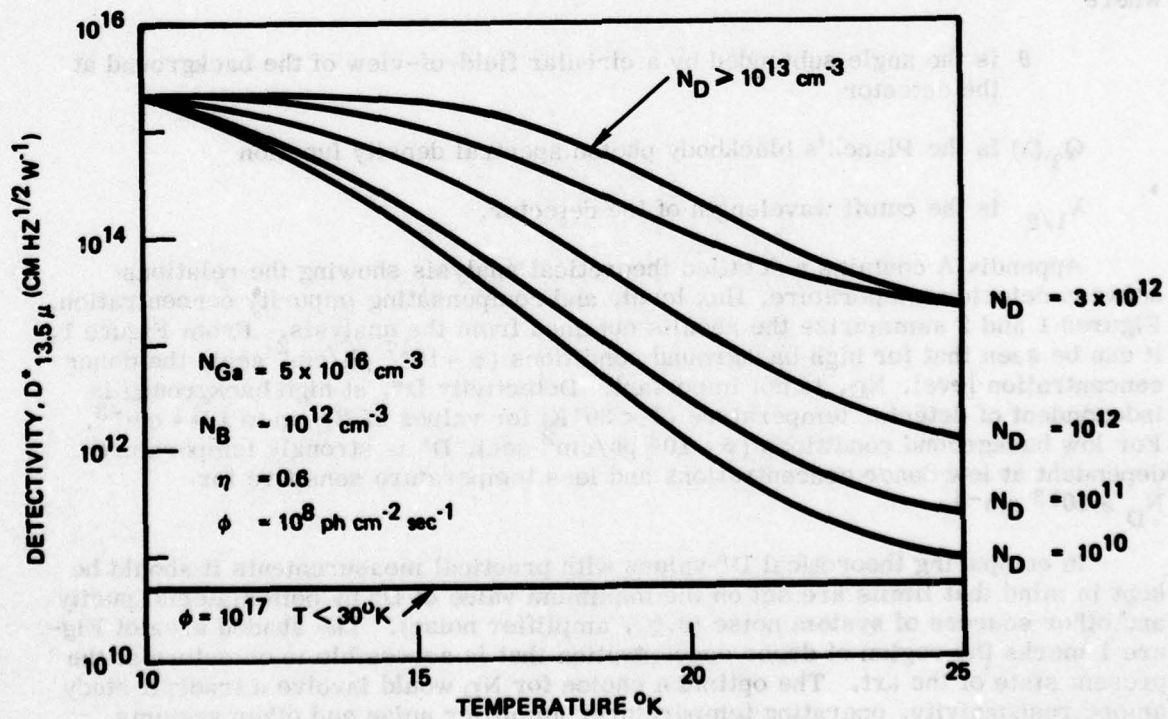
Figure 2. Detectivity vs Temperature

8

1.4 SILICON POLYCRYSTAL FABRICATION

Polycrystalline silicon is the starting material for the single crystal produced by the Czochralski and float zoning techniques. Polycrystalline rods are fabricated by a chemical reaction in which a gaseous silicon compound is purified by fractional distillation and then decomposed to form the polysilicon. A major goal in the process is to reduce the boron content to the minimum. Gaseous trichlorosilane ($Si:Cl_3H$) used in this process, provides the possibility of reducing the boron content to less than 0.02 ppb (parts per billion) or 10^{12} atoms cm^{-3}.

1.5 BORON LIMITATION ON IR SILICON DETECTORS

Extrinsic impurity doped silicon detectors operate at low temperatures where the detector becomes a near-insulator, because the free charge carriers are frozen out. In the presence of infrared, some of the trapped charge carriers are freed to provide a photoconductive response.

The responsivity of these detectors is proportional to the product of lifetime and mobility of the charge carriers (holes in the case of Si:Ga) generated by the absorption of infrared radiation. At low temperatures, electrons introduced by donor impurities will preferentially populate any shallow acceptor states like boron, leaving all donors in a positive charge state. The concentrations of positively charged donors and negatively charged acceptors will be numerically equal. The major reason for adding compensating donors is to ionize boron atoms without adding thermally generated holes to the dark current. However, if there is an excess of donors ($N_D > N_B$), some electrons will also populate gallium acceptor states. Thus, overcompensation will be detrimental to both the hole lifetime and hole mobility while not increasing the maximum detector operating temperature (see Eq (6) and (9)).

SECTION II

SILICON MATERIAL DEVELOPMENT FOR LADIR

This section details the technical considerations and processing steps required for the development of high quality gallium-doped silicon crystals for use in high performance silicon detectors with maximum responsivity in the 8 to 14 μm spectral region. Specific processing steps include methods to control the quality of purchased material, purification of the starting material, single crystal perfection, control of compensation, and well defined control of the gallium dopant in the final product.

Information, for optimizing each processing step and the final results, was obtained through comprehensive record keeping. This permitted the comparison of measurements taken at various points in the process. All processing steps were established in a repeatable manner and were completely documented. The resultant process is reported in Section III, Definition of the Growth Process.

2.1 TASK I – PURIFICATION OF INTRINSIC SILICON

The performance of a solid-state device depends largely upon the quality of the material, whose purity and crystallographic perfection are the two most important factors. The crystallographic orientation, the impurity distribution, and the dislocation density are material characteristics determined by the crystal growth process.

2.1.1 Float Zone Technique

The vertical float zone method was chosen for the crystal growth process. All major impurities are removed by float-zone refining with the exception of boron. Residual boron presents a specific problem in the silicon material preparation and represents the present limitation in silicon purity. The primary advantage of the float zone technique lies in the absence of many of the sources of contamination which are present in other crystal growing processes. Since the silicon surface effectively serves as a crucible for its own melt, crucible contamination is avoided. Since the heating is performed by a radio frequency induction coil, the only part of the crystal growing apparatus that is hot is the silicon itself. Growing in vacuum or inert gas isolates the silicon from atmospheric contamination and permits selective impurity outgassing (see Figure 3).

The two vertical float zoners (vacuum and gas) model number VZ A3* used at Rockwell were designed to grow single silicon crystals with a diameter of 0.5 to 1 inch and a maximum boule length of 18 inches. The dimensions of the crystal growth chamber are 12 inches wide by 8 inches deep by 26 inches high. The chamber walls are water cooled steel panels. The coil transport has two speed ranges: high, for crystal growth up to 1 to 5 inches (25 to 125 mm)/min and low, for crystal growth from 0.06 inch (1.5 mm)/min to 0.24 inches (6 mm)/min. Power demands due to crystal diameter changes are used for diameter control. These power change demands are corrected by an automatic stretch and squeeze mode which slightly alters

---

*Siemens A.G. D-8000, Muenchen 1, Germany

SILICON ROD →

LIQUID OR
MOLTEN ZONE

RF COIL →

SILICON SEED →
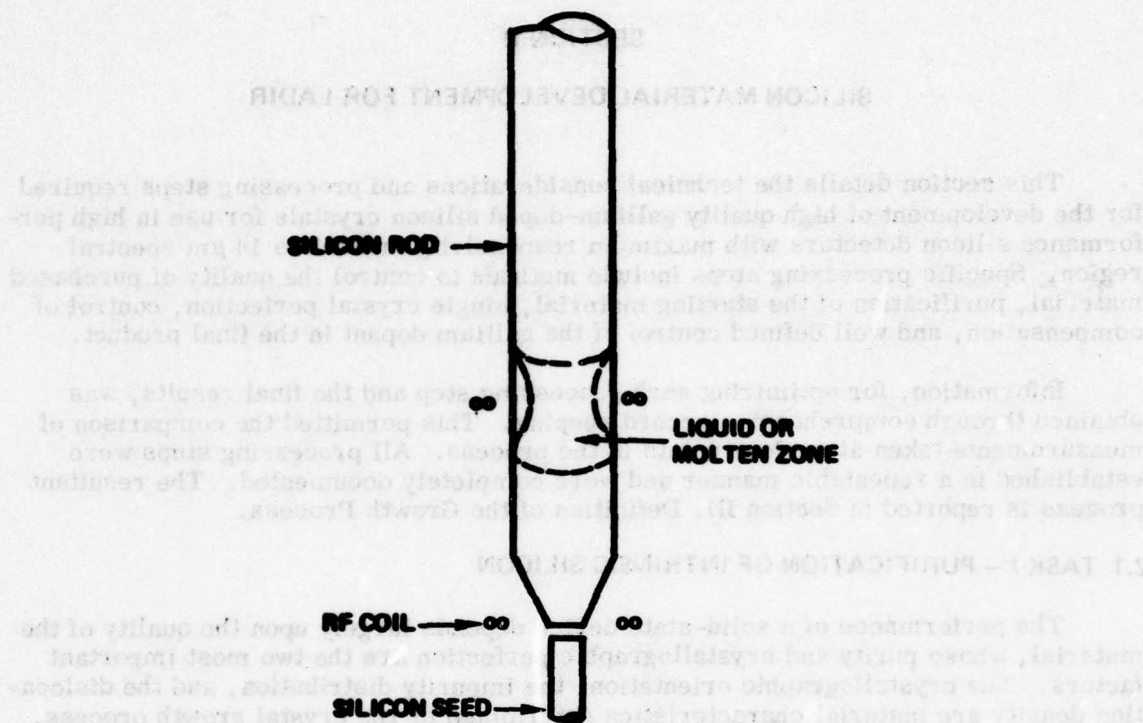
Figure 3. Principle of Vertical Float Zoning

the configuration of the zone and adjusts the coupling between the molten silicon and the coil. Radio frequency power is supplied by a 5 kW Siemens generator.

2.1.2 Polysilicon Evaluation

The purity of polysilicon may be characterized by the purity of single crystals zoned from the polysilicon. A basic assumption is that no impurity is added during the zone passing.

High quality polycrystalline silicon is purchased from Dow Corning* with an impurity content of less than 0.4 ppb donors (mainly phosphorus) and 0.02 ppb acceptors (mainly boron). The polycrystalline silicon is characterized by the supplier as to acceptor (p-type) and donor (n-type) concentrations.

The supplier checks the purity of the polysilicon by zoning a rod by the 1-2-3-7 pass method. A diagram of a 1-2-3-7 test crystal is shown in Figure 4. After the single crystal seed is connected with the molten end of the rod, the molten zone moves upward as the coil advances at a constant speed. Elements from Groups III and V either evaporate or are moved into the liquid zone as determined by their distribution coefficients. The impurities remaining in the different parts of the crystal after the passes are determined by resistivity measurements. The measurements must be taken in the centers of the rod areas with constant diameter. The undercuts on the

_____
* Dow Corning Corp., Hemlock, MI 48626
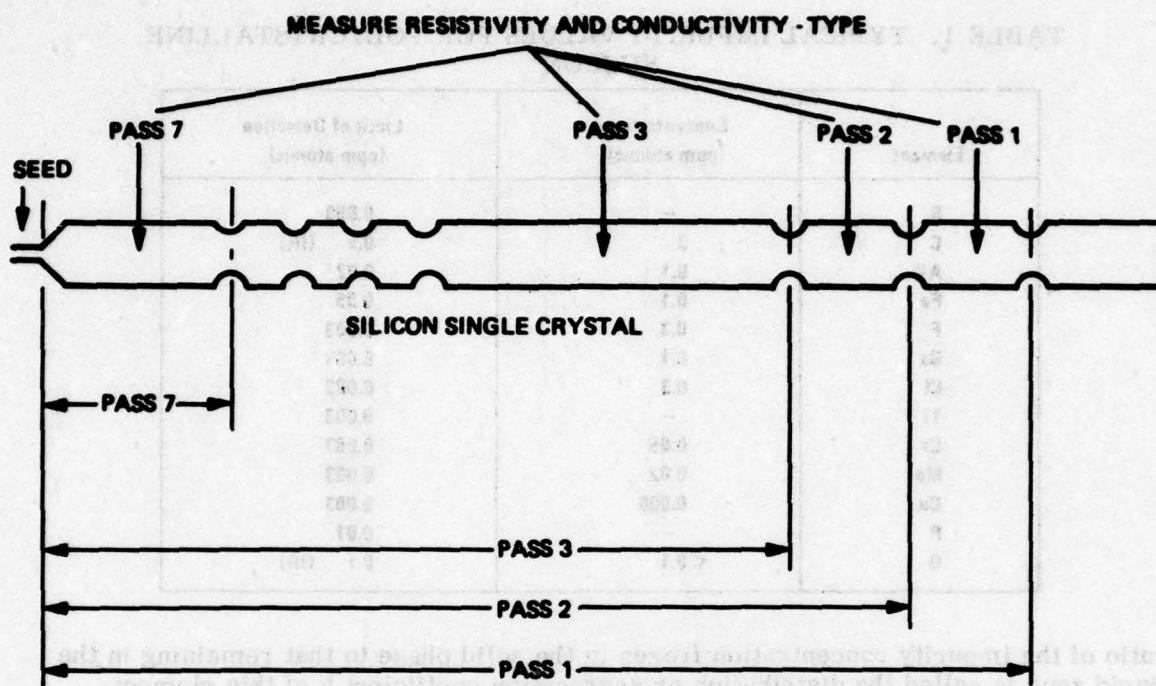
Figure 4. Polysilicon Evaluation – 1-2-3-7 Crystal

ingot are the last frozen liquid zones and contain the impurities removed. The conductivity-type is determined for each section of the rod by the thermal or rectifying probe method.

The 1-2-3 pass section of the ingot determines the donor concentration. The ratio of the impurity concentrations of two consecutive passes permits the calculation of the donor concentration of the polysilicon. The 7-pass section provides the data on the acceptor (boron) concentration which determines the purification limit of the material at this time.

Phosphorus and other impurities (at a lower concentration than phosphorus) are swept by the moving liquid zone and evaporate or accumulate at the end zone, which is cropped from the single crystal rod upon completion of the process.

Dow Corning provides a data sheet describing the impurity content of each silicon lot (see Table 1). The impurity concentrations are determined by mass spectroscopy and IR absorption (the latter for oxygen and carbon).

2.1.3 Silicon Purification

With the exception of boron, all of the important, electrically active impurities which are commonly found in silicon can be removed by the vertical vacuum float zoning method. These removable impurities remain preferentially in the liquid zone as the coil advances and the silicon solidifies at the interface (see Figure 3). The

13

TABLE 1. TYPICAL IMPURITY VALUES FOR POLYCRYSTALLINE SILICON

Element	Concentration (ppm atomic)	Limit of Detection (ppm atomic)
B	–	0.003
C	3	0.5 (IR)
Al	0.1	0.02
Fe	0.1	0.05
F	0.3	0.003
Ca	0.1	0.003
Cl	0.3	0.003
Ti	–	0.003
Cr	0.05	0.003
Mn	0.02	0.003
Cu	0.006	0.003
P	–	0.01
O	<0.1	0.1 (IR)

ratio of the impurity concentration frozen in the solid phase to that remaining in the liquid zone is called the distribution or segregation coefficient k of this element. Table 2 lists the distribution coefficient as the most important impurities in silicon (Ref. 6). The distribution k is expressed as:

$$k = N_s/N_L \tag{14}$$

where

    k is the distribution or segregation coefficient

    N_s is the impurity concentration frozen in the solid crystal at the interface

    N_L is the concentration remaining in the liquid at the interface.

Impurities with high vapor pressure like phosphorus and arsenic show a "modified distribution coefficient," which is characterized by the fact that evaporation increases the removal rate beyond the value of the segregation k if the purification process is performed in a vacuum (<0.1 mm Hg). (Ref. 5.) The modified distribution coefficient can be formulated as:

$$u = k + f/\alpha L \tag{15}$$

6. Trumbore, F.A., "Solid Solubility of Impurity Elements in Germanium and Silicon," Bell Sys. Tech. J., Vol. 39, pp 205-232, 1960.

TABLE 2. DISTRIBUTION AND DIFFUSION COEFFICIENTS AT THE MELTING POINT OF SILICON (Ref. 6)

Element	k Segregation or Distribution Coefficient in Silicon	Diffusion Coefficient (cm²/sec) Temp 1000 to 1350°C
Lithium	0.01	10^{-7} to 10^{-6}
Gold	2.5×10^{-5}	10^{-8} to 10^{-5}
Zinc	$\simeq 1 \times 10^{-5}$	5×10^{-7}
Boron	$\simeq 1$	10^{-13} to 10^{-12}
Aluminum	2×10^{-3}	2×10^{-12}
Gallium	8×10^{-3}	6×10^{-13}
Indium	4×10^{-4}	10^{-13}
Tin	1.6×10^{-2}	8×10^{-14}
Phosphorus	0.35	2×10^{-12}
Arsenic	0.3	10^{-14}
Antimony	2.3×10^{-2}	2×10^{-13}
Bismuth	7×10^{-4}	–
Oxygen	0.5	4×10^{-10}
Sulfur	10^{-5}	10^{-8}
Iron	8×10^{-6}	4×10^{-6}
Cobalt	8×10^{-6}	–
Manganese	$\simeq 10^{-5}$	2×10^{-7}
Magnesium	$\simeq 4 \times 10^{-6}$	$\simeq 10^{-7}$

where the modification term $f/\alpha L$ depends on the zone length L, growth rate (or coil speed) f, and the evaporation rate α, which is a function of the growth chamber pressure.

Figure 5 presents experimental data for the reduction of phosphorus at various growth rates (or coil speeds) and a constant growth chamber pressure (< 0.1 mm Hg). The curve shows that with the reduction of the growth rate from 2 mm/min to 1 mm/min, phosphorus reduction can be increased by a factor of two. This purification technique performed in the vacuum float zoner permits the reduction of the phosphorus concentration, which is always initially larger than the boron concentration, by multiple zone passing. Using the experimental data in Figure 5, the number of vacuum

15
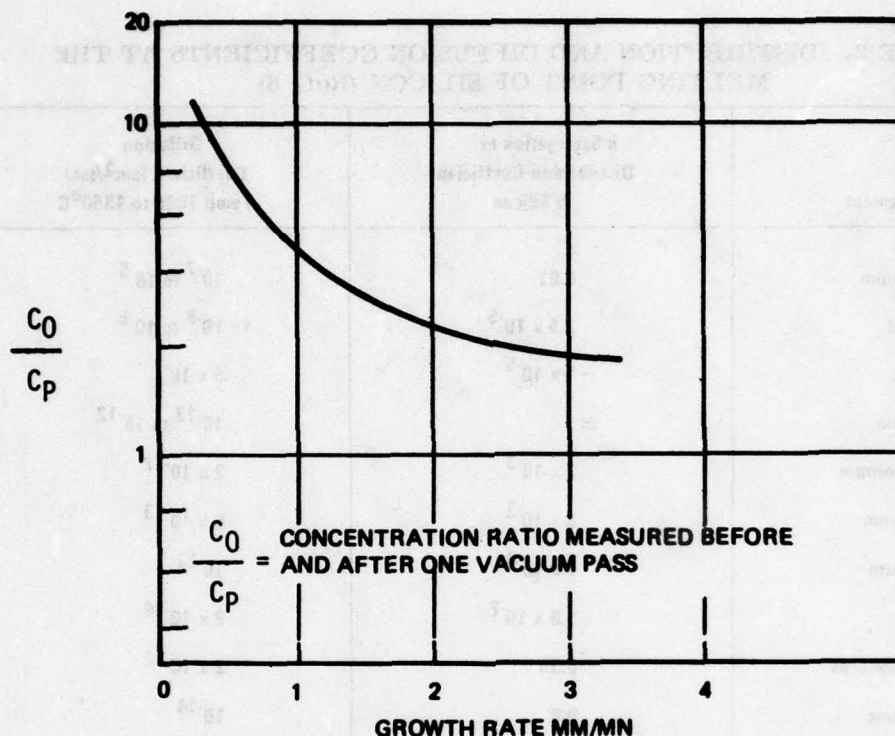
Figure 5. Phosphorus Reduction During Silicon Purification
by the Float Zoning Technique

passes needed to reduce the phosphorus concentration to a certain level can be calcu-
lated. Figure 6 compares experimental data of crystals purified in this program to a
calculated curve and shows good agreement.

Eighteen purification runs were started during this project (see Table 3). The
earlier purification runs showed the inadvertent addition of impurities during the
vacuum float zoning process. The following steps were adopted to minimize contamin-
ation of the crystal during the growth process:

1. A shutter arrangement was provided to cover the furnace window viewing
    port. This shutter provides the operator with the freedom of an "unlimited"
    number of passes without the need to open the furnace to clean the window.
    The shutter was equipped with high purity quartz panels to avoid
    contamination.

2. The achievable vacuum of the vacuum float zoner was improved through the
    addition of a liquid nitrogen trap and a water cooled chevron baffle. This
    installation further reduces contamination of the silicon by preventing
    back streaming of the diffusion pump oil into the growth chamber.

16
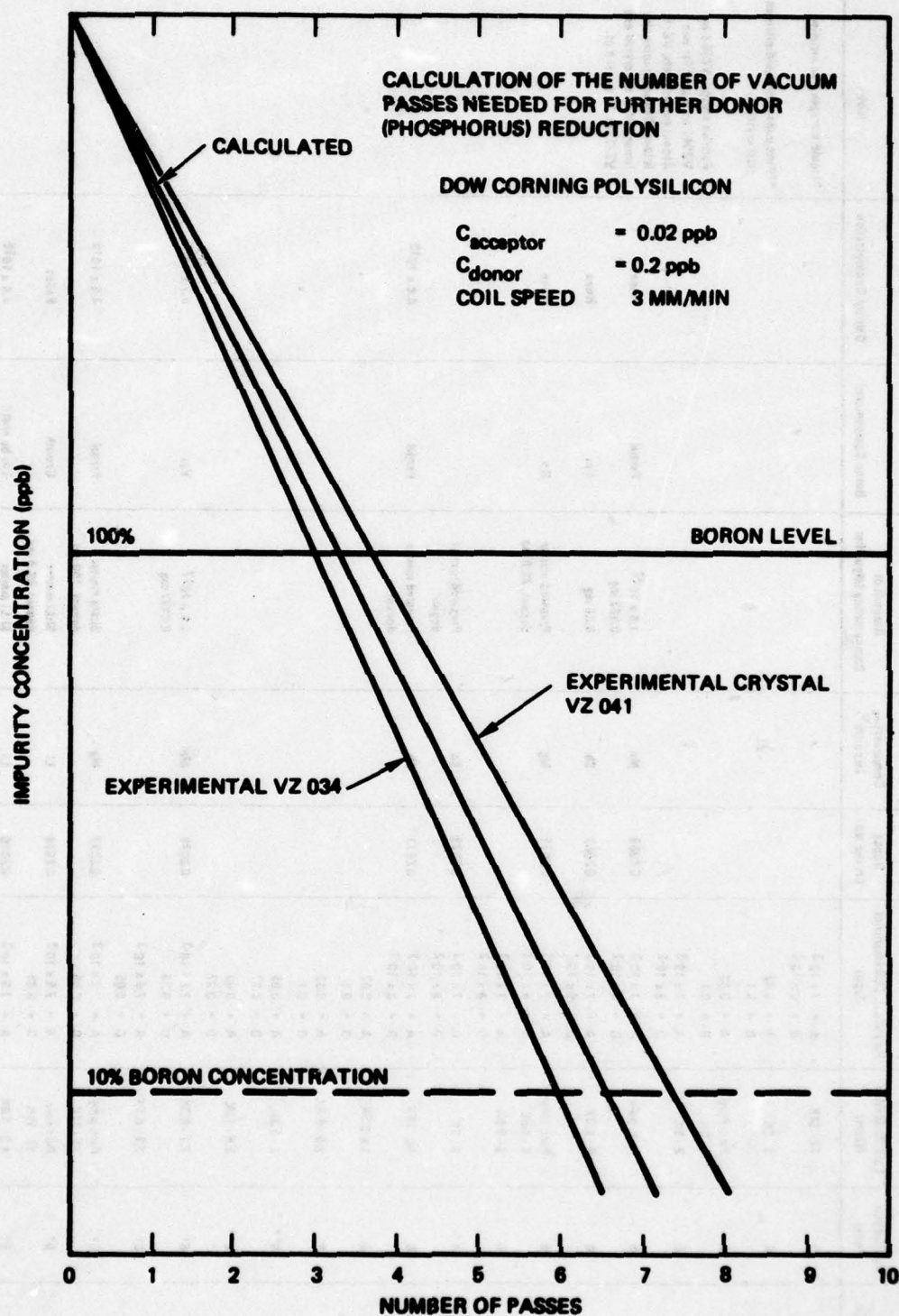
Figure 6. Number of Vacuum Passes for Phosphorus Purification in Silicon

17

TABLE 3. SILICON CRYSTAL GROWTH PROGRAM

Crystal No.	Purification Passes	Bulk Resistivity (Ω cm)	Polysilicon Characteristics (ppb)	Doped Crystal No.	Compensating Impurity	Amount of Compensating Impurities	Boron Component	Gallium Concentration	Notes
V2359	0	17 - 24K	A = 7 x 10³ D = 8 x 10⁻²						*Liquid nitrogen trap installed
V2360	0	8 - 9K	D = 0.02 D = 0.1						**Two pulls with liquid nitrogen trap (two crystals).
V2363	0	Purt. Poly 4 - 9K	A = 0.02 D = 0.1	G2360	Sb	1.8 x 10¹⁷ 0.482 mg	Partial	None	△ Purified crystals V2363 and V2363 were used for two dopant repetitions, V2/1 is identified when using the lower half of the crystal and V2/2 for the upper half.
V2367	0	2 - 9K	A = 0.02 D = 0.1	G2360	Sb	0.04 mg	Yes	None	
V2368	0	Purt. poly	A = 7 x 10³ D = 8 x 10⁻²	G2371	Sb	0.04 mg	No	None	
V2369	0	6 - 9.0K	A = 7 x 10³ D = 8 x 10⁻²	G2372	Sb	Prepared master dopant, 23.0 mg	Partial	4.5 x 10¹⁵	
V2366	0	Purt. poly 8 - 10K	A = 7 x 10³ D = 8 x 10⁻²	G2373	Ga	Prepared master dopant			
V2363	0	2 - 5.9K	A = 7 x 10³ D = 8 x 10⁻²			Prepared master dopant			
△V2364/1	0	5 - 9K	A = 7 x 10³ D = 8 x 10⁻²						
△V2364/2	0	10 - 16K	A = 0.02 D = 0.1						
V2365	0	1 x 2.6K	A = 0.02 D = 0.1						
V2366	0	2.5 - 4.2K	A = 0.02 D = 0.1						
V2369	4**	3 - 6.2K	A = 0.05 D = 0.27						
V2370	4**	3.5 - 12K	A = 0.05 D = 0.27	G2376	Sb	1.0 x 10¹⁷ 0.0277 mg	Yes	4.7 x 10¹⁵	
V2371	6*	7.1 - 9.2K	A = 7.5 x 10³ D = 0.05						
V2372	6*	7.3 - 9.6K	A = 7.5 x 10³ D = 0.05	G2377	Sb	5.64g master dopant, 100 mg	Partial	4.5 x 10¹⁵	
V2374	6*	Purt. poly 13 - 17K	A = 7.5 x 10³ D = 0.05	G2378	Li	5.64 master dopant, 45.4 mg	Growth	Failed	
V2375	6*	Purt poly 10 - 16K	A = 7.5 x 10³ D = 0.05	G2379	Li	5.64 master dopant, 45.3 mg	Yes by Hall No by IR	4.6 x 10¹⁵	
	6*	4.2 - 5.4K							

18

2.1.4 Float Zoner Preparation and Cleaning Procedure

Preparation and cleaning procedures were formulated for the float zone furnace chamber, the silicon, the seed, the coil, and all other parts used in connection with the crystal growth. These preparation procedures follow modified standard rules of cleaning and preparing silicon rods and growth environment for silicon crystal growth. The requirements in this contract specify a high degree of purity of the final single crystal, so the processed discussed in this report control the general handling procedures for the silicon and furnace parts.

The procedure for etching silicon boules is presented in the growth process writeup, as it is applicable for all silicon work. While the furnace cleaning procedures are tailored to our specific float zoner, they can be applied with modifications to other types.

2.1.5 Silicon Crystal Purification by Float Zoning

The silicon single crystals purified and grown under this program are listed in Table 3. The crystals are arranged by date and list the following:

1. The crystal number.

2. The number of purification passes in the vacuum zoner.

3. The bulk resistivity (maximum and minimum) measured on a 1 cm wide lapped strip on the ingot by a four-point probe. These data were correlated by slice resistivity and Hall measurements.

4. The characteristics of the polysilicon as listed by the supplier, given in ppb (parts per billion) of the A = acceptor (p-type) and D = donor (n-type) impurities.

The remainder of the data in Table 3 lists the further use of these purified crystals for boron compensation and gallium doping. A more detailed discussion about this subject is presented in the writeup on Tasks II, III, and IV.

Purification and uniformity in impurity concentration along the crystal boule and the radial resistivity gradient are plotted in Figures 7 and 8. Figure 7 shows the resistivity along the crystal boule for two purified crystals, VZ069 and VZ070 (see Table 3). Crystal VZ070 shows a low resistivity near the seed end reflecting the influence of a seed with lesser purity than that of the crystal material. The polysilicon used to grow VZ070 had an acceptor concentration of 7.5×10^{-3} ppb and a donor concentration of 0.05 ppb. The acceptor concentration provides the purification limit, corresponding to a single crystal resistivity of approximately 30,000 Ωcm. The difference in the resistivity between this limiting value and that measured for this crystal (4K to 10K Ωcm) is due to the seed influence and to the fact that apparently small amounts of boron were still added during the crystal growth process. A continuous effort was directed toward improving the purification process and increasing its consistency and repeatability.
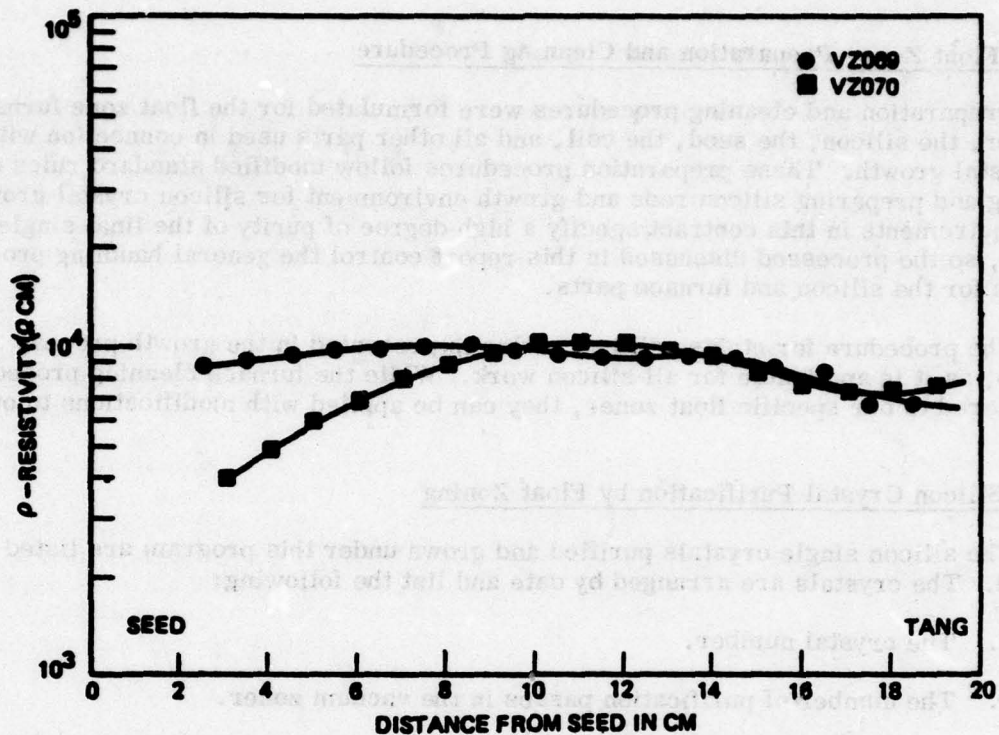
Figure 7. Skin Resistivity of Purified Crystals
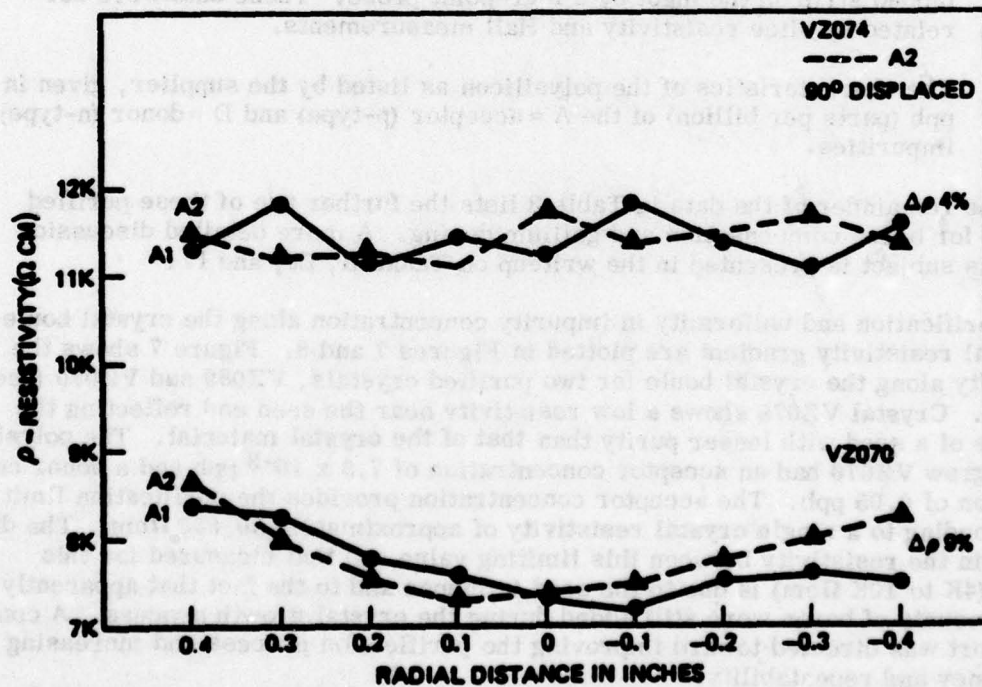
Figure 8. Radial Resistivity Gradient for Sample Wafers of Purified Crystals

20

The resistivity measurements on the bulk crystal were obtained by two- and four-point probes. It was found that four-point probe measurements on bulk silicon single crystals of high purity were erroneous when the contact pressure on the individual spring loaded points of the four-point probe varied. Lapping a level 1 cm wide strip along the ingot (final grit 5 μm) and thorough cleaning of the lapped strip provides reliable repeatable measurements in most cases (Figure 24, page 51).

The distribution of the impurity concentration in the bulk was evaluated by extracting wafers from different areas along the crystal. Resistivity topography in 90 deg x- and y-coordinates provided data reflecting uniformity on these slices. The collected test results are shown in Figure 8. The data points are A1 at the x coordinate and A2 at the y coordinate. The maximum resistivity variation between the data lines is indicated by a $\Delta\rho$ value.

The four- and two-point probes are the two most important techniques to measure the bulk resistivity along a silicon ingot by a non-destructive method. The purified silicon crystal has to be further processed in the gas zoner to compensate the boron and add the gallium. Only limited sample slices can be taken from the seed end to complement the bulk resistivity data. Sample slices taken less than one inch into the bulk from the seed end are not representative as the seed influence is still strong. Reliable Hall, IR, and photoconductive spectral response measurements require material samples from the bulk. These evaluation tests are imperative for the process development but consume large parts of the crystals and thereby reduce the yield of the final doped crystals. Improved consistency and reliability of the non-destructive bulk measurements is needed to narrow the uncertainty limits of the residual boron concentration which is used to calculate the needed compensating dopants.

2.1.6 Boron Reduction by Boron Redistribution in the SiO$_2$-Si System

Whenever two solids containing some specific impurities are brought into intimate contact, their impurities will redistribute in such a way that the chemical potential on the two sides of the interface will be equal. This concentration balance of the impurities in the two regions can be expressed as

$$a_1 c_1 = a_2 c_2$$

where

a_1, a_2 are the activity coefficients

c_1, c_2 are the concentrations of the impurities distributed in the two regions.

It has been theoretically and experimentally established that the impurity distribution within a semiconductor material can be altered during the thermal oxidation process. When a silicon surface is oxidized, an interface is created which separates the resulting two solid phases, the silicon oxide and the silicon. During the oxidation process,

21

the SiO_2-Si interface advances into the silicon, causing a redistribution of its original impurities. The redistribution depends on the segregation coefficient, m, where

$$m = \frac{\text{equilibrium concentration of impurity in Si}}{\text{equilibrium concentration of impurity in } SiO_2}$$

It compares the relative magnitude of the activity coefficients of a specific impurity in the oxide to that in the silicon. A second factor affecting the redistribution is the diffusion of the impurity within the oxide layer. This impurity may also have a tendency to leave the oxide and escape into the gaseous ambient. The rate of the escape then will be determined by the diffusion of the impurity through the oxide layer. A balance for this impurity is then established in the three parts of the system, silicon, oxide, and ambient.

A.S. Grove (Ref. 7) lists the segregation coefficient m for various impurities in the SiO_2-Si system. A segregation coefficient m < 1 corresponds to a situation where the oxide "takes up" the impurity. In such a case, the specific impurity will be depleted from the silicon. Gallium, boron, and indium have such specific characteristics (m $\simeq$ 0.3). Correspondingly, a rapid diffusion of these impurities through the oxide region further depletes their concentration in the silicon.

Purification by this method is most effective when silicon sample wafers are used. Other researchers (Ref. 8 and 9) have investigated boron redistribution in substrates with a boron concentration between 10^{15} and 10^{18} cm^{-3}. Four-point probe and spreading resistance measurements are quite accurate in this concentration range. Impurity (boron) contamination during oxidation as a competitor to out-diffusion is of little concern. However, silicon crystal material with a residual boron concentration of $\leq 10^{12}$ cm^{-3} is at a purity level where contamination by handling and specifically by high temperature processing drastically changes its characteristics. The experiments presented later in this section investigated the reduction of the boron concentration in silicon by boron out-diffusion into silicon dioxide.

To measure boron concentration below 1×10^{12} by the IR method, sample specimens of 3 to 7 cm in length (0.5 x 0.5 cm widths) are required. An ingot of three inches in length was needed to supply the test samples. Only small impurity changes are obtainable from such large size samples; by out diffusion. Therefore, further investigation of wafer material was only planned if the oxidation experiment of the boule at least retained the original silicon purity.

7. Grove, A.S., Leistiko, O., Sah, C.T., "Redistribution of Acceptor and Donor Impurities During Thermal Oxidation of Silicon," Journal of Applied Physics, Vol. 35, No. 9, p 2695, 1964.
8. Ar-Ron, M., Shatzkes, M., Burkhardt, P.T., "Distribution of Dopant in SiO_2-Si," Journal of Applied Physics, Vol. 34, No. 7, p 3159, 1976.
9. Kato, T., Nishi, Y., "Redistribution of Diffused Boron in Silicon by Thermal Oxidation," Japanese Journal of Applied Physics, Vol. 3, p 377, 1964.

Figure 9 shows the flow diagram of the SiO_2-Si experiment and Table 4 lists the results. The data of the experiments in both cases demonstrate the inability to retain the original purity of the silicon crystal, as obtained, through the vacuum float zoning process. Boron and oxygen contamination occurred during the diffusion process, while stripping the oxide, or while etching the ingot.

These test results confirm the conclusion of the previously referenced experiments that vacuum float zoning is the high temperature materials process best suited to achieve and retain optimum purity. Minimized handling and exposure to a contaminated environment is required in addition to rigid control of the etching and cleaning process. The float zone process still cannot decrease the residual boron concentration obtained in the original manufacture of the basic polysilicon material. At best, the float zone process maintains this boron impurity level while controlling the introduction of other elements.

2.2 TASK II – GROWTH OF DOPED SILICON CRYSTALS

Task II is concerned with: (1) boron compensation, and (2) gallium doping. These tasks were approached in separate experiments to determine the optimum procedures for each. These procedures were then used in combination to achieve the desired final results. Boron compensation and the gallium doping are achieved by adding impurities to the silicon ingot during the final crystal growth.

Dopants are added into the crystal near the seed end. The moving liquid zone carries the dopants into the silicon rod. The amount of dopant added is calculated as follows:

$$m = \frac{WC}{kAD} \tag{16}$$

where

   m   is the weight of the dopant in milligrams

   W   is the weight of the molten zone in grams

   C   is the concentration of impurities in the finished crystal in atoms/cm^3

   k   is the segregation coefficient (defined on page 14)

   A   is the number of atoms/milligram for the specific dopant

   D   is the density of silicon = 2.328 gm/cm^3.

2.2.1 Boron Compensation in Purified Silicon

Residual boron does not respond to the float zoning purification process or to any other established purification method. Photoconductivity in an extrinsic detector is a function of the impurities added to the silicon. The choice of the extrinsic impurity for this program is gallium which produces p-type conductivity. A gallium
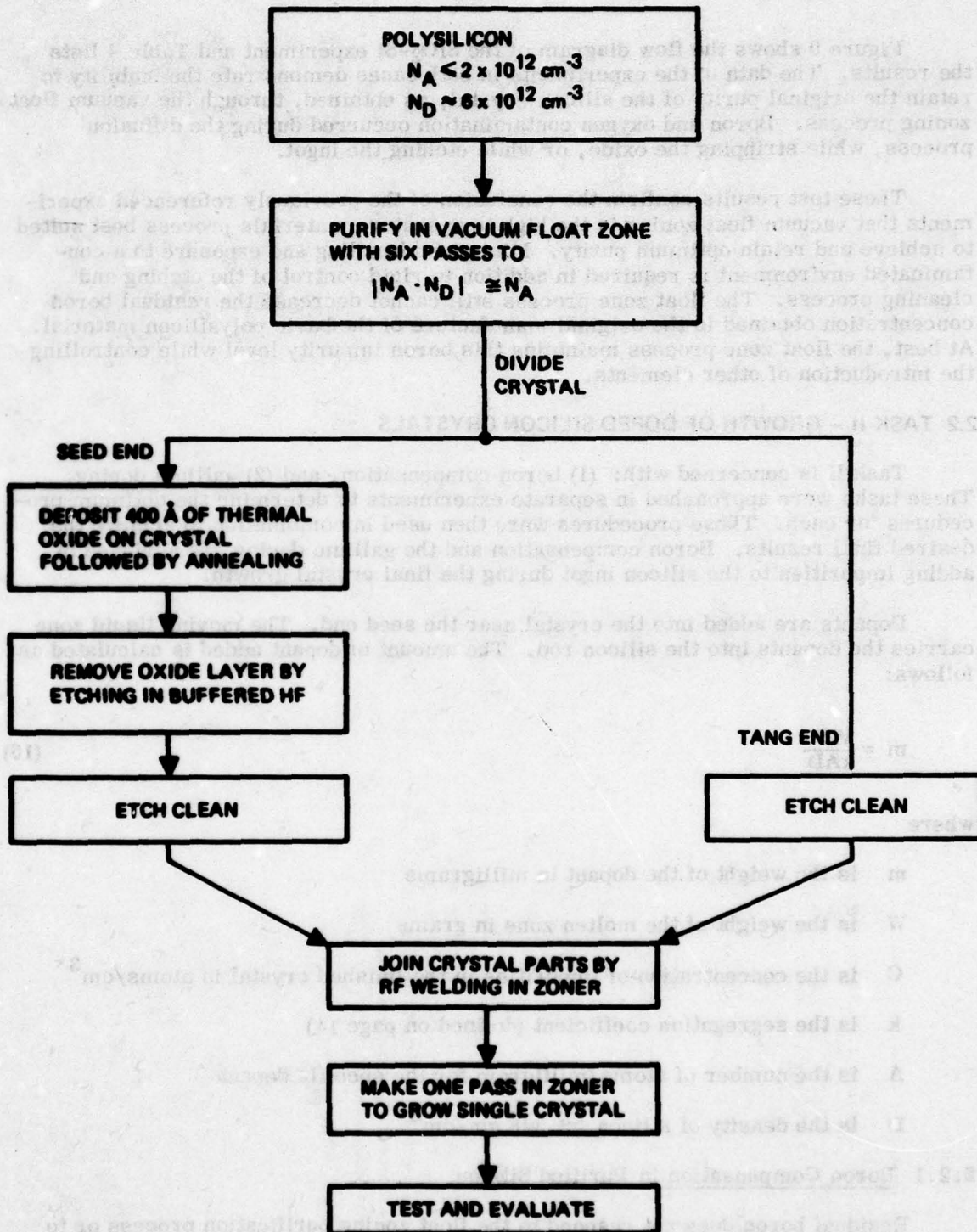
Figure 9. Flow Chart for SiO_2-Si Experiment

POLYSILICON
$N_A < 2 \times 10^{12}$ cm^{-3}
$N_D \approx 6 \times 10^{12}$ cm^{-3}

PURIFY IN VACUUM FLOAT ZONE
WITH SIX PASSES TO
$|N_A - N_D| \cong N_A$

DIVIDE CRYSTAL

SEED END

DEPOSIT 400 Å OF THERMAL OXIDE ON CRYSTAL FOLLOWED BY ANNEALING

REMOVE OXIDE LAYER BY ETCHING IN BUFFERED HF

TANG END

ETCH CLEAN

ETCH CLEAN

JOIN CRYSTAL PARTS BY RF WELDING IN ZONER

MAKE ONE PASS IN ZONER TO GROW SINGLE CRYSTAL

TEST AND EVALUATE

24

TABLE 4. TEST DATA FOR SiO_2–Si BORON REDISTRIBUTION EXPERIMENTS

	A			B			
Crystal Number	$\lvert N_A - N_B \rvert$ of Crystal Purified by Six Vacuum Passes (cm^{-3})	One Pass in	Experiment	Fourier Transform Absorption Data N_B (cm^{-3})	N_P (cm^{-3})	N_{Oxygen} (cm^{-3})	Comments
V2062	2×10^{12}	Vacuum Zoned	Seed End SiO_2–Si	5×10^{12}	1×10^{11}	7×10^{15}	Drastic contamination due to the oxidation process and during the final crystal growth
			Temp End	8.3×10^{12}	1×10^{11}		
V2101	1.28×10^{12}	Gas Zoned	Seed End SiO_2–Si	2.7×10^{12}	3×10^{11}	1×10^{16}	Boron and oxygen contamination of seed and crystal during the oxidation process
			Temp End	1.7×10^{12}	3×10^{11}	$< 5 \times 10^{15}$	

Column A shows the characteristics of crystal pulled by vacuum float zoning.
Column B shows characteristics of crystal after SiO_2–Si experiment and final single crystal growth.
N_B = Boron Concentration
N_P = Phosphorus Concentration

doped detector can be adversely affected by the presence of the uncompensated boron, a p-type impurity with a lower ionization energy. Boron, a shallow acceptor, can lower the operating temperature required for acceptable dark current values. To avoid this degradation of the detector, n-type impurities are added to compensate the boron. (For the theoretical discussion, see Section 1.3 and Appendix A.)

A minimum degradation in theoretical detector gain is expected when slightly more than exact compensation of the boron acceptors is accomplished. Excessive overcompensation is undesirable since it leads to additional acceptor and donor charged impurity centers. Such positively charged centers will reduce carrier mobility and lifetime and thereby the gain of the detectors.

Three experimental approaches were applied to investigate the effectiveness of the compensation of residual boron in gallium doped silicon. The material from the experimental crystals was then used to fabricate block detectors. These were then tested under high and low background conditions to evaluate the individual compensation method in terms of the final detector performance. The investigation of the three compensation methods was structured as follows:

1. Compensation of residual boron by adding interstitial (Mg or Li) or substitutional (Sb or Mn) impurities.

2. Compensation by nuclear transmutation doping $^{30}Si \rightarrow {}^{31}P$, boron compensated by ^{31}P.

3. Phosphorus reduction to a boron "plus" concentration by the float zoning method. This method is presently used in the industry and material obtained by this process was compared with that of methods (1) and (2).

2.2.1.1 Various n-Type Impurities for Boron Compensation

The investigation of n-type impurities that lend themselves to this kind of compensation is part of this project. Desirable characteristics for these dopants are that the distribution coefficient is in the range of 10^{-2} to 10^{-3} (see Table 2) and that the solubility limit of this element in silicon is at least as large as the highest expected values of boron concentration (approximately 10^{13} cm^{-3}). The added dopant has to have a melting point below 1420°C (melting point of silicon) and/or the ability to readily diffuse into silicon for the preparation of a "master dopant." The process of preparing a master dopant is performed by diffusing the impurity into an ultra pure silicon slice to such a concentration that a small part of this doped wafer provides the impurity atoms needed for the compensation.

Magnesium, lithium, manganese, and antimony were the n-type impurities considered for use in the LADIR program. Magnesium and lithium, the two interstitial impurities, were investigated because of their potential for complexing with boron. The experiments are discussed in the next subsections. Manganese and antimony, the substitutional impurities, were chosen because of their favorable segregation coefficients, melting points, and vapor pressures at 1420°C.

2.2.1.2 Magnesium and Lithium for Boron Compensation

The optimum condition of accurate compensation of the residual boron, without concern for the boron distribution in the silicon, can only be achieved by introducing an n-type impurity (X) that complexes with each available boron atom to form a stable XB compound.

Furthermore, a bond strong enough to hold the compensating impurity atom to the boron atom may cause the solubility of the compensating impurity to be dependent upon the density of the boron atoms. Magnesium and lithium are two elements considered for this compensation process. Diffusion experiments with lithium and magnesium indicate that their solubility limit is dependent upon the boron concentration contained in the silicon. Diffusion data reported in the literature cover diffusion temperatures up to 1340°C for magnesium and 1100°C for lithium. The compensation of the residual boron, while doping and growing a single crystal by the float zoning method in the gas zoner, has to be achieved at a temperature of 1420°C (the melting point of silicon). The vapor pressure, diffusion coefficient and stability of the compound XB at this temperature will be the limiting factors in establishing the utility of lithium and magnesium for boron compensation during the crystal growth process. (Refs. 10 through 21.)

10.   Franks, R.K. and Robertson, J.B., "Magnesium as a Donor Impurity in Silicon," Solid State Communications, Vol. 5, p 479, 1967.
11.   Fuller, G.S. and Ditzenberger, J.A., "Diffusion of Lithium Into Ge and Si," Physical Review, Vol. 91/1, p 193, 1953.
12.   Reiss, H. and Fuller, C.S., "Influence of Holes and Electrons on the Solubility of Lithium in Boron-Doped Silicon," Journal of Metals, p 276, February 1956.
13.   Reiss, H., Fuller, C.S., and Peitruszkiewicz, J., "Solubility of Lithium in Doped and Undoped Silicon, Evidence for Compound Formation," J. Chem. Phys., Vol. 25/4, p 650, 1956.
14.   Reiss, H., Fuller, C.S., and Morin, F.J., "Chemical Interactions Among Defects in Germanium and Silicon," Bell Sys. Tech. J., p 535, May 1956.
15.   Weiser, K., "Theory of Diffusion and Equilibrium Position of Interstitial Impurities in the Diamond Lattice," Physical Review, Vol. 126/4, p 1427, 1962.
16.   Aggarwal, R.L. and Fisher, P., et al, "Excitation Spectra of Lithium in Silicon and Germanium," Physical Review, Vol. 138/3A, p A882, 1965.
17.   Ho, L.T., "A Spectroscopic Study of Helium-Like Donors in Silicon," Purdue University, 1971.
18.   Pratt, B. and Friedman, F., "Diffusion of Lithium Into Ge and Si," J. Appl. Phys., Vol. 37/4, p 1893, 1966.
19.   Seeger, A., and Chik, K.P., "Diffusion Mechanism and Point Defects in Silicon and Germanium," Phys. Stat. Solids, Vol. 29, p 455, 1968.
20.   Pell, E.M., "Diffusion Rate of Li in Si at Low Temperatures," Physical Review, Vol. 119, p 1222, 1960.
21.   Pall, E.M., "Diffusion of Li in Si at High Temperatures and the Isotope Effect," Physical Review, Vol. 119, p 1014, 1960.

Lithium introduced in low-resistivity p-type silicon can form pairs bound by coulomb forces with Group III impurities. The localized modes of the Li^+B^- pair, as well as those of the Li^+Al^- pair, have been observed and reported in the literature. Compensation of boron doped silicon with interstitial lithium is achieved by a process in which a lithium atom or a Li-O complex, both donors, compensates an acceptor by the formation of a neutral Li^+B^- pair.

It is expected that magnesium, can also form a Mg^+B^- pair. This pair may further release an electron, leaving the ionized $Mg^{++}B^-$ pair.

2.2.1.3 Magnesium Experiments

Experimental work on extrinsic detector material at Rockwell International done prior to the LADIR contract included the introduction of magnesium into silicon. Magnesium doped silicon samples prepared by a specific diffusion technique were reported by L.T. Ho of Purdue University (Ref. 17). Ho's technique became the basis for two further experiments (labelled 6 and 7) at Rockwell, which are listed in Table 5.

Experiment 6 investigated the workability of the diffusion technique. This technique uses the diffusion of magnesium into an optically polished silicon slice sandwiched between two other silicon slices. These outside silicon "cover slices" contact the center slice on all surfaces covered with magnesium to avoid the escape of the magnesium into the ambient. The boiling point of magnesium is $1107°C$. This is much lower than $1340°C$, the temperature at which the diffusion coefficient of magnesium is a useful value of 10^{-7} cm^2/sec.

To avoid contact between the quartz tube and the silicon sandwich, a tantalum plate supports the wafer package. Quenching this sample package after diffusion caused breakage due to thermal shock. Therefore, to avoid this effect, the slice sandwich was placed between two thick silicon slabs, as shown in Figure 10, before quenching. This diffusion method succeeded and was used in all further diffusion experiments with magnesium and lithium.

Experiment 7 was conducted in two parts:

a) To establish the maximum solubility of magnesium in silicon by quenching (rapidly cooling by immersion in cold water) one sample to avoid outdiffusion during a slow cooling process.

b) To investigate the magnesium concentration remaining in the material when using slow cooling to imitate the float zoning process.

The impurity characteristics of two wafers from crystal VZ021 (with four vacuum passes) used for experiment 7 were measured to be:

$$\left| N_B - N_P \right| = 1.9 \times 10^{12} \text{ cm}^{-3} \quad \text{for } 7(a)$$

$$\left| N_B - N_P \right| = 2.2 \times 10^{12} \text{ cm}^{-3} \quad \text{for } 7(b)$$
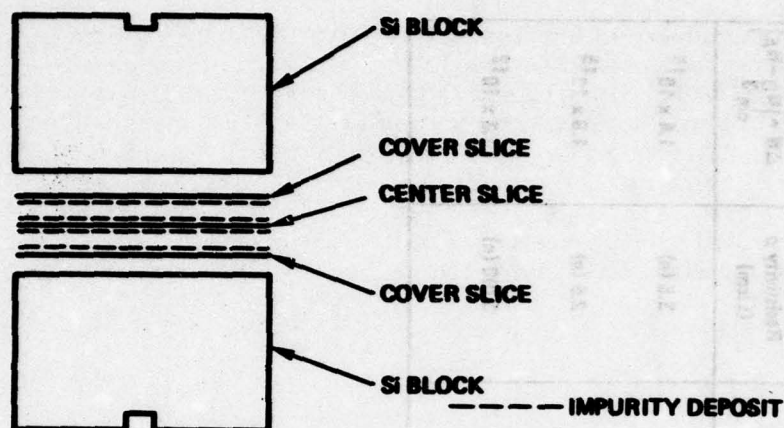
Figure 10. Diffusion Arrangement

The calculated phosphorus concentration is 0.8×10^{12} cm^{-3} (see Section 2.1.3 method of calculation).

After magnesium diffusion the impurity balance can be formulated as follows:

$$\Delta N = N_D - N_A = N_{Mg} + N_P - N_B$$

$$N_{Mg} \text{ (quenched)} = 1.9 \times 10^{15} \text{ cm}^{-3}$$

$$N_{Mg} \text{ (slowly cooled)} = 3.5 \times 10^{12} \text{ cm}^{-3}$$

The published (Ref. 10) maximum solid solubility limit of magnesium in silicon was confirmed by our experimental data as 1.9×10^{15} cm^{-3}. This low solubility limit, together with the segregation coefficient value of 0.01, would demand the use of a relatively large amount of master dopant. This complicates the crystal growth. Alternatively, the amount of pure elemental magnesium needed to compensate the boron in the purified crystal is so small that weighing and transferring it into the doping slot or welding it into the crystal is impractical. Therefore, an alternate method was developed to introduce the magnesium into the silicon ingot. Magnesium was evaporated onto a high purity silicon wafer. The slice was weighed before and after magnesium deposition. The wafer with the dopant was then broken into pieces and a small piece containing the approximate calculated amount of magnesium was welded into the ingot. The results are discussed in Sections 2.2.1.5 and 2.4.

2.2.1.4 Lithium Doped Silicon Study

Lithium is an interstitial impurity with a diffusion constant of 10^{-5} at approximately 850°C. In contrast, substitutional impurities from Groups III and V have a diffusion coefficient of 10^{-12} to 10^{-13} at the source temperature (see Table 2).

29

TABLE 5. Si:Mg EXPERIMENTS TO PRODUCE Si:Mg AS A MASTER DOPANT FOR BORON COMPENSATION

Experiment No. Crystal No.	Original Resistivity ρ (Ωcm)	$|N_B - N_P|$ cm^{-3}	Diffusion Temp (°C)	Diffusion Time (min)	Specimen Quenched or Slowly Cooled	Final Resistivity ρ (Ωcm)	ΔN Measured after Diffusion $\Delta N = |N_{Mg} - N_A|$ cm^{-3}
Expt No. 6 HPT no number	4000.0 (p)	3.4×10^{12}	1340	90	Quenched	3.5 (n)	1.4×10^{15}
Expt No. 7(a) VZ821	7157.0 (p)	1.9×10^{12}	1340	75	Quenched	2.5 (n)	1.9×10^{15}
Expt No. 7(b) VZ821	8183.0 (p)	2.2×10^{12}	1340	75	Slowly Cooled	3700 (n)	1.3×10^{12}

The diffusion rate and solubility limit of lithium in silicon have been reported in References 11 through 21. The dependence of the lithium solubility on the boron concentration in silicon (Ref. 13) was used to investigate the use of this element for boron compensation. A theoretical and experimental curve for lithium in doped silicon for the temperature range from 200 to 1200°C was used as the guideline of our first experiment (see Figure 11). A sharp maximum in the solubility curve around 650°C was reported (Ref. 13) when doping silicon with a boron concentration between 5×10^{17} to 1×10^{19} cm^{-3}.

Data for very low concentrations, in our case $< 3 \times 10^{12}$ cm^{-3}, were not available and the characteristics of the behavior of lithium at the silicon melting temperature had to be investigated.

Experiments to compensate residual boron impurities by formation of a Li-B complex were performed. Our initial study required producing a Si:Li master dopant for the compensation of boron during crystal growth. A simple procedure for doping silicon with lithium was developed by using the diffusion method used for magnesium.

Experiment No. 1

A sketch of the location of the silicon slices and blocks in the experiment is shown in Figure 12. A slice from single crystal VZ050, purified by six vacuum zone passes, with a resistivity of 5.58 kΩcm, was optically polished and used as the center slice. This slice and the inside surfaces of the cover slices were generously coated

SOLUBILITY OF Li IN Si VS TEMPERATURE

A   IS THE CURVE FOR LITHIUM IN UNDOPED SILICON

B   IS THE THEORETICAL CURVE FOR SOLUBILITY OF LITHIUM IN DOPED SILICON

CONCENTRATION OF Li ATOMS PER cm³

TEMPERATURE IN DEGREES C
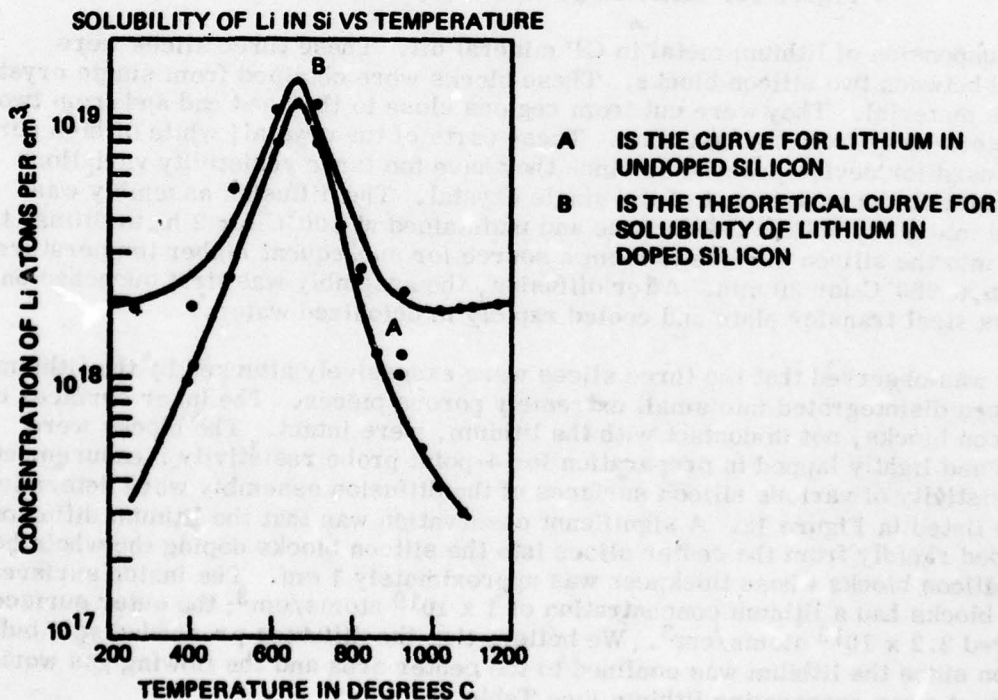
Figure 11. Solubility of Lithium in Silicon as a Function of Temperature
(Ref. 13)

31
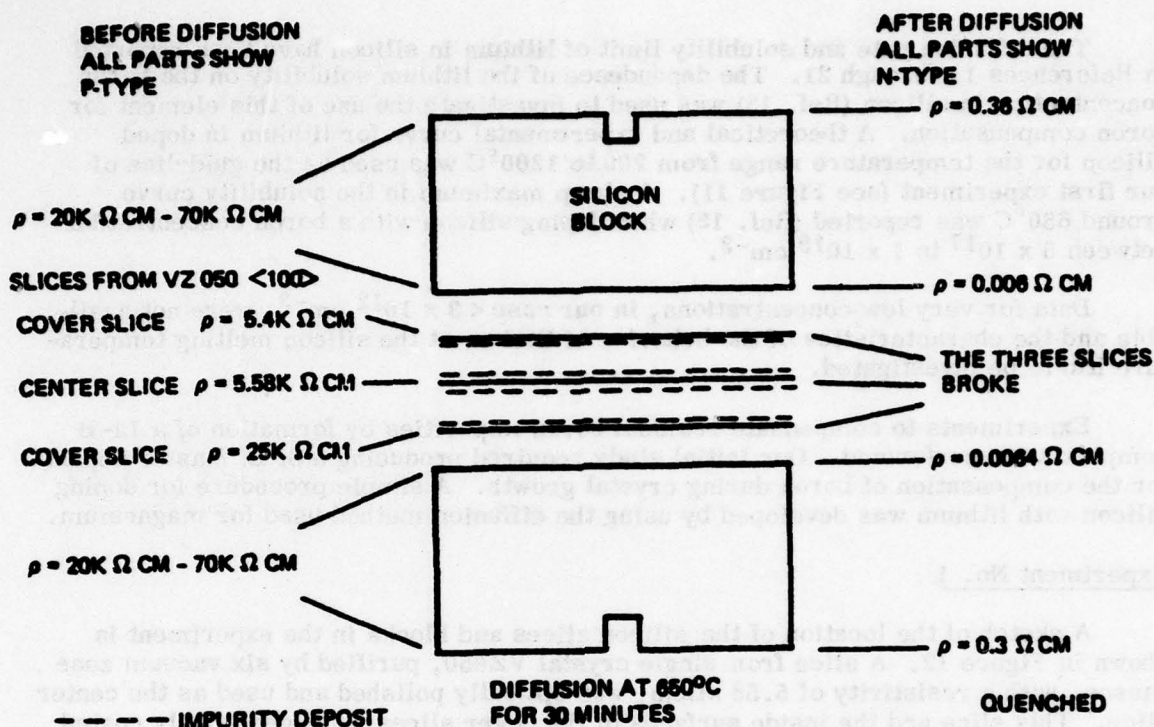
Figure 12. Lithium Diffusion Experiment No. 1

with a suspension of lithium metal in CP mineral oil. These three slices were fastened between two silicon blocks. These blocks were obtained from single crystal, six-pass material. They were cut from regions close to the seed end and from two centimeters away from the last zone. These parts of the crystal, while of high purity, are not used for device processing since they have too large resistivity variations compared with the center part of the single crystal. The diffusion assembly was inserted into a dry helium gas furnace and maintained at 200°C for 2 hr to diffuse the lithium into the silicon surface to form a source for subsequent higher temperature diffusion at 650°C for 30 min. After diffusion, the assembly was first quenched on a stainless steel transfer plate and cooled rapidly in deionized water.

It was observed that the three slices were excessively attacked by the lithium. The slices disintegrated into small extremely porous pieces. The inner surfaces of the silicon blocks, not in contact with the lithium, were intact. The blocks were cleaned and lightly lapped in preparation for 4-point probe resistivity measurements. The resistivity of various silicon surfaces of the diffusion assembly were determined and are listed in Figure 12. A significant observation was that the lithium diffusion proceeded rapidly from the center slices into the silicon blocks doping the whole bulk of the silicon blocks whose thickness was approximately 1 cm. The inside surfaces of both blocks had a lithium concentration of 1×10^{19} atoms/cm^3; the outer surfaces measured 2.2×10^{16} atoms/cm^3. We believe that the diffusion proceeded as a bulk diffusion since the lithium was confined to the center area and the flowing gas would have swept away evaporating lithium (see Table 6).

TABLE 6. DIFFUSION EXPERIMENTS Si:Li

Experiment No.	Silicon Wafer ρ (Ωcm)	Silicon Wafer $|N_B - N_P|$ (cm^{-3})	Silicon Block inside ρ (kΩcm)	Cooling Process Used	Diffused Slice ρ (Ωcm)	Diffused Slice N_{Li} (cm^{-3})	Silicon Block ρ (Ωcm) N_{Li} (cm^{-3})	Comments
1	5.50 k	2.6 x 10^{12}	20 - 70	Quenched	Slice Broke	Could not be obtained	0.008 / 10^{19}	Extensive amount of Lithium
2	10.25 k	1.4 x 10^{12}	20 - 70	Slowly Cooled	0.033	4.5 x 10^{17}	0.05 / 2.7 x 10^{17}	Lithium Some Excess $N_{Li} \gg N_B$
3	13.3 k	1.2 x 10^{12}	Reused from Exp. 2	Quenched	3.18	6 x 10^{15}	0.03 / 10^{17}	$N_{Li} \gg N_B$

ρ = Resistivity (Ωcm)

$|N_B - N_P|$ = Net Impurity Concentration (atoms/cm^3), $N_{boron} - N_{phosphorus}$

Experimental parameters held constant:
Silicon wafers from V208
Diffusion temperature 650°C
Diffusion time 30 min

In conclusion, lithium was observed to be a very fast diffuser in silicon confirming data in the literature ($D \simeq 10^{-5}$ cm^2/sec at 650°C) (Ref. 11). Deterioration of the slice was due to the excessive amount of lithium applied to the slice surfaces. It was clear from this first experiment that our lithium source was too high in concentration.

Experiment No. 2

The purpose of this experiment, a sketch of which is shown in Figure 13, was to study the lithium diffusion process with a cooling cycle which approximates that of the crystal growth process. Experiment No. 1 showed that a more dilute lithium source should be used to prevent disintegration of the slices. Using a new diffusion assembly, the center slice was coated with a thin film of the lithium suspension. The two cover slices were not coated. The diffusion experiment was performed again as in Experiment No. 1. The sample was not removed or quenched but was allowed to remain in the furnace where it cooled slowly.

The diffusion assembly was disassembled in deionized water. It was observed that the slices were intact; the center slice which had been coated with lithium was slightly pitted. The lithium concentrations for the three slices and end blocks were measured and are recorded in Figure 13. A lithium concentration of 4.5×10^{17} cm^{-3} was measured for the slowly cooled diffused wafer, establishing that a higher lithium content than needed for boron compensation remained in the silicon material. The outer surfaces of the silicon blocks did not type convert and measured high resistivity values correlating to exact compensation of the residual boron in this material.
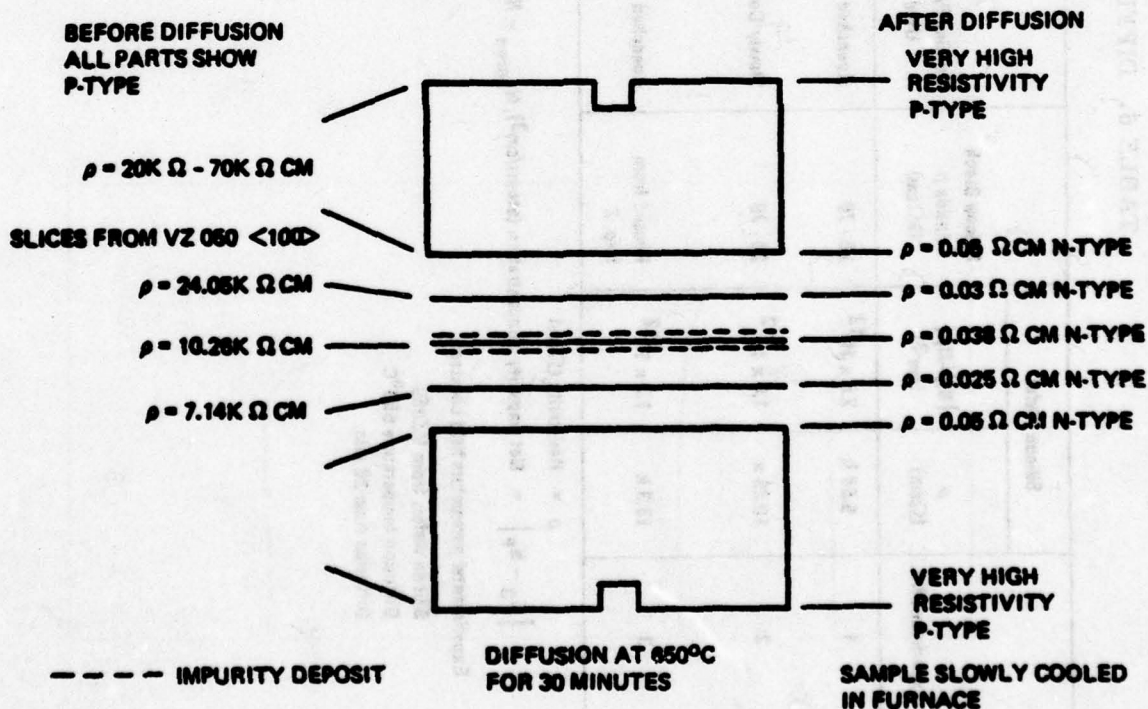
Figure 13. Lithium Diffusion Experiment No. 2

34

The conclusion of this study is that the LiB complexing mechanism is operable and could provide a means of compensation of boron over a large concentration range. The effectiveness of this procedure indicated that an improved method to add the lithium could be to use the lithium contaminated block as the diffusion source instead of a master doped alloy or an elemental lithium source on the surface of the slice. Experiment No. 3 explored this possibility.

Experiment No. 3

A sketch of Experiment No. 3 is shown in Figure 14. The two end blocks of the previous experiment, heavily contaminated with lithium, were used to enclose one slice of optically polished p-type silicon with a resistivity of 13.3 kΩcm. The diffusion assembly was again inserted in the furnace and maintained at 650°C for 30 min. To explore the amount of lithium transferred into the slice, the sample was quenched using the procedure of Experiment No. 1.

The data of Experiment 3 (listed in Figure 14) show that the silicon center slice type converted and a lithium concentration of 6×10^{15} cm^{-3}, corresponding to 3.18 Ωcm, was obtained. Changes in the lithium concentration on the silicon blocks could be verified on the inside surfaces only. This experiment shows that the silicon blocks which were heavily doped lend themselves as a lithium source, suggesting a simplified method to introduce this impurity into silicon bulk material as shown in Figure 15.

BEFORE DIFFUSION

VERY HIGH RESISTIVITY P-TYPE

N-TYPE 0.05 Ω CM

P-TYPE 13.3K Ω CM

N-TYPE 0.05 Ω CM

VERY HIGH RESISTIVITY P-TYPE

DIFFUSION AT 650°C AT 30 MINUTES

AFTER DIFFUSION

VERY HIGH RESISTIVITY P-TYPE

N-TYPE 0.09 Ω CM

3.18 Ω CM N-TYPE

N-TYPE 0.1 Ω CM

VERY HIGH RESISTIVITY P-TYPE

QUENCHED
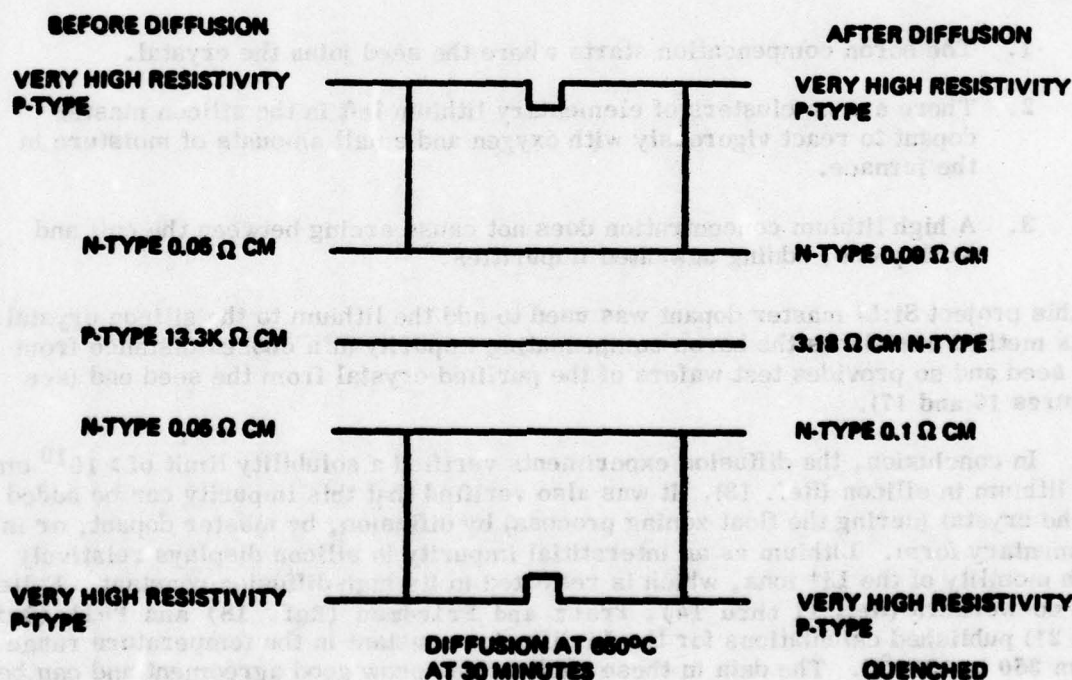
Figure 14. Lithium Diffusion Experiment No. 3

35
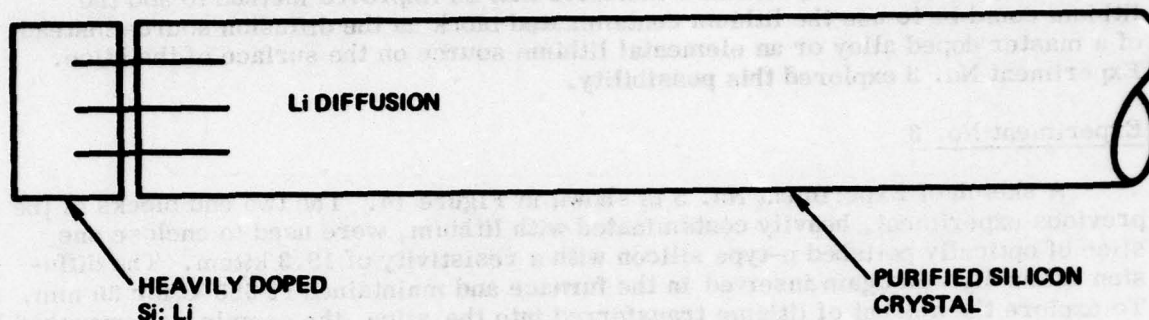
Figure 15. Diffusion of Lithium into Silicon Bulk

The purified silicon crystal in contact with a heavily doped Si:Li slab is held at an elevated temperature of 650°C for 30 min in a diffusion tube. Enough lithium will diffuse into the lower end to provide a sufficient number of impurity atoms to compensate the residual boron. It had to be assumed that the excess of lithium, not bound as a LiB complex, would evaporate to provide optimum compensation.

This method seems to provide some advantage over the master dopant method, because:

1. The boron compensation starts where the seed joins the crystal.

2. There are no clusters of elementary lithium left in the silicon master dopant to react vigorously with oxygen and small amounts of moisture in the furnace.

3. A high lithium concentration does not cause arcing between the coil and work piece, adding unwanted impurities.

In this project Si:Li master dopant was used to add the lithium to the silicon crystal. This method introduces the boron compensating impurity at a chosen distance from the seed and so provides test wafers of the purified crystal from the seed end (see Figures 16 and 17).

In conclusion, the diffusion experiments verified a solubility limit of $> 10^{19}$ cm^{-3} for lithium in silicon (Ref. 13). It was also verified that this impurity can be added to the crystal (during the float zoning process) by diffusion, by master dopant, or in elementary form. Lithium as an interstitial impurity in silicon displays relatively high mobility of the Li$^+$ ions, which is reflected in its high diffusion constant. Fuller and co-workers (Ref. 11 thru 14), Pratt and Friedman (Ref. 18) and Pell (Ref. 20 and 21) published calculations for the Li diffusion constant in the temperature range from 360 to 1350°C. The data in these publications show good agreement and can be represented by the expression:

$$D_{Li} = (2.5 \pm 0.2) \; 10^{-3} \exp (15400 \pm 235)/RT \tag{17}$$
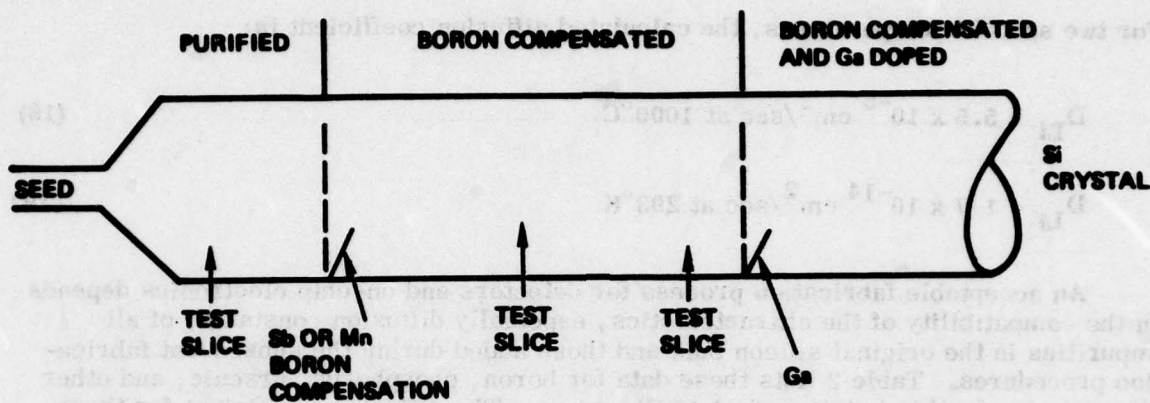
Figure 16. Boron Compensation with Substitutional Impurities
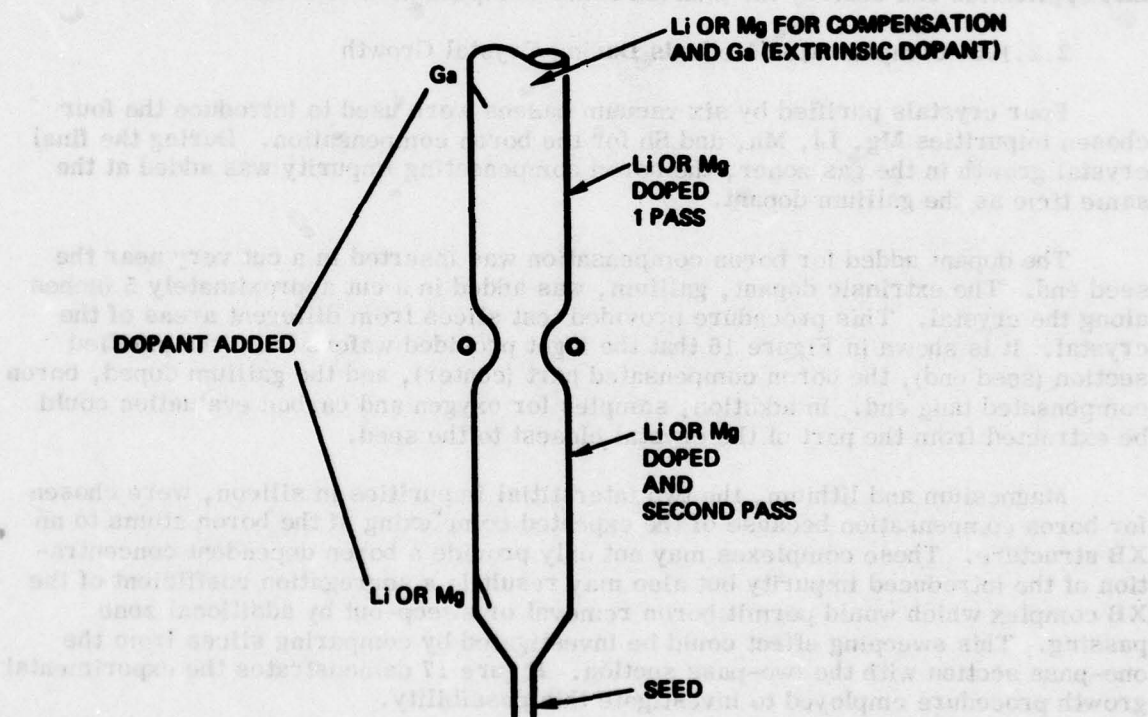
Figure 17. Crystal with Boron Compensation by Li or Mg

For two specific temperatures, the calculated diffusion coefficient is:

$$D_{Li} = 5.5 \times 10^{-6} \text{ cm}^2/\text{sec at } 1000°C \tag{18}$$

$$D_{Li} = 1.7 \times 10^{-14} \text{ cm}^2/\text{sec at } 293°K \tag{19}$$

An acceptable fabrication process for detectors and on-chip electronics depends on the compatibility of the characteristics, especially diffusion constants, of all impurities in the original silicon bulk and those added during the subsequent fabrication procedures. Table 2 lists these data for boron, phosphorus, arsenic, and other elements involved in building the LADIR arrays. The diffusion coefficient for these impurities at 1000°C, a conventional processing temperature, is on the order of 10^{-12} to 10^{-14} cm^2/sec, a factor of 10^8 lower than that for lithium (Eq 18). As an illustration of this problem, Hall data (Figure 23) indicate out-diffusion during contact application can destroy the planned donor compensation of boron.

2.2.1.5 Compensation Methods During Crystal Growth

Four crystals purified by six vacuum passes were used to introduce the four chosen impurities Mg, Li, Mn, and Sb for the boron compensation. During the final crystal growth in the gas zoner, the boron compensating impurity was added at the same time as the gallium dopant.

The dopant added for boron compensation was inserted in a cut very near the seed end. The extrinsic dopant, gallium, was added in a cut approximately 5 inches along the crystal. This procedure provided test slices from different areas of the crystal. It is shown in Figure 16 that the ingot provided wafers from the purified section (seed end), the boron compensated part (center), and the gallium doped, boron compensated tang end. In addition, samples for oxygen and carbon evaluation could be extracted from the part of the crystal closest to the seed.

Magnesium and lithium, the two interstitial impurities in silicon, were chosen for boron compensation because of the expected complexing of the boron atoms to an XB structure. These complexes may not only provide a boron dependent concentration of the introduced impurity but also may result in a segregation coefficient of the XB complex which would permit boron removal or sweep-out by additional zone passing. This sweeping effect could be investigated by comparing slices from the one-pass section with the two-pass section. Figure 17 demonstrates the experimental growth procedure employed to investigate this possibility.

2.2.1.6 Boron Compensation by Nuclear Transmutation

Nuclear transmutation doping promises several advantages over conventional doping techniques for producing the desired compensating donor concentration. The nuclear reaction of the transmutation process is based on the conversion of the isotope ^{30}Si to ^{31}P, the desired donor impurity. This process is dose dependent, slow enough to provide accurate control of the dopant concentration, and the created phosphorus atoms are distributed uniformly throughout the lattice.

The nuclear reactions of interest for this transmutation doping are as follows:

<div align="right">

Reaction

</div>

$$^{28}Si \, (n, \gamma) \, ^{29}Si \tag{1}$$

$$^{29}Si \, (n, \gamma) \, ^{30}Si \tag{2}$$

$$^{30}Si \, (n, \gamma) \, ^{31}Si \rightarrow \, ^{31}P + \beta^{-}; T_{1/2} = 2.62h \tag{3}$$

$$^{31}P \, (n, \gamma) \, ^{32}P \rightarrow \, ^{32}S + \beta^{-}; T_{1/2} = 14.3d \tag{4}$$
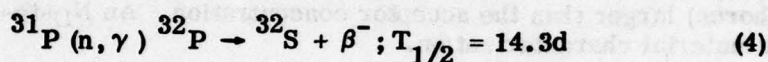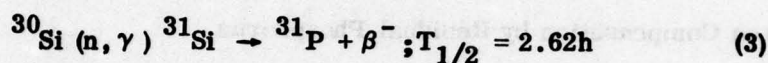
The natural abundance, thermal neutron absorption cross section (n, γ) and half-life of the relevant isotopes of silicon and phosphorus are listed in Table 7. The production rate of the desired dopant can be calculated from these data. Since the total number of Si atoms/cm^3 is 4.996×10^{22} atoms/cm^3, the density of ^{30}Si isotopes is

$$N(^{30}Si) = 0.0305 \, N(Si) = 1.524 \times 10^{21} \text{ atoms/cm}^3.$$

The theoretical production rate for phosphorus is then found from the expression:

$$\frac{d\left[^{31}P\right]}{d\Phi} = N(^{30}Si) \, \sigma \left[^{30}Si \, (n, \gamma) \, ^{31}Si\right] = 1.676 \times 10^{-4} \, ^{31}P \text{ atoms/cm}^3/n/cm^2$$

TABLE 7. NUCLEAR DATA

Natural Abundance (%)	Isotope	$\sigma(n, \gamma)$	$T_{1/2}$
92.27	^{28}Si	0.08 ± 0.03 b	Stable
4.68	^{29}Si	0.28 ± 0.09 b	Stable
3.05	^{30}Si	0.11 ± 0.01 b	2.62h
100	^{31}p	0.10 ± 0.02 b	14.3d

Atomic Weight: Si = 28.086, N(Si) = 4.996 x 10^{22} atoms/cm^3
Density: Si = 2.33 gm/cm^3

where ϕ is the irradiation fluence of thermal neutrons (n/cm^2). Table 8 lists the theoretical production of donors in Si in several useful sets of units.

The transmutation dopant techniques were investigated by MURR using sample material from silicon single crystals of different sources. Rockwell supplied two purified ingots, VZ072 and VZ083. The identification data are listed in Table 9 and the wafer resistivity topographies are shown in Figures 18 and 19, evidencing the uniform boron distribution in this material. MURR's results indicated that the trans-mutation doping method could be applied to compensate low boron concentrations. The transmutation doping technique with intrinsic silicon was then applied to gallium doped silicon with the results described in Section 2.4.

2.2.1.7 Boron Compensation by Residual Phosphorus

High quality polycrystalline silicon is generally supplied with a donor concentra-tion (mainly phosphorus) larger than the acceptor concentration. An N_D-to-N_A ratio of ≥ 10 is the usual material characterization.

Wherever this n-type polysilicon is used to fabricate extrinsic silicon by doping with a p-type impurity other than boron, the phosphorus concentration is reduced by the sweep-out and evaporation effects of the vacuum float zoning process. The phosphorus reduction per vacuum pass follows the calculation on page 16, and the number of passes to retain a boron concentration "plus" level follows the graph of Figure 6. The silicon crystal with low conductivity is then further processed by doping to the desired gallium concentration.

2.2.2 Gallium Doping

Extensive work has been done at Rockwell on gallium doped silicon. The accumulated data were compared to the recent test data and were then used as an aid in evaluating the recommended growth process for the gallium doped LADIR material.

Figure 20 illustrates the resistance of gallium doped silicon samples versus reciprocal temperature. The data presented show the effect of varying the gallium concentration between 3.0×10^{16} and 1.5×10^{17} cm^{-3} over a temperature range from 7.3 to 50°K. The change in slope of log R versus reciprocal temperature for Si:Ga

TABLE 8. ^{31}P THEORETICAL PRODUCTION RATES

Production Rate (K)	Units
1.676×10^{-4}	P atoms/cm^3 per n/cm^2
1.676×10^{14}	P atoms/cm^3 per 10^{18} n/cm^2
3.355	ppb per 10^{18} n/cm^2

40

TABLE 9. IDENTIFICATION DATA FOR PURIFIED CRYSTALS, VZ072 AND VZ083

Dow Corning Polysilicon Data	Rockwell Data	
	Number of Vacuum Passes	Residual Impurities After Purification*
VZ072 N_A = 0.0075 ppb $< 0.5 \times 10^{12}$ cm^{-3} N_D = 0.05 ppb $= 2.5 \times 10^{12}$ cm^{-3}	6	$N_A - N_D = 5 \times 10^{12}$ cm^{-3}
VZ083 N_A = 0.075 ppb $< 0.5 \times 10^{12}$ cm^{-3} N_D = 0.05 ppb $= 2.5 \times 10^{12}$ cm^{-3}	4	$N_A - N_D = 10^{12}$ cm^{-3}

*Measured with 4-point probe at RT.

near 25°K is due to conduction in the gallium impurity band. The secondary slope and the temperature at which it appears depend strongly on the gallium impurity concentration and also on the concentration of the compensating impurity in the material. For the gallium concentration of 1.5×10^{17} cm^{-3} the secondary slope is about 0.007ev. The calculation of the secondary slope can be approached using Ref. 22, page 113, Eq 4.

Spectral responsivity curves (such as shown in Figure 21) provide a valuable tool for the study of the effects of impurity concentration and the detector geometry. The responsivity R is proportional to the product $\lambda\eta$ (see Eq 2). The wavelength dependence of the IR absorption cross section σ_A for a specific impurity produces the major wavelength variation of R_λ.

22. Mott, N.F. and Twose, W.D., "Theory of Impurity Conduction," Advances in Physics, Vol. 10, p 107, 1961.
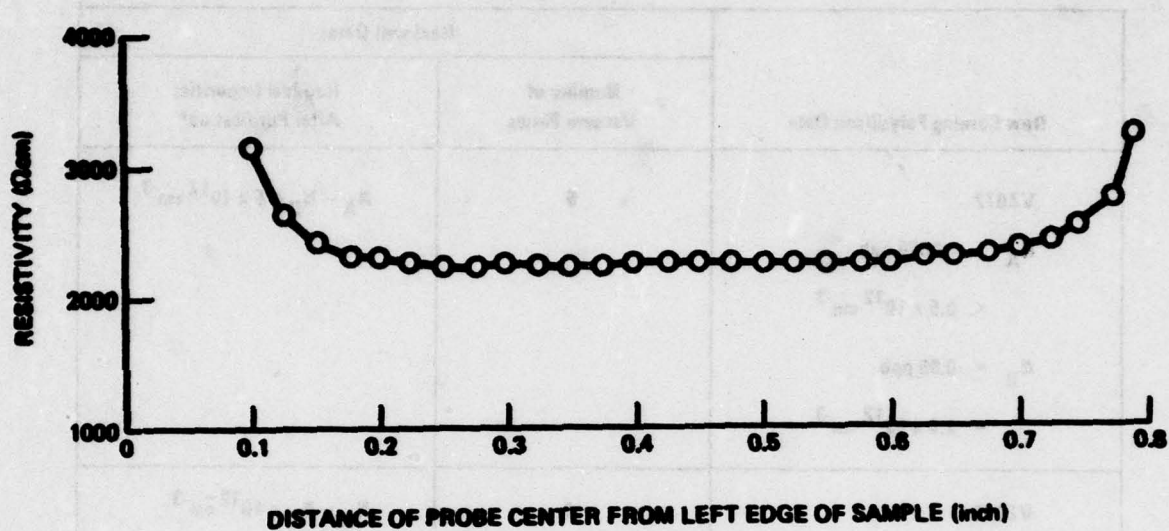
Figure 18. Radial Resistivity of VZ072-1, Top
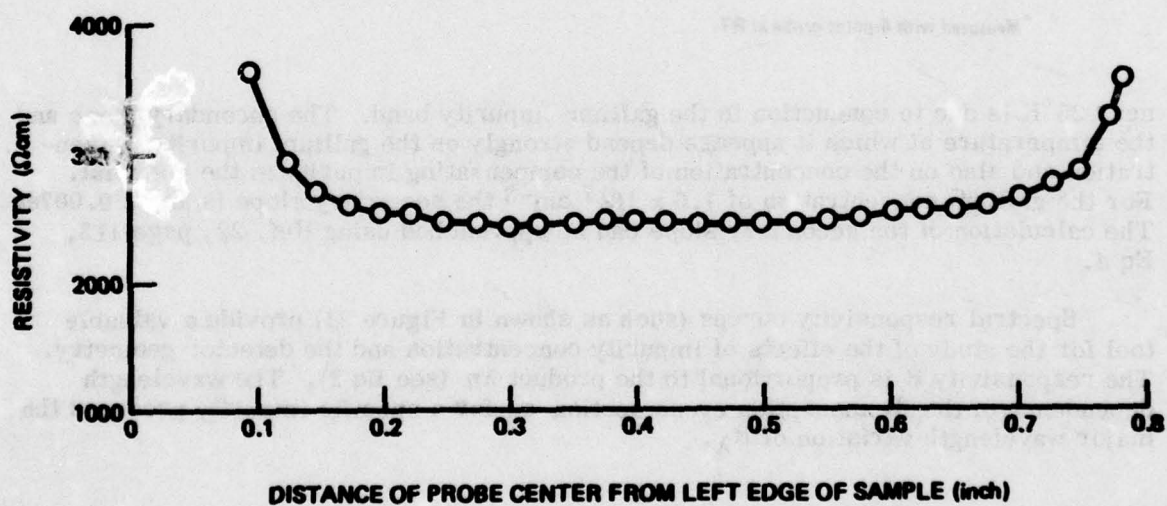
Figure 19. Radial Resistivity of VZ072-5, Bottom

42
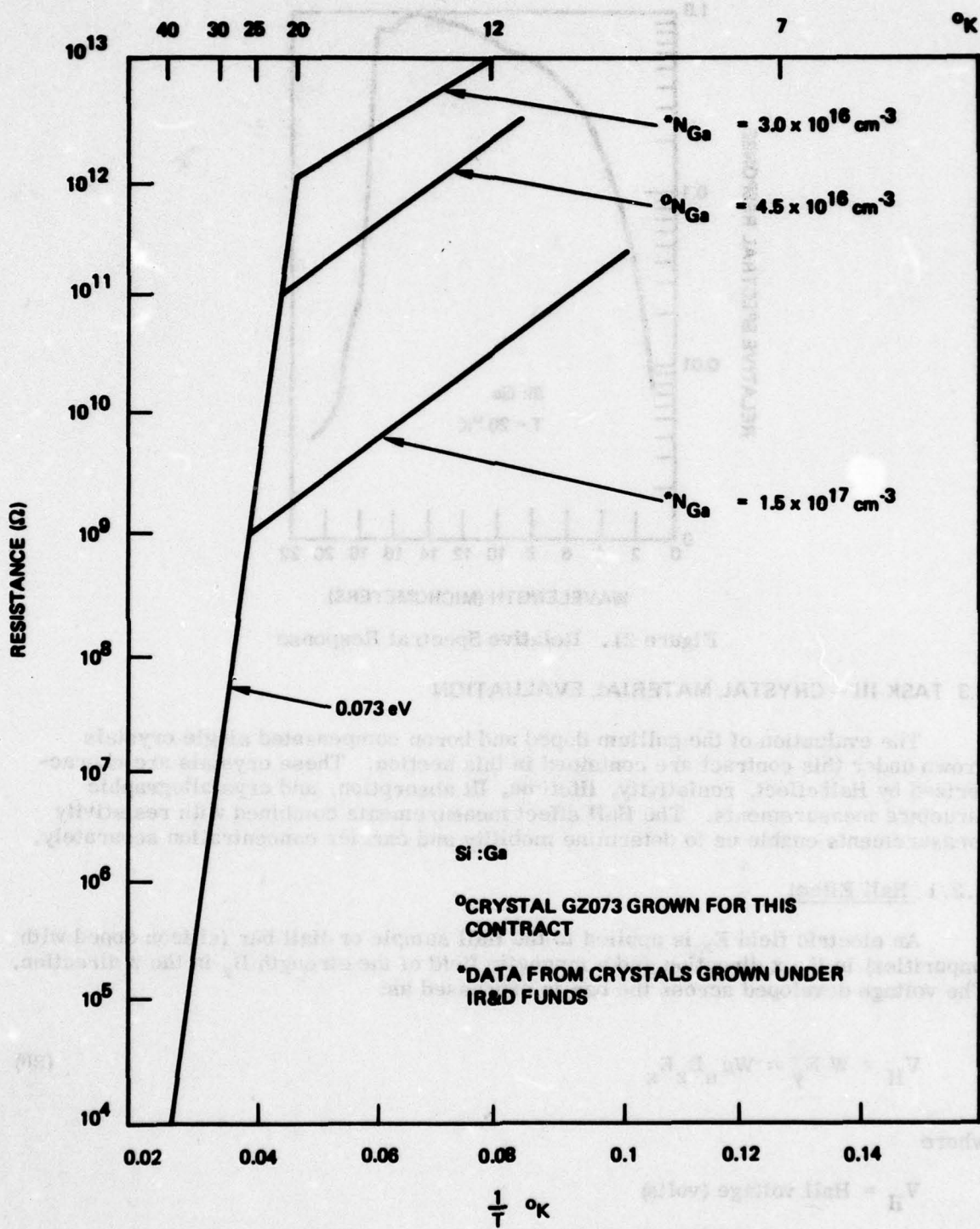
Figure 20. Resistance vs Reciprocal Temperature for Si:Ga
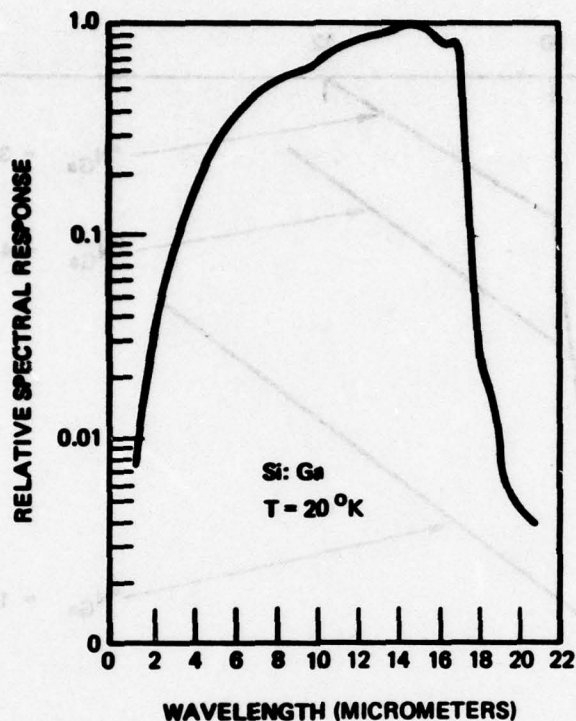
Figure 21. Relative Spectral Response

2.3 TASK III – CRYSTAL MATERIAL EVALUATION

The evaluation of the gallium doped and boron compensated single crystals grown under this contract are contained in this section. These crystals are characterized by Hall effect, resistivity, lifetime, IR absorption, and crystallographic structure measurements. The Hall effect measurements combined with resistivity measurements enable us to determine mobility and carrier concentration separately.

2.3.1 Hall Effect

An electric field E_x is applied to the Hall sample or Hall bar (silicon doped with impurities) in the x direction and a magnetic field of the strength B_z in the z direction. The voltage developed across the bar is expressed as:

$$V_H = W E_y = W\mu_n B_z E_x \tag{20}$$

where

V_H = Hall voltage (volts)

W = Width of the Hall bar (cm)

44

B_z = Strength of the magnetic field (gauss)

E_x = Strength of the electric field (volt/cm) (Ref. 23).

Expressing Eq (20) in terms of the Hall constant gives

$$V_H = I_x B_z \frac{R_H}{t} \tag{21}$$

where

    I_x is the current flowing through the bar

    R_H is the Hall constant

    t   is the thickness of the Hall bar (cm).

The Hall constant is expressed as

$$R_H = \frac{1}{qn} \text{ (cm}^3\text{/coulomb)} \tag{22}$$

where

    q   is the electronic charge

    n   is the free electron density.

The carrier mobility (μ_p or μ_n) can be obtained from the Hall measurement by

$$\sigma_{p \text{ or } n} = qn\mu_{p \text{ or } n} \ (\Omega \text{cm})^{-1} \tag{23}$$

or

$$\mu = \sigma R_H \text{ (cm}^2\text{/volt sec)} \tag{24}$$

The Hall measurement vs temperature gives the carrier concentration as a function of the temperature which can be used to determine thermal activation energies in the semiconductor.

---

23.   Matare, H.F., "Electronic Measurements of Semiconductor Material Parameters," North American Aviation, Anaheim, CA, 1967.

The mobility is the velocity of a charge per unit electric field and is strongly dependent upon the purity of the material, temperature, and the crystallographic quality of the crystal. In a perfect undoped semiconductor crystal, the charge carrier mobility would only depend upon the lattice vibrations of the crystal. As the temperature increases, the excursions of the atoms from their equilibrium positions will increase and the free path and mobility will become shorter (Réf. 23 through 27). The departures from perfection caused by the presence of vacant lattice sites, atoms in interstitial positions, ionized atoms, dislocations, and the surfaces of the crystal will also have strong effects on mobility particularly at the low temperatures of importance for detectors.

In the early stages of this program, impurity contamination during the vacuum float zoning was apparent (see Table 3). Hall Effect, resistivity and IR absorption measurements were performed to monitor the silicon purification process. Contamination by boron and other impurities was verified by these tests. Subsequently, several improvements were made in the vacuum system of the vacuum float zoner. The purification process now provides single crystals with a residual impurity concentration of less than 2×10^{12} boron atoms per cm^3 and a calculated donor concentration of less than 10^{11} per cm^3.

In order to conduct Hall measurements at low temperature some special sample preparative techniques had to be developed. An extensive analysis of Ref. 28 and 29 yielded the four methods (listed below) for applying ohmic contacts onto high purity silicon:

1. Aluminum evaporation approximately 1μ thick sintered at 450°C for 30 min. Measurements showed 5 to 20 kΩ resistance independent of the sample resistance.

2. Laser drive-in alloying of the aluminum and gold. This method did not improve the linearity of the impedance.

3. Capacitance discharge of aluminum or indium into the silicon. This method probably breaks the SiO_2 layer between the silicon and the metal and reduces the impedance providing linear voltage current characteristics.

4. Ion implantation of boron to provide a degenerate contact (approximately $10^{19}/cm^3$) followed by annealing at 425°C, using indium and spring contacts (Ref. 30).

24. Logan, R.A. and Peters, A.J., "Impurity Effects Upon Mobility in Silicon," J. Appl. Phys., Vol. 31/1, p 122, 1960.

25. Debye, P.P., "Electrical Properties of N-Type Germanium," Physical Review, Vol. 93/4, p 693, 1954.

26. Morin, F.J. and Maita, J.P., "Electrical Properties of Silicon Containing Arsenic and Boron," Physical Review, Vol. 96/1, 1954.

27. Conwell, E.M., "Properties of Silicon and Germanium: II," Proceedings of IRE, p 1281, June 1958.

28. Messier, J. and Flores, J.M., "Temperature Dependence of Hall Mobility and μ_H/μ_D for Si," J. Phys. Chem. Solids, Vol. 24, p 1539, 1963.

The third method gave the best results, permitting measurements down to 30°K, and was applied on test samples.

Figure 22 presents the Hall mobility versus temperature of purified undoped float zoned crystals. The six pass crystals to follow the theoretical mobility curve for p-type silicon determined by lattice scattering only. (Ref. 24.) Crystal VZ053 with one vacuum pass shows the mobility reduction due to residual ionized impurities, at temperatures below 100°K.

▲ P-TYPE SILICON WHERE LATTICE SCATTERING IS THE DOMINANT MECHANISM (EXPERIMENTAL)[24]

● VZ059 6 PASS CRYSTAL

✕ VZ083 6 PASS CRYSTAL

■ VZ052 6 PASS CRYSTAL

○ VZ053 1 PASS CRYSTAL (IR&D)
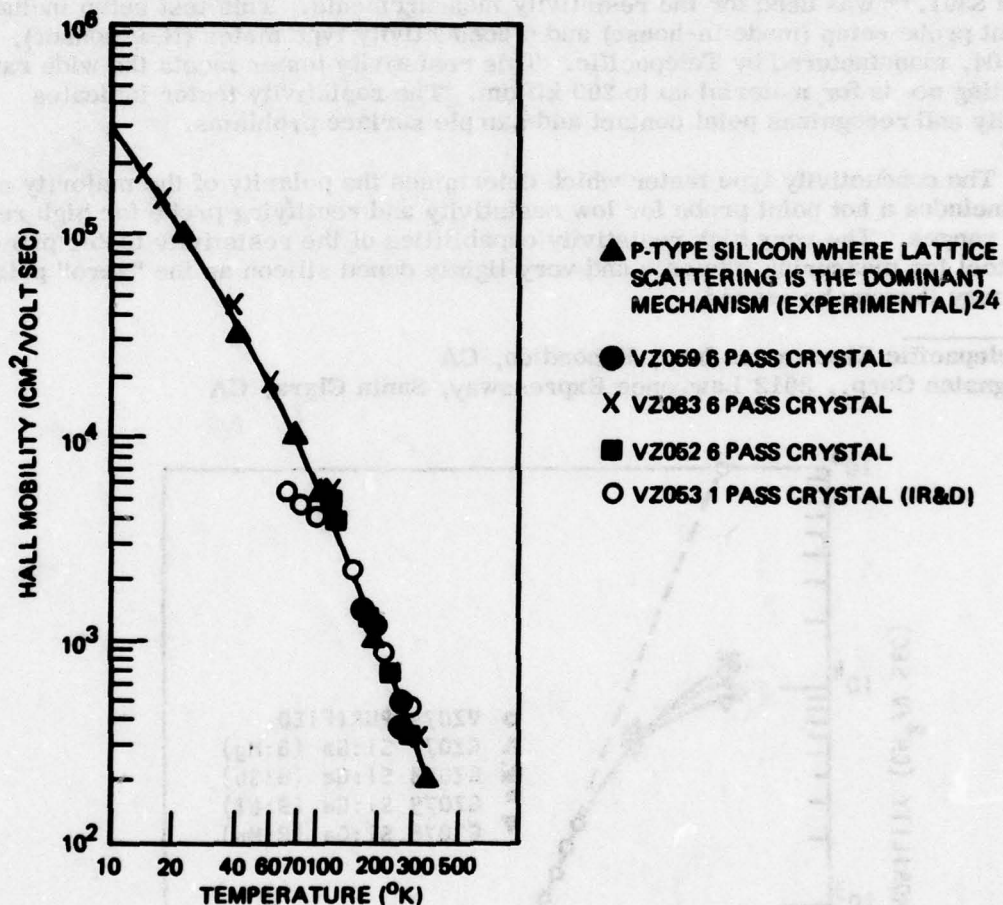
Figure 22. Mobility vs Temperature for Purified Crystals

29. Rideout, V.L., "A Review of the Theory and Technology for Ohmic Contacts to Group III-V Compound Semiconductors," Solid State Electronics, Vol. 18, pp 541-550, 1975.

30. Gibbons, James F., "Ion Implantation in Semiconductors," Proceedings of the IEEE, Vol. 60, p 1062, 1972.

Figure 23 shows mobility versus temperature for Si:Ga material samples grown with various n-type (compensating) impurities. All four doped samples show a mobility reduction at low temperatures compared to the purified samples in Figure 22. Ionized impurity scattering causes these reduced mobilities (Ref. 24). The n-type impurity concentrations in the individual crystals are listed in Table 10, column ③.

2.3.2 Resistivity Measurements

A Telepacific resistivity tester, model TPP-17,* with a Signaton 4-point probe, model S301,** was used for the resistivity measurements. This test setup includes a 2-point probe setup (made in-house) and a conductivity type meter (N-P sensor), model TPP-04, manufactured by Telepacific. This resistivity tester meets the wide range of testing needs for material up to 200 kΩ cm. The resistivity tester indicates polarity and recognizes point contact and sample surface problems.

The conductivity type meter which determines the polarity of the majority carrier includes a hot point probe for low resistivity and rectifying probe for high resistivity ranges. The very high resistivity capabilities of the resistivity tester provide a good tool for measuring intrinsic and very lightly doped silicon as the "zero" polarity point may thereby be sensed.

*Telepacific Electronics Inc., Escondido, CA
**Signaton Corp., 3012 Lawrence Expressway, Santa Clara, CA
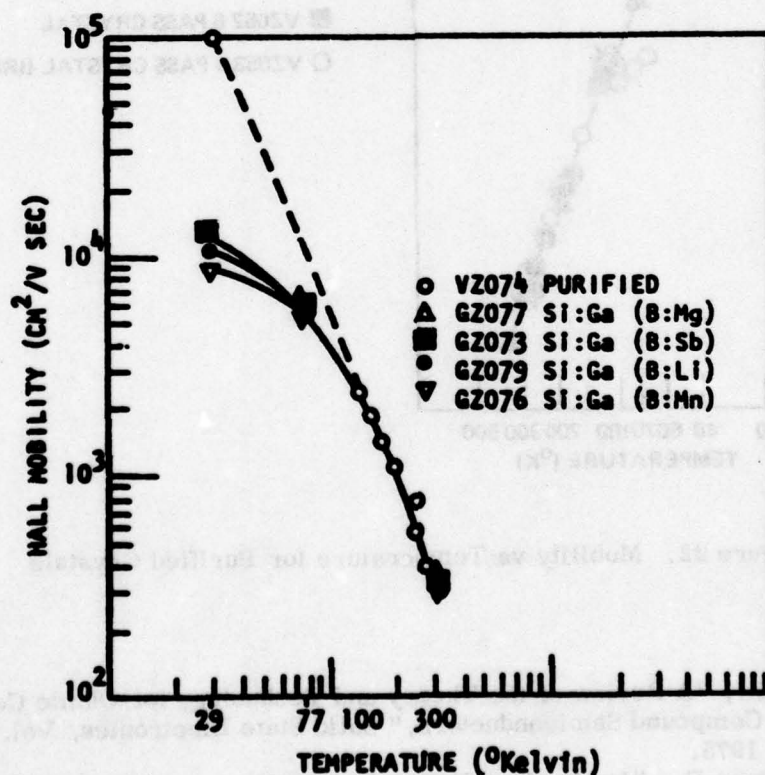
Figure 23. Mobility vs Temperature for Doped Crystals

48

TABLE 10. WORK SUMMARY DATA

	Purified Crystal		Compensated Crystal	For IR by Kelthane Method (Fourier Spectrophotometer)			Relative Spectral Response	Gallium Doped Crystal — Hall Data at RT			
Crystal	$N_A - N_D$ (cm-3)	Lifetime at RT (μsec)	$N_D - N_A$ (cm-3)	IR Radiation Only Mg Uncompensated (cm-3)	IR Plus Band Gap Light Mg Total (cm-3)	Calculated Mg Compensated (cm-3)	Present at 31.2 μ	$(N_A - N_D)$ 4 Pt Probe (cm-3)	$(N_A - N_D)$ Hall (cm-3)	Resistivity ohm-cm at RT
Q2072 Si:Ga (B:Ga)	4×10^{12} V2064	140	Sb, added by master dopant	2.6×10^{12}	3.6×10^{12}	1.5×10^{12}	2.68	4.5×10^{16}	4.46×10^{16}	287
Q2076 Si:Ga (B:Ga)	1.5×10^{12} V2076	280	Sb 1.2×10^{12}	Below Detection 0.3×10^{12}	≈ 1.5×10^{12}	1.2×10^{12}	0.88	4.5×10^{16}	4.46×10^{16}	288
Q2077 Si:Ga (B:Mg)	2×10^{12} V2073	180	Mg** p-Type 2.6×10^{12} Two Pass	1.5×10^{12} / 1.1×10^{13}	B:Mg IR Data Questionable 2.5×10^{13} / 1.4×10^{13}	1×10^{12} / 3.8×10^{12}	0.64	4.5×10^{16}	4.46×10^{16}	288
Q2070 Si:Ga (B:Li)	1.4×10^{12} V2076	210	Li 0 no Pass 6.1×10^{13} / Two Pass 2.61×10^{12}	1.4×10^{12} / 1.9×10^{12}	1.4×10^{12} / 1.9×10^{12}	Compensation not Detected by IR Technique	0.64	4.5×10^{16}	4.46×10^{16}	288

**Fig. 33, page 62
**Crystal growth program for interstitial impurities (See Fig. 17, page 37
***Percent of Spectral Response for boron (31.3 μm) relate to gallium (15 μm) concentration peak for $N_{Ga} = 4.5 \times 10^{16}$ cm-3 as 100%.

N_A = Acceptor Concentration
N_D = Donor Concentration
N_B = Boron Concentration
RT = Natural at room temperature

The thickness of the silicon slice, which enters into the calculation of wafer resistivity, is monitored by a wafer thickness gage ADE model 6033.* This setup works on the capacitance principle providing a noncontact method for wafer thickness identification.

2.3.2.1 Four-Point Probe - Theory

The most straightforward method of determining resistivity is to measure the resistance R (in ohms) of a sample with uniform cross section A (in square centimeters) and length L (in centimeters), either by applying a voltage to the sample and measuring the resultant current or applying a current and measuring the resultant voltage.

In making such measurements on a semiconductor sample, it is imperative that the contact resistance at the end of the sample is negligible compared with the resistance of the sample. The process of applying good contacts is time consuming and often leads to incorrect measurements. Using the 4-point probe method to take resistivity measurements eliminates these problems. In this method, four equally spaced pressure contacts are so arranged that the two outer contacts deliver a current through the sample while the two inner contacts measure the voltage developed across the semiconductor path used for the current flow.

The resistivity ρ, expressed in terms of ΔV, the voltage sensed between the two inner probe points spaced at a distance s, is expressed as:

$$\rho = \frac{2\pi S \Delta V}{I} \tag{25}$$

Most 4-point probe test stations have the value of I, the current through the outer points, adjusted so that the instrument reads the ΔV (in mv) directly in $|\Omega cm|$ after correct calibration. For example, our tester utilizes a distance s between probes of 0.0625 inch and a current through the sample of 10 mA.

2.3.2.2 Bulk Measurements

The grown single crystals undergo conductivity and resistivity measurements. Using the N-P sensor and four-point probes for resistivity values near the intrinsic range, the surface condition of the crystal is critical to the measurements. Four-point probe measurements taken at the ingot surface, may not reflect the characteristics of the bulk silicon crystal. The method developed to achieve reliable results is shown in Figure 24.

---

*ADE Corp., 127 Coolidge Hill Rd., Watertown, MA

0.8–1 CM WIDE LAPPED STRIP

POSITION OF FOUR POINTS FOR RESISTIVITY MEASUREMENTS
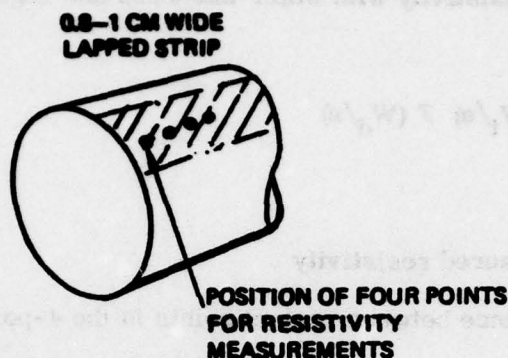
Figure 24. Four-Point Probe Position on Purified Ingot

A 0.8 to 1 cm wide strip is lapped along the crystal. The final grit used should be 5 μ. After lapping, the crystal is washed in a surface cleaning solution and rinsed in DI water. The ASTM Standards Book, Volume 43 (F43 and F84)* was consulted for additional suggestions on surface preparation. During the measurements, the 4-point probe is placed in the center of the strip and the data are taken along the boule length.

An additional test slice taken from the seed end of the ingot can be used to correlate to the bulk data. In this regard, the importance of using a seed with as high a purity as the bulk material should be mentioned again. It avoids contamination of the ingot at the seed end and inconclusive data from the test slice.

2.3.2.3 Resistivity Measurements of Sample Slices

When 4-point probe resistivity measurements are made on small specimens such as crystal slices, the nonconducting surface boundaries of the specimen modify the current paths introduced by the current probes. The two center probes (the voltage probes) see these changes as additional current sources. The result is an increased potential at the voltage probes and an erroneously high measurement of resistivity. The effect of crystal boundaries has to be included as a correction factor whenever a boundary is within a distance of about two and one-half times the dimensions between the 4-point probes (Ref. 23).

For the case of resistivity with wafer thickness correction only, the relationship between the resistivity of the single crystal material, ρ, to the measured resistivity ρ_0 is as follows:

$$\rho = \rho_0 \, 2 \pi \, s \, F \, (W/s) \tag{26}$$

---

*ASTM Standards, American Society for Testing and Materials, 1916 Race St., Philadelphia, PA.

51

And, for the case of resistivity with wafer thickness and edge boundary correction, the relationship is

$$\rho = \rho_o \, 2\pi \, s \, F\,(W_t/s) \, F\,(W_d/s) \tag{27}$$

where

ρ_o is the measured resistivity

s   is the distance between contact points in the 4-point probe

W_d is the distance of the 4-point probe from edge boundary

W_t is the thickness of the sample

The function F (W/s) is plotted in Figure 25 for all cases of practical importance.

Data previously shown in Figures 7 and 8 used the correction factor shown in Figure 25. The data for various sections of the crystals evaluated in this program are listed in Table 10, columns ②, ③, and ⑥.
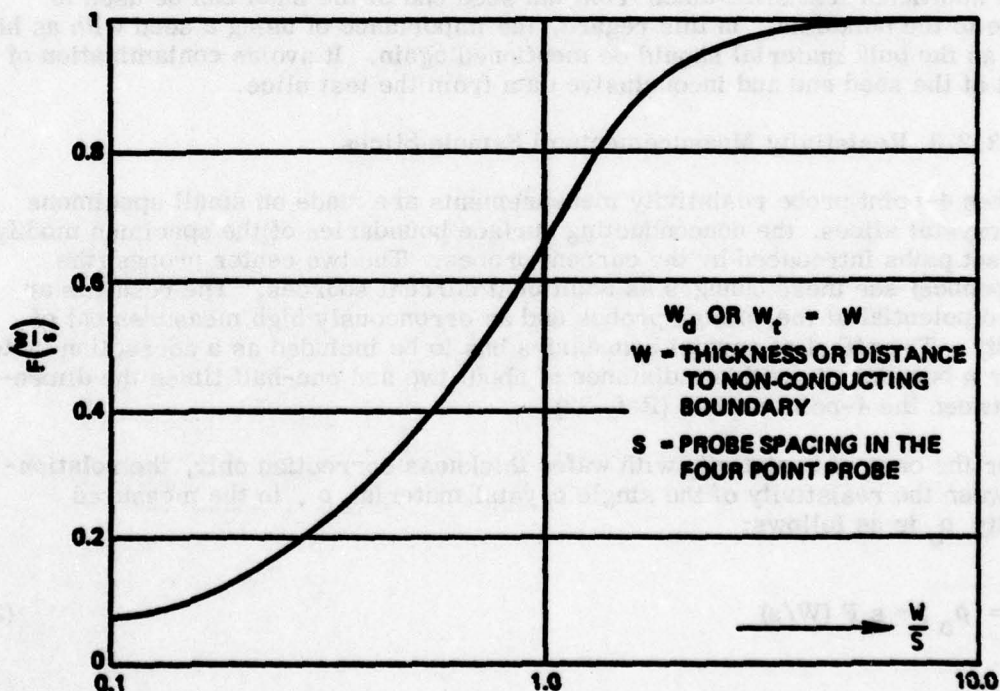
Figure 25. Correction Factor Applied in Resistivity
Measurements of Silicon Samples

52

2.3.3 Lifetime

This section describes the procedures and techniques used to measure the recombination time of compensated, uncompensated, and doped high purity silicon. (Ref. 31 and 32.) The photoconductive decay measurement method was employed and all measurements were made at room temperature. The light source used to generate excess carriers was either a TEA CO_2 laser or a Xenon lamp. Boules, as grown, or filaments, cut from a boule, can be accommodated by the test hardware.

Because of the great variation in the resistivity of the test specimens, two different test configurations were required to make the measurements. Figure 26 shows the test circuitry to be used on the doped material, while Figure 27 shows the test circuit used for the lifetime measurements on the high purity material.

31. ASTM Standards, F 28-66, Electronics, Measuring the Minority-Carrier Lifetime in Bulk Germanium and Silicon, Part 43.
32. Keller, Wolfgang, "Messung der Traegerlebensdauer in Siliziumkristallen mit Hochfrequenz," Zeitschrift fur Angewandte Physik, Vol. II, September 1959.
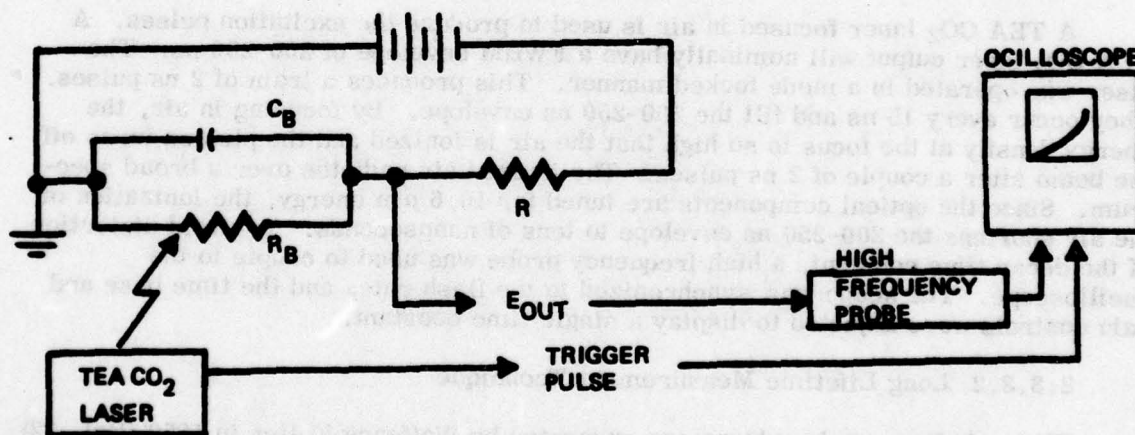
Figure 26. Simplified Schematic for Photoconductive Decay Lifetime Measurements of Doped Silicon
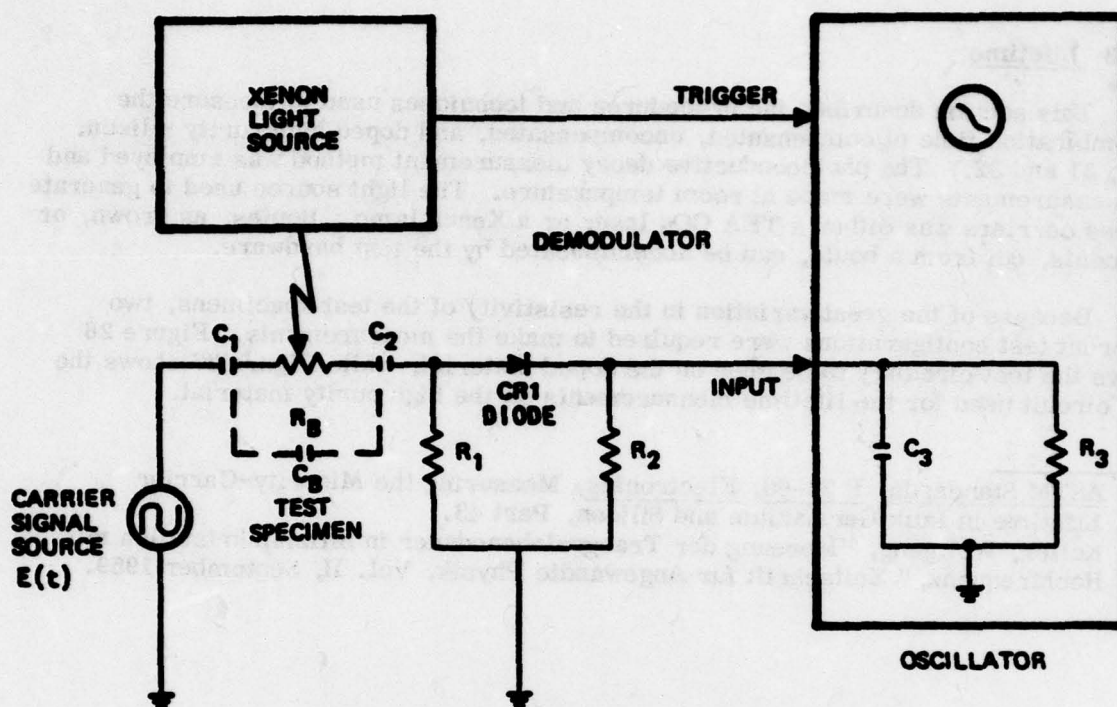
Figure 27. Simplified Schematic for High Purity Photoconductive Decay Lifetime Measurements

2.3.3.1 Short Lifetime Measurement Technique

A TEA CO_2 laser focused in air is used to produce the excitation pulses. A TEA CO_2 laser output will nominally have a FWHM envelope of 200-250 ns. The laser was operated in a mode locked manner. This produces a train of 2 ns pulses. They occur every 15 ns and fill the 200-250 ns envelope. By focusing in air, the energy density at the focus is so high that the air is ionized and the plasma turns off the beam after a couple of 2 ns pulses. The ionized air radiates over a broad spectrum. Since the optical components are tuned for 10.6 μm energy, the ionization of the air shortens the 200-250 ns envelope to tens of nanoseconds. To avoid distortion of the decay time constant, a high frequency probe was used to couple to the oscilloscope. The scope was synchronized to the flash rate, and the time base and gain controls were adjusted to display a single time constant.

2.3.3.2 Long Lifetime Measurement Technique

The technique employed was one suggested by Wolfgang Keller in 1959 (Ref. 32). Basically, the scheme involves detecting and displaying the decay of a 35 MHz carrier frequency modulated by the generation and recombination of excess carriers (introduced by photoexcitation) in the test specimen. As shown in Figure 27, a high frequency current is capacitatively coupled to the ingot. The advantage of this method is that the test sample does not require the application of contacts and the ingot can be measured while wrapped in a protective plastic cover, thus avoiding contamination by handling.

54

Purified crystals (see Table 10, column ②) measured 140-200 μsec and one purified crystal counterdoped with manganese for boron compensation showed a lifetime of 28 μsec (Si:Mn experiment GZ068).

2.3.3.3 Minority Carrier Lifetime Data

Minority carrier lifetime up to 1500 μsec have been measured in purified ($|N_A - N_D| \sim 10^{12}$ cm^{-3}) dislocation free float zone silicon single crystals (Ref. 32). Data obtained from purified crystals, grown on this program, measured only 100-400 μsec and high dislocation density was correlated to these lower lifetime values. T. Noack (Ref. 33) reports on the negative factors affecting lifetime, such as dislocations, contaminations, vacancies and small angle boundaries. He states the relation between dislocation density and lifetime as

$$N_d \tau = 15 \ (\text{sec cm}^{-2}) \tag{28}$$

where

$$N_d = \text{dislocation density}$$

and

$$\tau = \text{lifetime in seconds.}$$

Lifetime data from the crystals listed in Table 10, then imply a dislocation density of $3.75 \times 10^4 - 1.5 \times 10^5$ cm^{-2}. This agrees with data from dislocation density measurements reported in para. 2.3.5.2

2.3.4 IR Measurements

The impurity concentrations in the silicon crystals were investigated by infrared absorption, using both room temperature and low temperature techniques. In addition, the IR response method was used to determine the spectral sensitivity of detectors fabricated from boron compensated gallium doped crystals.

Three test arrangements, available at Rockwell, were utilized for silicon crystal characterization by IR absorption. These test methods are described in the following paragraphs and the test data are presented in Table 10.

---

33. Noack, T., "Measurement of Minority Carrier Lifetime in Silicon of Low Dislocation Density," Phys, Stat., Vol. 32, K17, 1969.

2.3.4.1 IR Spectral Response with the Perkin-Elmer 112

A Perkin-Elmer 112* spectrophotometer (Figure 28) with a wavelength range from 2 to 35 μm is in routine use to measure the relative spectral response of all extrinsic detectors fabricated and tested at the Rockwell material laboratory. The spectral response of gallium doped detectors from this program measured at 5°K is shown in Figure 29.

In addition to the monochromatic IR, the optical system supplies a background flux ϕ which is also absorbed by the gallium and boron impurities. The effects of this background flux on detector properties under various temperature conditions are discussed in App. A, pp. 121-122. Application of this theoretical treatment to the conditions under which the spectral response data were taken ($10^8 < \phi < 10^{15}$ photons/cm² sec) indicates that both the boron and gallium impurities are only slightly ionized. The detector under these conditions will show a response proportional to the boron concentration in the appropriate spectral region.

Figure 30 shows the charge state of the levels for very low background ($\phi << \phi_{min}$), where the Fermi distribution applies. For a sufficiently high background such that $\phi >> \phi_{min}$, the charge state distribution of the levels is determined by the photon flux spectrum, the values of the photon absorption cross-sections for Ga and B and their hole capture cross-sections.

The high background case shown would apply to a background spectrum having a sufficient number of photons available for absorption by both neutral boron and gallium impurities.

The response spectrum at wavelengths longer than about 20 μm is due to photoionization of the boron centers. A prominent feature of this region is a spectral peak at 31.3 μm (320 cm⁻¹). A strong absorption peak is observed at this energy
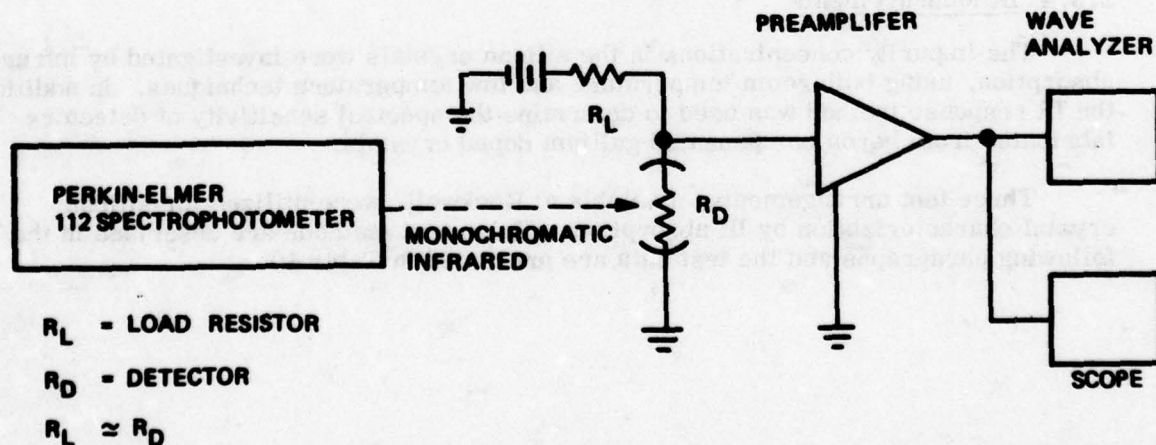
Figure 28. Sketch of Measurement Apparatus for Relative Spectral Response
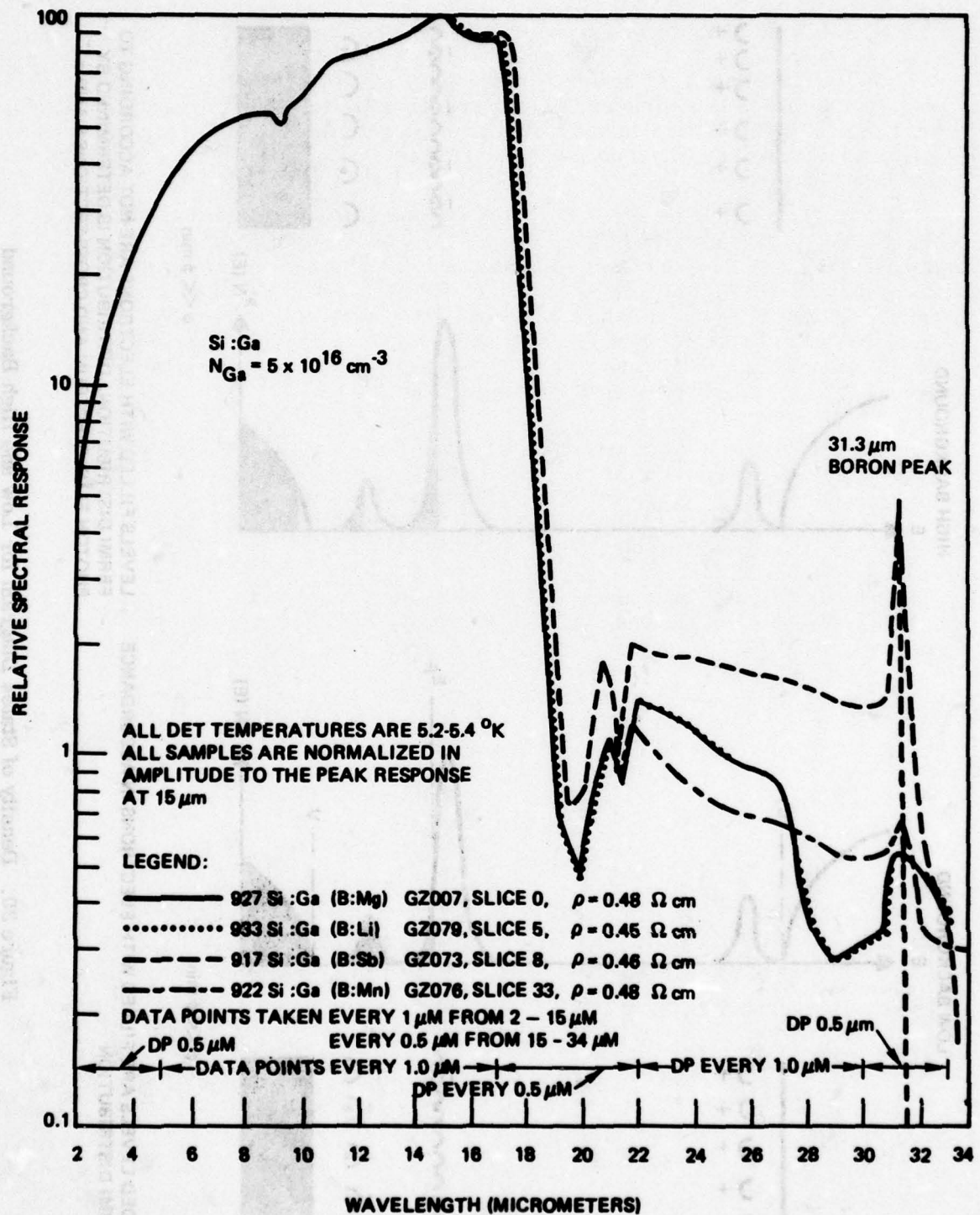
Figure 29. Residual Boron Concentration Detected in the Relative
Spectral Response of Si:Ga Detectors

57

Figure 30. Density of States Diagram for Low and High Background

LEVELS FILLED WITH ELECTRONS ARE NOT ACCORDING TO FERMI DISTRIBUTION. DISTRIBUTION IS DETERMINED BY PHOTON FLUX SPECTRUM AND CROSS-SECTIONS S AND σ
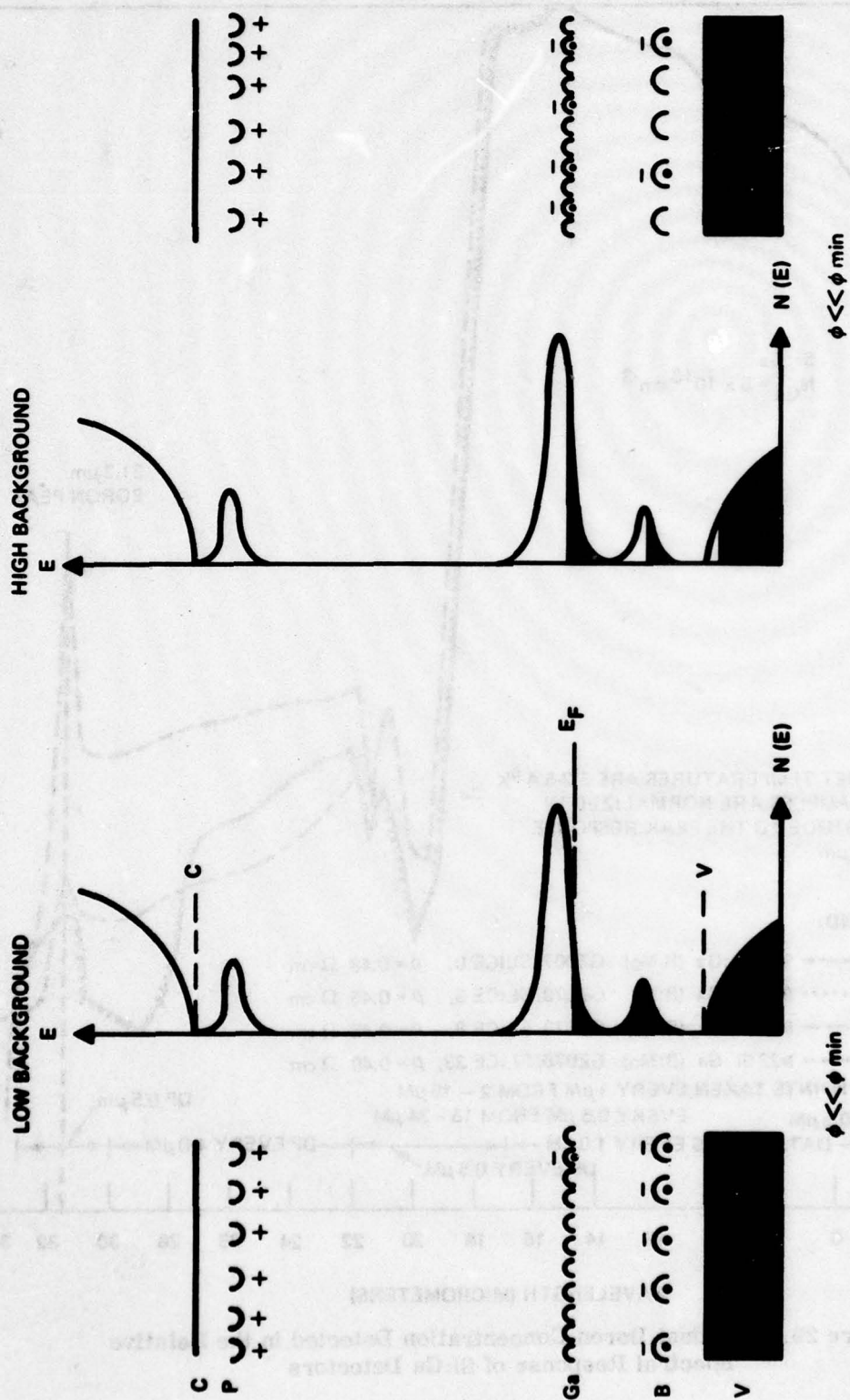
THE SHADED LEVELS ARE FILLED WITH ELECTRONS IN ACCORDANCE WITH FERMI DISTRIBUTION

in the absorption spectrum of boron acceptors (Ref. 34 through 37) and is due to a transition of a hole from the ground state to a bound excited state lying about 40 cm^{-1} below the ionization limit. Although some contribution to the photoconducting from this absorption line is expected, presumably due to a thermal or hot carrier ionization from the excited state, it is surprising that it is so strongly exhibited here. In any event, as a means of analysis, the magnitude of the spectral response due to the boron at 31.3 μm was normalized to the gallium photoresponse at 15 μm which, for all samples, was in the range of 4 to 5 x 10^{16} cm^{-3}. The normalized boron response data are plotted in Figure 31 against boron concentration data obtained by Fourier

34. Kolbesen, B.O., "Simultaneous Determination of the Total Content of Boron and Phosphorus in High Resistivity Silicon by I.R. Spectroscopy at Low Temperatures," Appl. Phys. Letters, Vol. 27/6, p 353, 1975.
35. Pajot, B., "Impurity Lines of Boron and Phosphorus in Silicon," J. Phys. Chem. Solids, Vol. 25, p 613, 1964.
36. Hrostowski, H.J. and Kaiser, R.H., "Infrared Spectra of Group III Acceptors in Silicon," J. Phys. Chem. Solids, Vol. 4, p 148, 1958.
37. Burstein, E., Picus, G., Henvis, B. and Wallis, R., "Absorption Spectra of Impurities in Silicon I," J. Phys. Chem. Solids, Vol. 1, p 65, 1956.

1. GZ073 N$_{BORON}$ 3.6 x 10^{12}
2. GZ076 N$_{BORON}$ 1.5 x 10^{12}
3. GZ077 N$_{BORON}$ 2-2.5 x 10^{12}
4. GZ079 N$_{BORON}$ 1.4 x 10^{12}

Figure 31. Boron Concentration by Spectral Response

59

transform absorption spectroscopy. Clearly the data are insufficiently accurate (e.g., they do not even show a linear relationship between the boron concentration and spectral response) to provide more than an approximate measure of boron concentration.

2.3.4.2 IR Absorption Measurements with Beckman FS-720

A Beckman FS-720 Fourier Transform Spectrophotometer* was used to make the IR absorption measurements. It was connected to a PDP-11/05 digital computer with a 16K word memory, a high speed papertape input-output, and analog CRT and graphic display capabilities. The programmed resolution limit on the current data is 1.25 wave numbers, although the maximum possible resolution limit for this system is 0.05 to 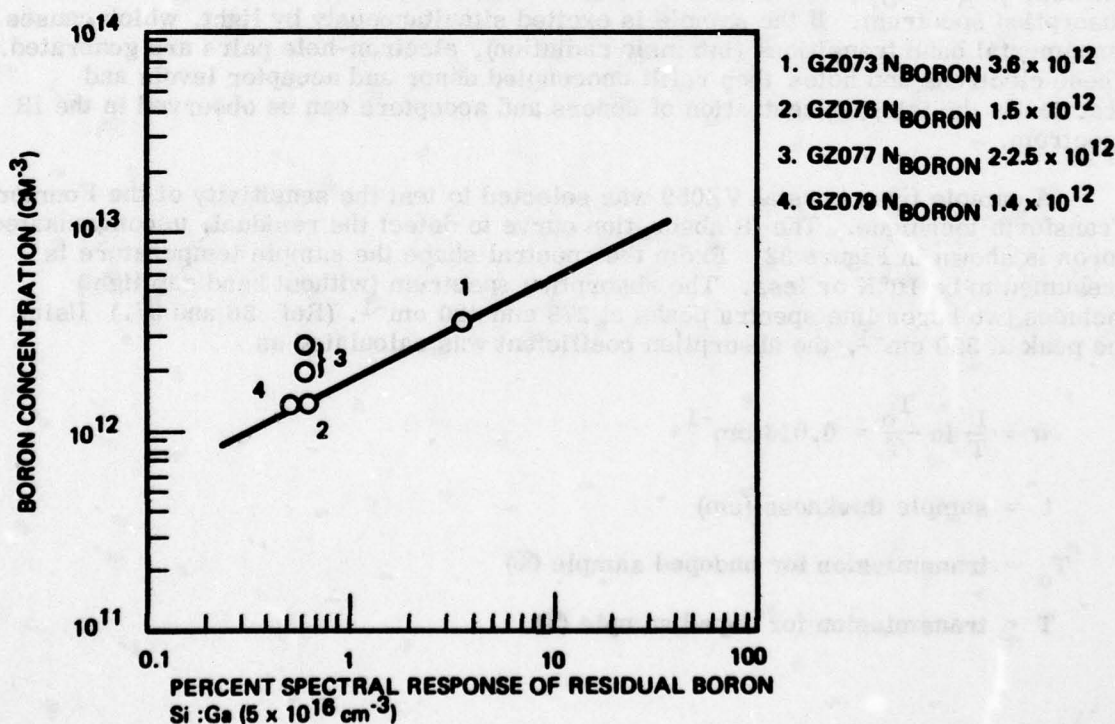0.1 wave numbers. The detector was a doped silicon bolometer operated at 1.2°K. The cryostat has sufficient space to accommodate samples greater than 10 cm long at this low temperature.

While investigating the residual boron concentrations in the crystals, we experimented with measurements using the Kolbesen absorption method. (Ref. 34.) This spectroscopic method provides a simultaneous analysis of the total phosphorus and boron content in as-grown silicon samples. At low temperatures, the absorption spectrum of neutral donors or acceptors consists of a series of bands at energies lower than the ionization energies of the impurities in silicon, e.g., for B and P in the 200 to 400 cm^{-1} (25 to 50 μm) region. Generally, only the uncompensated centers, $|N_A - N_D|$, of the total content of acceptors and donors contribute to the absorption spectrum. If the sample is excited simultaneously by light, which causes fundamental band transitions (intrinsic radiation), electron-hole pairs are generated. These electrons and holes then refill unoccupied donor and acceptor levels and practically the total concentration of donors and acceptors can be observed in the IR spectrum.

A sample from crystal VZ059 was selected to test the sensitivity of the Fourier Transform technique. The IR absorption curve to detect the residual, uncompensated boron is shown in Figure 32. From the spectral shape the sample temperature is presumed to be 10°K or less. The absorption spectrum (without band gap light) includes two boron line spectra peaks at 278 and 320 cm^{-1}. (Ref. 36 and 37.) Using the peak at 320 cm^{-1}, the absorption coefficient was calculated as

$$\alpha = \frac{1}{T} \ln \frac{T_o}{T} = 0.016 \text{ cm}^{-1}$$

t = sample thickness (cm)

T_o = transmission for undoped sample (%)

T = transmission for doped sample (%)

---

*Beckman Instruments, 2500 N. Harbor Blvd., Fullerton, CA.
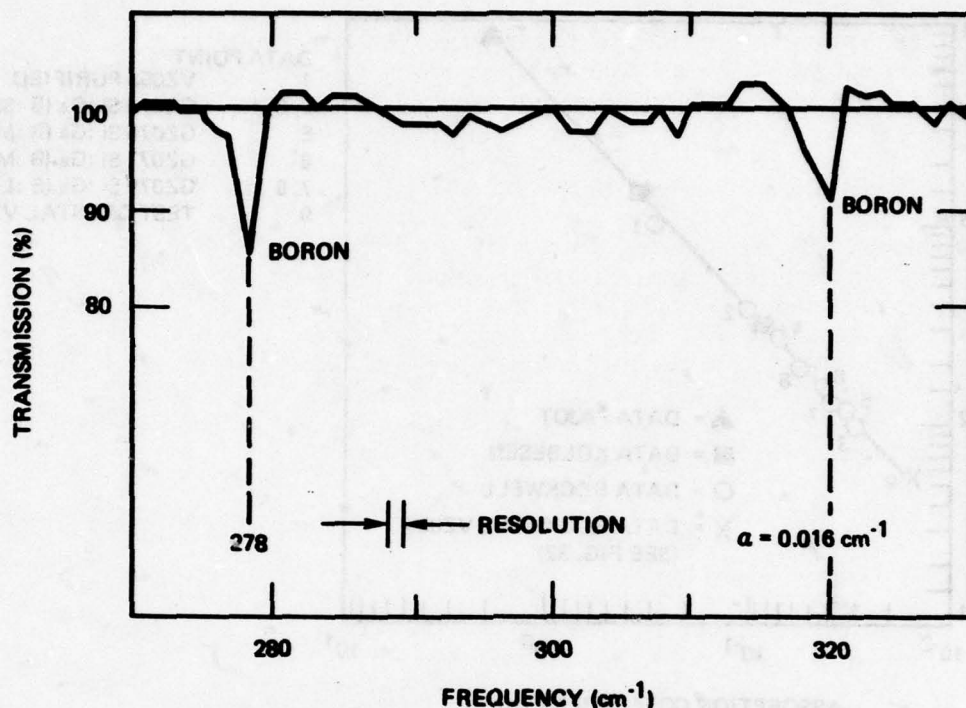
Figure 32. Optical Transmission Spectrum of a 6.7 cm
Thick Sample of Si:B

Correlating this experiment with data reported by Kolbesen (Ref. 34) and Pajot
(Ref. 35) (see Figure 33), the 10 percent absorption at 320 cm^{-1} in the 6.7 cm long
sample corresponds to approximately 6×10^{11} cm^{-3} boron. The noise level in
Figure 32 indicates a minimum detectable concentration at this sample of approxi-
mately 1×10^{11} atoms/cm^3.

Figure 34 shows the relative absorption of two identical silicon samples of
different lengths. By reducing the sample length by half, the absorption strength is
reduced by the same amount verifying that all samples have been uniformly pumped
by band gap light. In addition, experiments decreasing the intensity of the pump
light showed no reduction of the intensity of the absorption, indicating that the
impurity states were all neutralized. Further investigation into the validity of this
test method is shown graphically in Figure 35, which presents Fourier transform
spectra of a material sample (3 cm long) from crystal GZ073 Si:Ga (B:Sb).

N_B and $N_{\bar{B}}$ of the four test crystals (Table 10) was obtained from Figure 33
using experimental transmission values to calculate the absorption coefficient .
These boron and boron compensation data were compared with test data from
4-point probe resistivity and Hall measurements (Table 10, columns ② through ⑤).
There is good agreement between the relationship of absorption coefficient and total
boron concentration found here and in prior data. Compensated samples (e.g. Sb and
Mg) showed the expected increases in absorption due to band gap pumping.

61
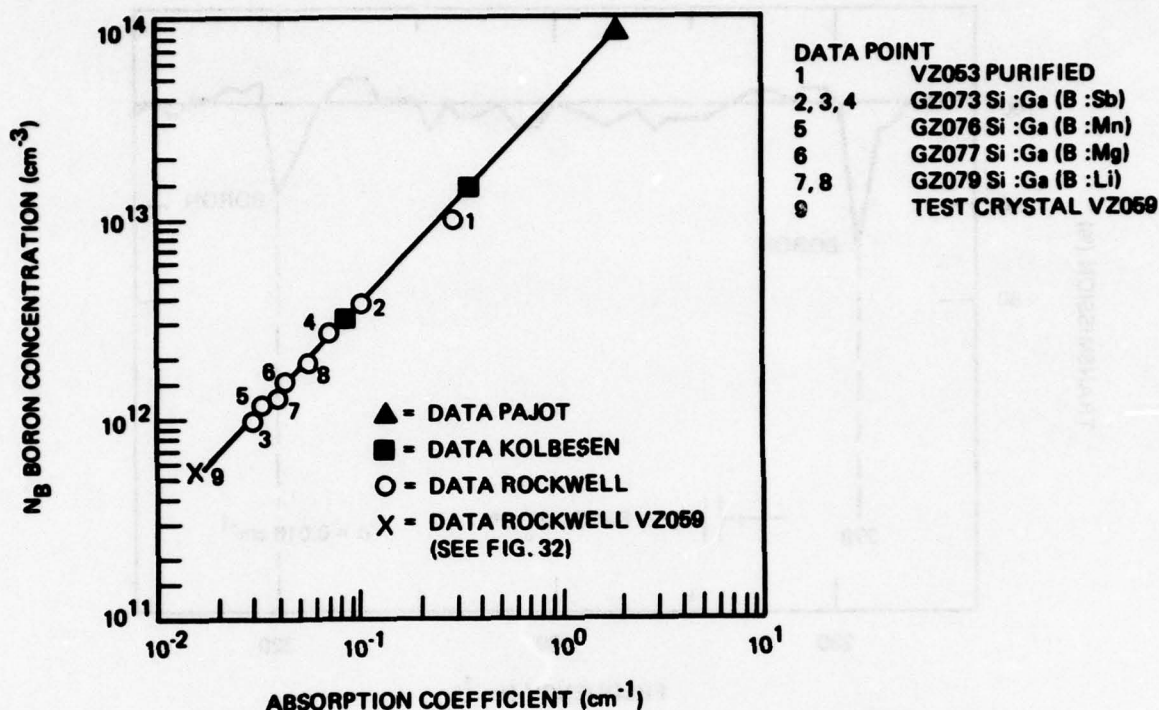
Figure 33. Boron Concentration in Silicon by Fourier Transform
Absorption Measurements at 320 cm^{-1}

Samples from crystal (GZ077 Si:Ga (B:Mg) did not provide satisfactory infrared measurements. Crystal GZ079, counterdoped with lithium, showed no compensation by IR, while resistivity and Hall data measured $N_D > N_A$ with a lithium concentration of 5×10^{13} cm^{-3} compared to a boron concentration of 1.4×10^{12} cm^{-3}. The second pass on this crystal showed a reduction of the lithium to 3.81×10^{12} cm^{-3}, which should still be sufficient to compensate a boron concentration of 1.9×10^{12} cm^{-3}, but compensation could not be verified by IR measurement.

2.3.4.3 Carbon and Oxygen Concentration

Infrared absorption spectroscopy has been used to determine the oxygen and carbon content of single crystal silicon material. Interstitial oxygen could be detected with absorption bands at 1130 cm^{-1} (9 μm) (Ref. 38, 39, 40) and substitutional carbon

38. Runyan, W.R., Silicon Semiconductor Technology, T.I. McGraw-Hill, N.Y., 1965.
39. Kaiser, W., Keck, P.H. and Lange, C.F., "Infrared Absorption and Oxygen Content in Silicon and Germanium," Physical Review, Vol. 101/4, p 1264, 1956.
40. Gross, C. and Gaetano, G., "Comparison of Infrared and Activation Analysis Results in Determining the Oxygen and Carbon Content in Silicon," J. Electro-Chem. Soc., Vol. 119, p 926, 1972.
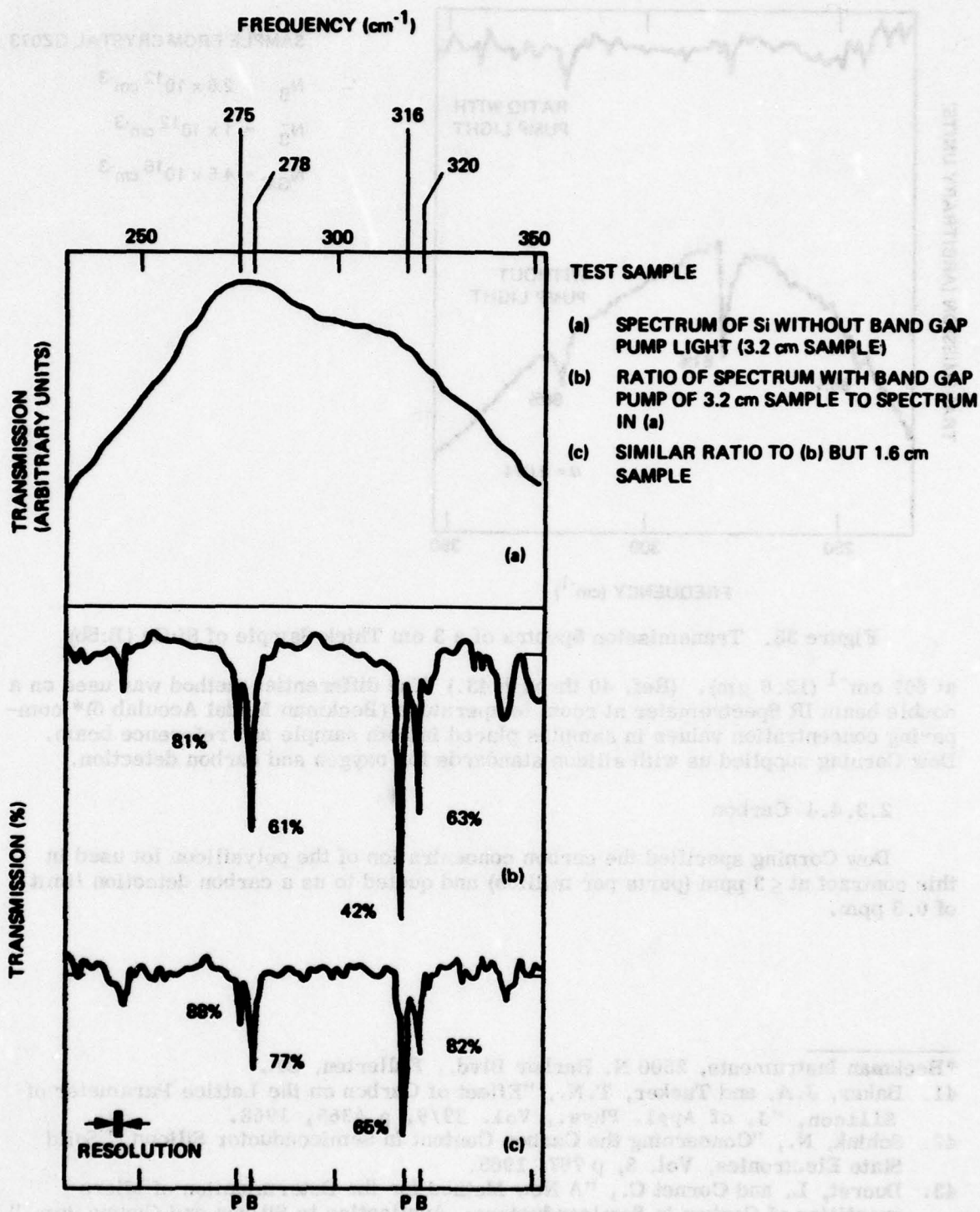
Figure 34. Transmission Spectra of Compensated Si

SAMPLE FROM CRYSTAL GZ073

$N_B = 2.6 \times 10^{12} \, cm^{-3}$

$N_B^- = 1 \times 10^{12} \, cm^{-3}$

$N_{Ga} = 4.5 \times 10^{16} \, cm^{-3}$
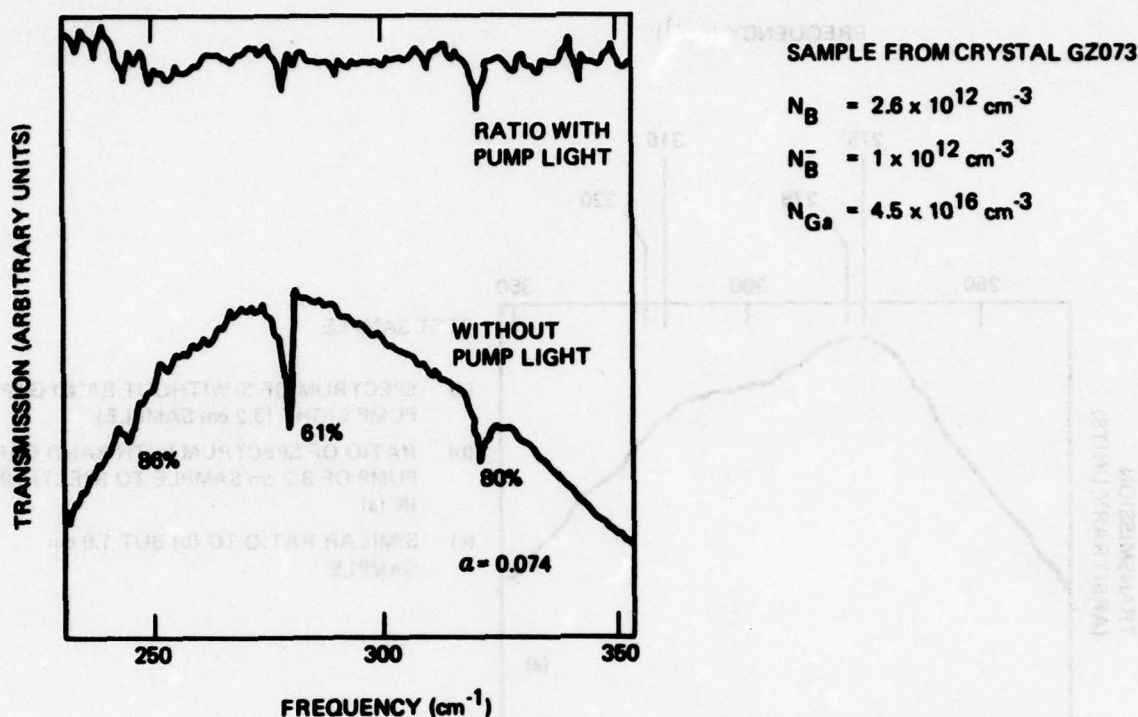
Figure 35. Transmission Spectra of a 3 cm Thick Sample of Si:Ga (B:Sb)

at 607 cm^{-1} (12.6 μm). (Ref. 40 through 43.) The differential method was used on a double beam IR Spectrometer at room temperature (Beckman Model Acculab 6)* comparing concentration values in samples placed in both sample and reference beam. Dow Corning supplied us with silicon standards for oxygen and carbon detection.

2.3.4.4 Carbon

Dow Corning specified the carbon concentration of the polysilicon lot used in this contract at ≤ 3 ppm (parts per million) and quoted to us a carbon detection limit of 0.3 ppm.

*Beckman Instruments, 2500 N. Harbor Blvd., Fullerton, CA.
41. Baker, J.A. and Tucker, T.N., "Effect of Carbon on the Lattice Parameter of Silicon, "J. of Appl. Phys., Vol. 39/9, p 4365, 1968.
42. Schink, N., "Concerning the Carbon Content in Semiconductor Silicon," Solid State Electronics, Vol. 8, p 767, 1965.
43. Ducret, L. and Cornet C., "A New Method for the Determination of Micro-quantities of Carbon in Semiconductors: Application to Silicon and Germanium," Centre National d'Etudes Des Telecommunications Issy Les Moulineaux, Seine, France, p 461.

Polished crystal slabs of uniform and equal thickness from a polyrod, a purified crystal, and a doped single crystal were measured against the calibrated standards (Figure 36). All three samples showed an impurity concentration below the detection limit. It can be concluded that the first exposure to the carbon preheater in the vacuum furnace and the second exposure during the start in the gas float zones do not raise the carbon level above 0.3 ppm, the detection limit. It is assumed that the variation between the mass spectroscopy data of Dow Corning and our IR absorption data are within the range of averaging data for one large material lot. Dow Corning also stated that analysis of the poly material is not accurate to the desired levels due to impurity collection in the grain boundaries.

2.3.4.5 Oxygen

A method similar to that used for the carbon detection was also used to measure the change in the oxygen content of the crystals during the various processing steps. The oxygen content of the poly material was specified as below 4.4×10^{16} cm^{-3}. Samples of poly material, purified material, and compensated and gallium doped material were measured and compared to the oxygen standards. No oxygen could be detected in any of the material.

These results (see Figure 37) are within the range of expectation. Low carbon and oxygen concentration or, better, the avoidance of adding these two impurities into the silicon is a great advantage of the float zoning process over the Czochralski method.
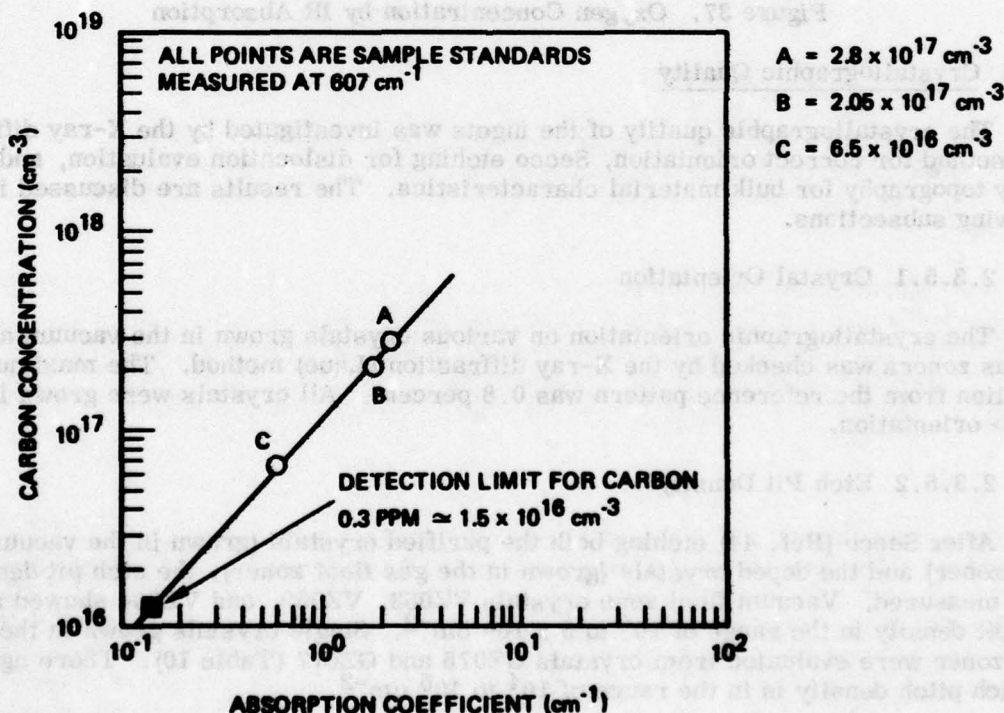
Figure 36. Carbon Concentration by IR Absorption
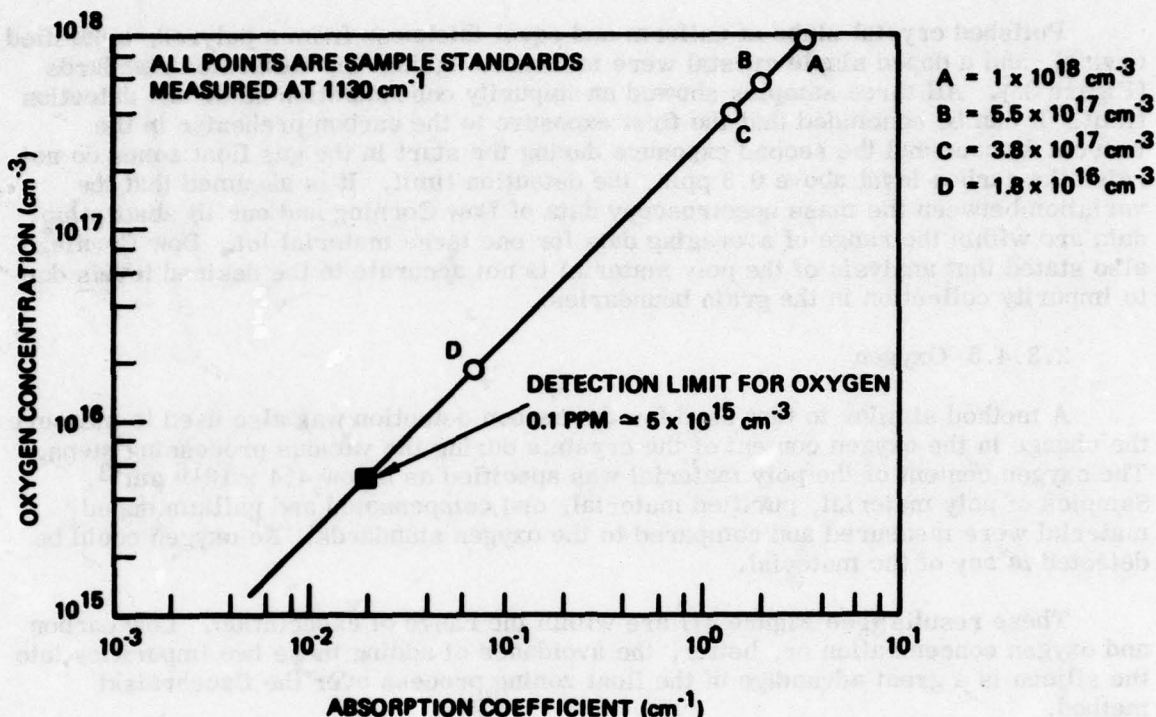
Figure 37. Oxygen Concentration by IR Absorption

2.3.5 Crystallographic Quality

The crystallographic quality of the ingots was investigated by the X-ray diffraction method for correct orientation, Secco etching for dislocation evaluation, and X-ray topography for bulk material characteristics. The results are discussed in the following subsections.

2.3.5.1 Crystal Orientation

The crystallographic orientation on various crystals grown in the vacuum and the gas zoners was checked by the X-ray diffraction (Laue) method. The maximum deviation from the reference pattern was 0.8 percent. All crystals were grown in <100> orientation.

2.3.5.2 Etch Pit Density

After Secco (Ref. 44) etching both the purified crystals (grown in the vacuum float zoner) and the doped crystals (grown in the gas float zoner), the etch pit densities were measured. Vacuum float zone crystals VZ053, VZ059, and VZ064 showed an etch pit density in the range of 10^4 to 5×10^5 cm^{-2}. Single crystals grown in the gas float zoner were evaluated from crystals GZ076 and GZ077 (Table 10). There again, the etch pitch density is in the range of 10^4 to 10^5 cm^{-2}.

---

44. Secco d'Aragona, "Dislocation Etch for (100) Planes in Silicon," J. Electrodium. Soc., Vol. 119, p 948, 1972.

This undesirable growth condition had two main causes.

1. The furnaces were not on isolation pads and the building around the crystal room contains large power equipment. To improve this condition, some crystals were grown at night under reduced external vibration conditions, but the improvement was not enough to justify this schedule.

2. The power control on the two-float zoners needed to be upgraded. It did not provide sufficient sensitivity to make small power changes when growing the thin neck of the crystal.

Both of these problems will be corrected with a relocation and modification of the zoners.

2.3.5.3 X-Ray Topography

X-Ray diffraction topography provides a means of obtaining photographic images of crystalline materials. In general, an X-ray is incident on a specimen, which is oriented to satisfy the conditions for diffraction from a particular set of atomic planes having Miller indices (hk1). The diffracted beam is recorded on a photographic film or plate to form the topographic image. A perfect crystal would give rise to a topograph having a uniformly grey appearance. The contrast effects observed in topographs are due to the presence of crystal imperfections in the specimen.

One of the best known topographic methods is the one developed by Lang (Ref. 45) and used in our analysis. The apparatus is shown in Figure 38. The X-ray beam from

---

45. Lang, A.R., "Studies of Individual Dislocations in Crystals by X-Ray Diffraction Microscope," J. of Appl. Phys. 30, p 1748, 1959.
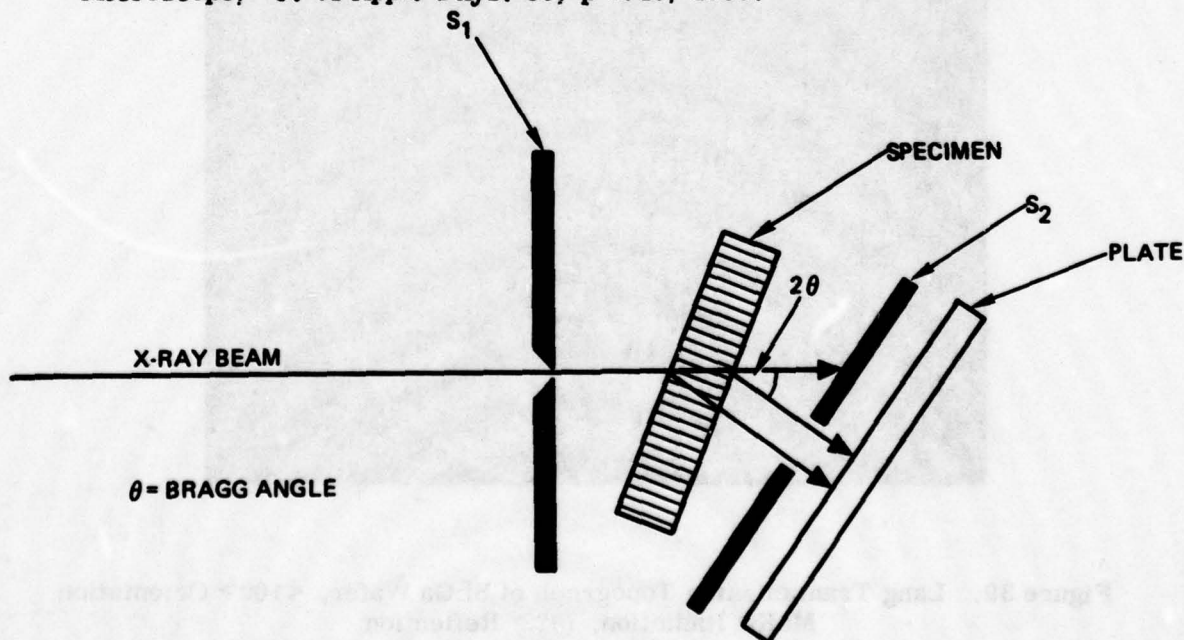
Figure 38. Transmission Lang Topographic Geometry

a geometrically small source is collimated by the slit S_1 and impinges upon the specimen crystal. Kα characteristic radiation is generally used and the specimen is set to diffract this radiation in transmission, i.e., the incident beam enters one side of the wafer-like specimen and the diffracted beam exits through the opposite face. In Figure 38, the diffracting planes are perpendicular to the specimen faces. This is the symmetric case where the incident and the diffracted beams make equal angles with the specimen face.

The diffracted beam is recorded on the photographic plate. Since the X-rays do not provide any magnification, the plate must be very fine grained to allow for subsequent magnification by optical means. The beam that is incident on the crystal is very narrow. To record a topographic image of a complete wafer, the Lang camera includes a mechanism for translation of specimen and plate.

Figure 39 is a Lang transmission topograph of a gallium doped silicon wafer in <100> orientation. The wafer (from GZ077) was about 12 mils thick, and the topograph was made with MoKα radiation using the (022) reflection. The exposure was made using Ilford Nuclear* plates, G-5 emulsion, 50 μ thick and was of the order of 8 hours.

---

*Ilford, Ltd., Ilford, Essex, England.
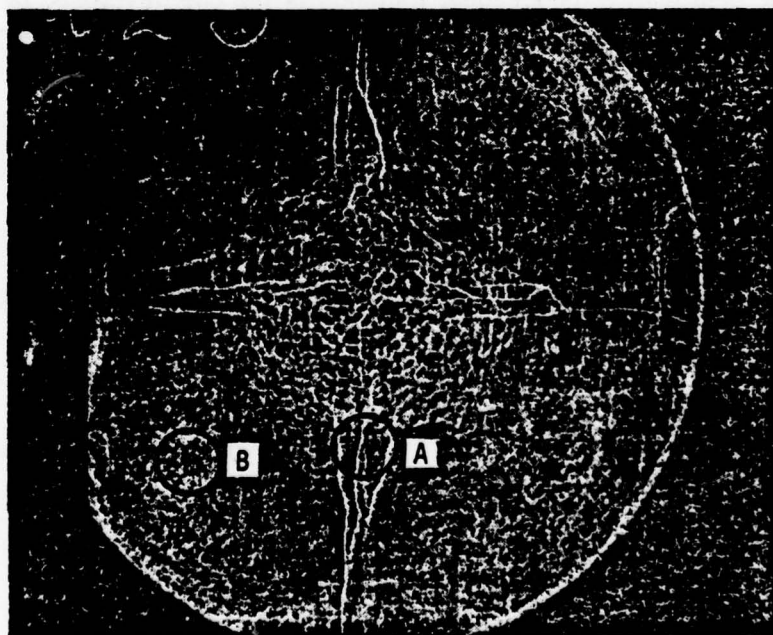
Figure 39. Lang Transmission Topograph of Si:Ga Wafer, <100> Orientation, MoKα Radiation, (022) Reflection

The wafer shown in Figure 39 shows a dislocation density of approximately 1×10^4 cm^{-2}. The converging lines directed from the outside of the wafer toward the center are arranged in 90 deg intervals. These lines are dislocation lines, branching out into lines with a diminished number of defects in the center of the wafer.

The two areas indicated by A and B in Figure 39 were Seeco etched and photographed with a 500 magnification. The results are shown in Figure 40 and 41, respectively. Figure 40 shows the diminished number of defects in the center, while Figure 41 shows an area between the converging lines. This slightly marbled structure in the topograph (enlarged in Figure 40) corresponding to a dislocation density of approximately 10^3 cm^{-2}.
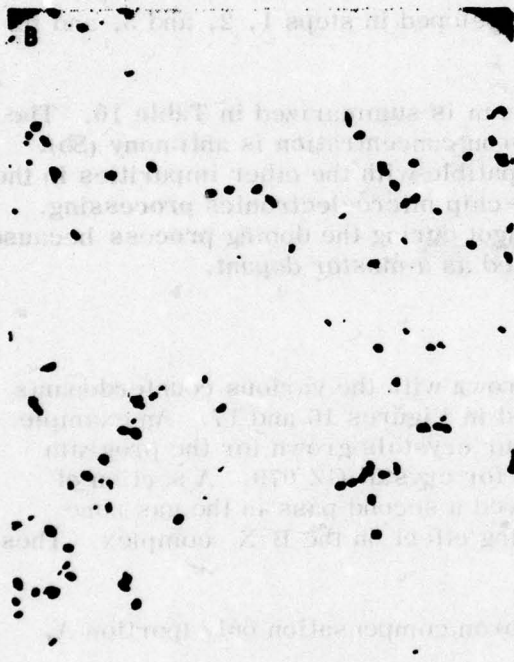
Figure 40. Diminishing Number of
Defects in Center of Wafer, 500X
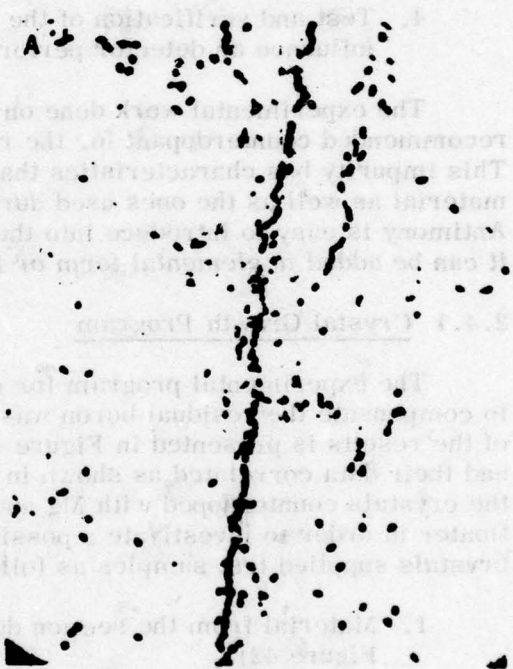
Figure 41. Dislocation Lines,
500X

2.4 TEST RESULTS AND CONCLUSIONS

The LADIR material project has developed a process for producing highly purified, boron compensated, gallium doped single crystals. This task was structured into the following steps:

1. Purification by vacuum float zoning to a donor (phosphorus) level of less than 10 percent of the residual boron. The boron acceptor content, which is not affected by the vacuum float zoning process, determined the resistivity of the purified crystal.

2. Compensation of boron by adding the calculated amount of n-type dopant during the final growth in the gas zoner.

3. Simultaneous addition of the desired, calculated, and accurately weighed amount of gallium dopant.

4. Test and verification of the process developed in steps 1, 2, and 3, and its influence on detector performance.

The experimental work done on this program is summarized in Table 10. The recommended counterdopant for the residual boron concentration is antimony (Sb). This impurity has characteristics that are compatible with the other impurities in the material as well as the ones used during the on-chip microelectronics processing. Antimony is easy to introduce into the silicon ingot during the doping process because it can be added in elemental form or incorporated as a master dopant.

2.4.1 Crystal Growth Program

The experimental program for crystals grown with the various counterdopants to compensate the residual boron was illustrated in Figures 16 and 17. An example of the results is presented in Figure 42. All four crystals grown for the program had their data correlated as shown in Figure 42 for crystal GZ 079. A section of the crystals counterdoped with Mg and Li received a second pass in the gas zone floater in order to investigate a possible sweeping effect on the B^-X^- complex. These crystals supplied test samples as follows:

1. Material from the section doped for boron compensation only (portion A, Figure 42).

2. Material from the section doped with gallium and the compensating impurity (portion B, Figure 42).

3. Material from the section (seed end) grown during a second pass in the gas float zoner (portion C, Figure 42).
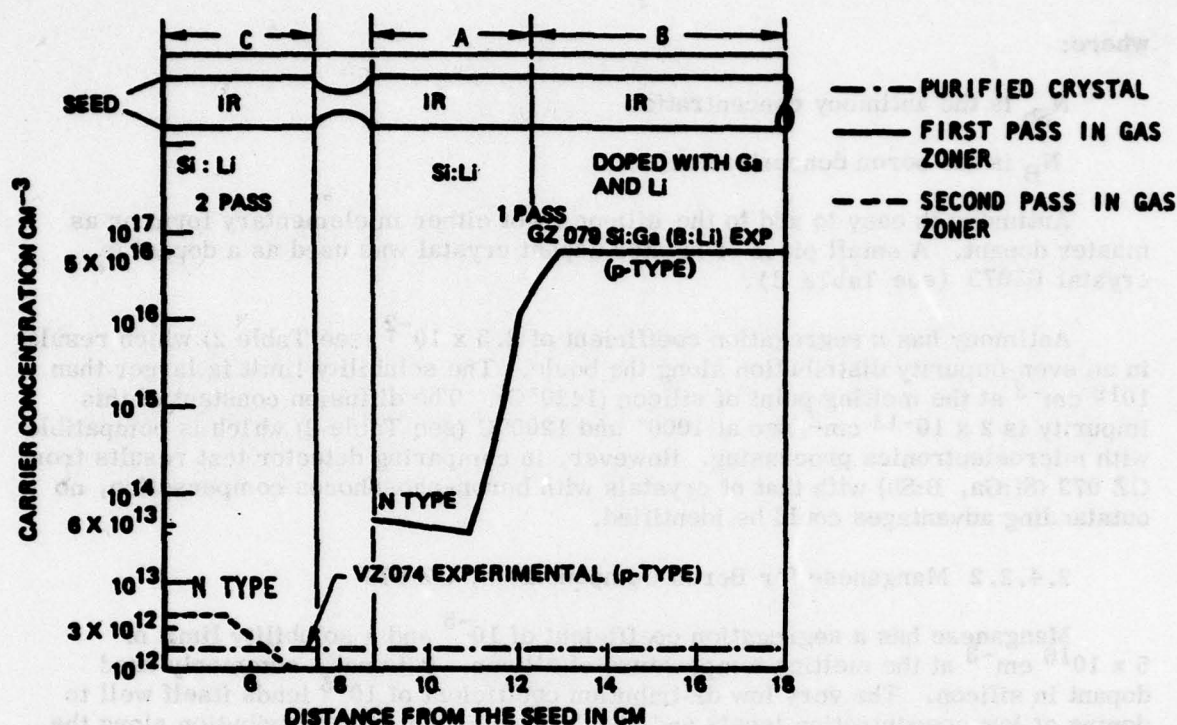
Figure 42. Crystal Growth Program.

2.4.2 Work Summary Data Discussion

The four single crystals (boron compensated and gallium doped) listed in Table 10, provided samples for material characterization and detector fabrication. Resistivity, Hall measurement, lifetime, IR absorption, and photo-conductive spectral response data are listed in this table. The gallium impurity concentration of 4 to 5 x 10^{16} cm^{-3} used for all doped crystals in this contract was previously selected as optimum for the LADIR program.

Short, general descriptions and evaluations of the crystals with the various boron-counterdopants will now be presented. This is followed by the evaluation of the relevant detector data.

2.4.2.1 Antimony for Boron Compensation, GZ -73

The purified crystal VZ 064 used for the GZ073 crystal growth had a higher boron concentration than originally measured on the vacuum zone refined boule. Measurement problems precluded determination of the proper concentration of antimony to be used for boron compensation. IR data (see Table 10) showed a low boron compensation ratio.

$$\frac{N_{Sb}}{N_B} = 0.28$$

71

where:

N_{Sb} is the antimony concentration

N_B is the boron concentration

Antimony is easy to add to the silicon ingot either in elementary form or as master dopant. A small piece of master dopant crystal was used as a dopant in crystal GZ073 (see Table 3).

Antimony has a segregation coefficient of 2.3×10^{-2} (see Table 2) which results in an even impurity distribution along the boule. The solubility limit is larger than 10^{19} cm^{-3} at the melting point of silicon (1420° C). The diffusion constant of this impurity is 2×10^{-13} cm^2/sec at 1000° and 1200° C (see Table 2) which is compatible with microelectronics processing. However, in comparing detector test results from GZ 073 (Si:Ga, B:Sb) with that of crystals with boron-phosphorus compensation, no outstanding advantages could be identified.

2.4.2.2 Manganese for Boron Compensation, GZ 076

Manganese has a segregation coefficient of 10^{-5} and a solubility limit of 5×10^{16} cm^{-3} at the melting temperature of silicon. It is not a commonly used dopant in silicon. The very low distribution coefficient of 10^{-5} lends itself well to doping at low concentration levels and should produce an even distribution along the crystal boule. Manganese is a deep level impurity in silicon. It has a high diffusion coefficient of approximately 2×10^{-7} cm^2/sec at 1200° C. This high diffusion coefficient suggests that manganese diffuses interstitially in the silicon lattice, but Schibli and Milnes (Ref. 46) report manganese in substitutional positions if vacancies are available. The diffusion coefficient is considerably larger than boron, phosphorus, and gallium. This implies an undesirable accelerated out diffusion of manganese atoms at wafer processing temperatures.

A test slice from the ingot section containing only boron and manganese impurities was measured by 4-point probe (n-type, 11 kΩcm) and cycled through a high temperature (1000° C) annealing process similar to a contact fabrication process. After remeasuring, it showed p-type conductivity and a resistivity of 4.5 kΩcm, indicating out diffusion of the n-type impurity manganese, exposing the boron level. Therefore, manganese cannot be considered a desirable element for stable boron compensation in silicon.

2.4.2.3 Magnesium for Boron Compensation, GZ 077

Magnesium as an n-type impurity was considered for boron compensation because it may complex with boron atoms as Mg^+B^-. Experiments to investigate the behavior of magnesium atoms in silicon containing residual boron were described in section 2.2.1, and the data were listed in Table 5. The added magnesium concentration was calculated as approximately 10^{13} cm^{-3} compared with residual boron

46. Schibli, E. and Milnes, A.G., Deep Impurities in Silicon, Master Sci Eng. Vol. 2, p 173, 1967.

concentration of 2×10^{12} cm^{-3} measured in the purified crystal. Room temperature Hall measurements indicated the impurity concentration $|N_A - N_D|$ to be 3.6×10^{12} cm^{-3}, i.e., greater than the residual boron concentration. IR measurements also indicated a smaller than desired Mg concentration has been incorporated in the crystal. The inability to add sufficient magnesium during the float zoning process to compensate the residual boron eliminated magnesium as a useful compensation impurity.

2.4.2.4 Lithium for Boron Compensation, GZ 079

The solubility of lithium in doped silicon crystals markedly exceeds that in the undoped material. Experimental investigations (Figure 11) showed a solubility dependence on the boron concentration in silicon. These experiments were made with silicon containing a boron concentration from 10^{17} to 10^{19} cm^{-3} and diffusion temperatures $\leq 1150°$C. This program has extended these experiments to lower boron concentrations, approximately 10^{13} to 10^{12} cm^{-3}. These experiments are also described in para 2.2.1, and the results are listed in Table 6. The lithium concentration of 5.4×10^{13} cm^{-3}, (see Table 10, GZ 079, Column 3) is more than 10 times the boron concentration in the crystal ($N_{boron} = 1.4 \times 10^{12}$ cm^{-3}). Conductivity-type measurements showed this crystal to be n-type. Compensation could not, however, be verified by IR measurements and complexing with other atoms is suspected.

An attempt was made to prove this theory by adding another zone pass on the crystal segment containing boron and lithium impurities only (Figure 15). The lithium concentration was reduced by the float zone pass; however, IR measurements showed that the remaining Lithium did not compensate the boron present.

Lithium did not seem to form the desired Li^+B^- complex at the low boron concentration and did not create a complex sweep-out effect that would reduce the boron concentration. In addition, lithium has a diffusion coefficient that is much higher than the other elements in silicon (see Table 2). Therefore, lithium was eliminated as a choice for the counterdopant for the residual boron in float zoned silicon crystals.

2.4.2.5 Neutron Transmutation Doping for Boron Compensation

One crystal purified by four vacuum passes and doped to a gallium concentration of approximately 5×10^{16} cm^{-3} was grown for the transmutation doping experiment. This crystal identified as GZ 156 was dedicated to provide detector grade silicon wafer material with $N_{phosphorus}/N_{boron}$ ratios of from 1 to 20.

Identification data of the crystal are listed in Table 11. Table 12 lists the wafers provided to MURR for the planned irradiation procedure. The topography data verify the gallium doping uniformity along the boule, and Figure 43 verifies it across the wafer diameters. The impurity distribution of the residual boron in this crystal is shown in Figure 44. The data were obtained by four-point probe resistivity measurements across a half wafer cut from the undoped seed end of the crystal.

TABLE 11. IDENTIFICATION DATA FOR CRYSTAL CZ 156 Si:Ga CRYSTAL PURIFIED BY FOUR VACUUM PASSES AND BORON NOT COMPENSATED

Down Corning Data Polysilicon	Rockwell Data		Doped Crystal Gallium Concentration
	Purified Crystal VZ107 Residual Impurity Concentrations		
	4-Pt Probe	IR Absorption	
$N_A = 0.006$ ppb $= 3 \times 10^{12}$ cm^{-3} $N_D = 0.1$ ppb $= 5 \times 10^{12}$ cm^{-3}	$\rho = \lvert N_A - N_D \rvert$ $= 5.42 \times 10^{12}$ cm^{-3}	$N_{Boron} = 4.3 \times 10^{12}$ cm^{-3} $N_{Phosporus} = 0.9 \times 10^{12}$ cm^{-3}	$5 - 6 \times 10^{16}$ cm^{-3} See resistivity topographs in Table 13.

The irradiated wafers (Table 12) were returned from MURR to Rockwell with the compensation concentration characteristics listed in the irradiation log shown in Table 13. These wafers were processed into standard detectors as elaborated in para 2.4.3.

2.4.2.6 Compensation by Residual Phosphorus

Detectors fabricated from silicon crystal with the compensation methods developed on this program were compared with detectors from gallium doped crystals where the boron-phosphorus balance was achieved by vacuum float zoning. Material from crystal GZ -65 grown for another project was used to fabricate the comparison detectors. Table 14 presents the identification data for this crystal or wafer.

2.4.3 Fabrication of Test Detectors

Test detectors of standard geometry were fabricated using silicon wafers from the gallium doped boron compensated materials described in section 2.4.2. The detectors were fabricated as follows:

1. Cut silicon wafers to approximately 22 mils thick.

2. Lap wafers with 9μ grit to approximately 20 mils.

3. Diffuse boron (from boron tribromide) at 1050°C to a depth of 2.5μ. The boron surface concentration is approximately 5×10^{19} cm^{-3}.

4. Plate nickel and indium on both wafer sides.

74

TABLE 12. RESISTIVITY TOPOGRAPHY FOR GZ 156, BORON NOT COMPENSATED, Si:Ga, p-TYPE

Slice Number	Thickness (mils)	Center (Ωcm)	North (Ωcm)	South (Ωcm)	East (Ωcm)	West (Ωcm)	Average (Ωcm)	Comment
5	23.6	0.523	0.632	0.593	0.588	0.632	0.594	Used for Detectors
6	24.4	0.523	0.618	0.600	0.600	0.596	0.588	
7	25.8	0.539	0.608	0.620	0.610	0.600	0.595	
8	25.1	0.530	0.607	0.631	0.592	0.599	0.592	
9	26.1	0.530	0.604	0.611	0.598	0.616	0.592	
10	26.3	0.526	0.604	0.601	0.601	0.582	0.583	
11	26.3	0.521	0.595	0.608	0.614	0.584	0.594	
12	25.7	0.526	0.616	0.600	0.600	0.592	0.587	
13	26.5	0.517	0.605	0.629	0.584	0.600	0.587	
14	25.8	0.536	0.636	0.632	0.630	0.656	0.618	
15	26.9	0.526	0.596	0.620	0.636	0.649	0.606	
16	24.7	0.540	0.647	0.642	0.620	0.635	0.617	
17	25.7	0.526	0.601	0.608	0.630	0.630	0.599	
18	26.1	0.535	0.636	0.605	0.630	0.594	0.600	
19	27.4	0.521	0.619	0.652	0.620	0.641	0.611	
20	25.0	0.534	0.648	0.659	0.674	0.625	0.628	
21	26.8	0.533	0.599	0.624	0.598	0.600	0.598	
22	24.6	0.538	0.644	0.634	0.610	0.644	0.620	
23	27.2	0.530	0.631	0.624	0.617	0.635	0.607	
24	25.9	0.540	0.626	0.636	0.604	0.654	0.612	
25	25.1	0.527	0.626	0.642	0.611	0.632	0.607	
26	25.9	0.523	0.582	0.592	0.594	0.594	0.575	
A	25.2	1.222						
B	25.3	1.392						
C	25.5	4.56K						
D	25.5	4.61K						
E	30.2	0.696						Not Included
F	30.2	0.662						Not Included
G	25.4	1.40K						
H	26.4	2.66K						

Note: A through H from seed end of GZ156

75
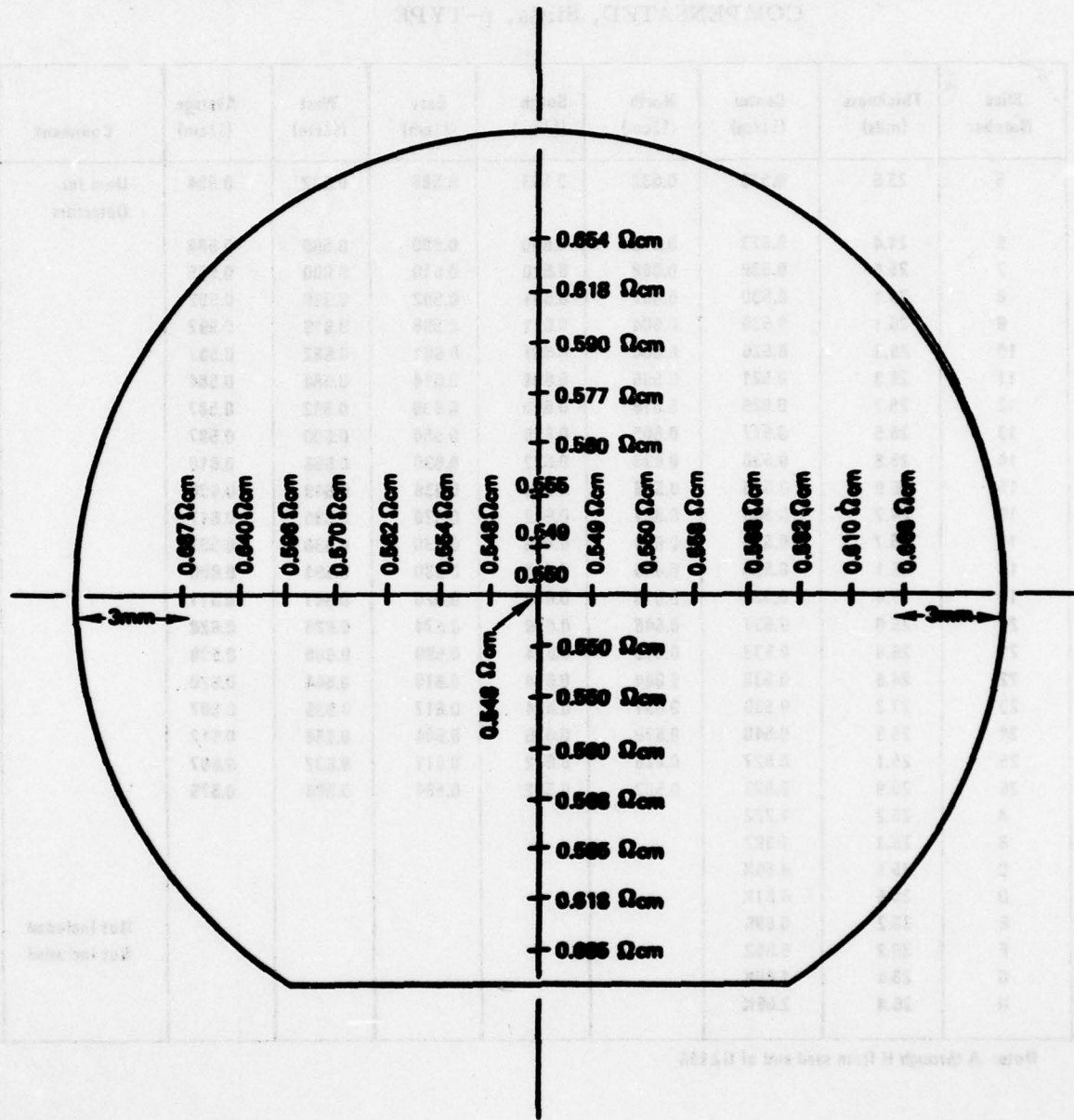
Figure 43. Resistivity Profile, GZ 156, Wafer 2, Si:Ga

GZ 156

UNDOPED
SEED-END
Si :B

RESISTIVITY
(Ωcm)

6×10^3

5×10^3

4×10^3

0   0.1   0.2   0.3   0.4   0.5   0.6   0.7   0.8

DISTANCE OF PROBE CENTER FROM LEFT EDGE OF SAMPLE (in.)
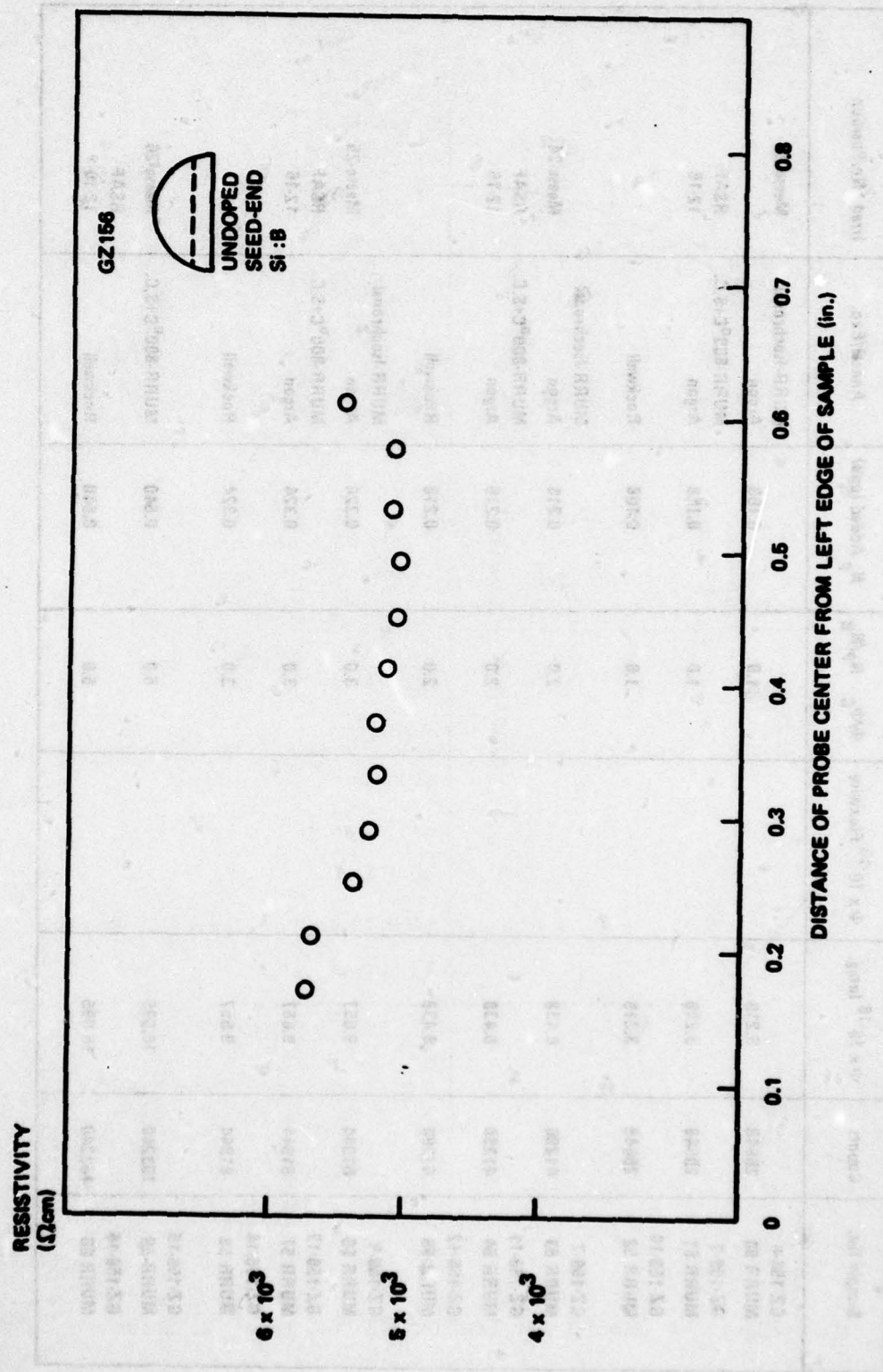
Figure 44. Boron Distribution in Undoped GZ 156

77

TABLE 13. IRRADIATION LOG (1322 COUNTS/HOUR) FOR Ga DOPED CRYSTAL GZ156.

Sample No.	Counts	$\Phi \times 10^{-16}$ Integ.	$\Phi \times 10^{-16}$ Fluxwire	Φ/Φ_C N_p/N_B	N_p Added (ppb)	Anneal/Exp.	Irrad. No/Position
GZ-156-6 MURR 50	20648	3.219		1.0	0.108	MURR-isochronal Argon	Meese-23
GZ-156-9 MURR 51	20648	3.219		1.0	0.108	MURR-800°C+S.C. Argon	RSAF 12-16
GZ-156-10 MURR 52	20648	3.219		1.0	0.108	Rockwell	
GZ-156-7 MURR 53	41296	6.438		2.0	0.216	MURR-isochronal Argon	Meese-24
GZ-156-11 MURR 54	41296	6.438		2.0	0.216	MURR-800°C+S.C. Argon	RSAF 12-16
GZ-156-12 MURR 55	41296	6.438		2.0	0.216	Rockwell	
GZ-156-8 MURR 56	61944	9.657		3.0	0.324	MURR-isochronal Argon	Meese-25
GZ-156-13 MURR 57	61944	9.657		3.0	0.324	MURR-800°C+S.C. Argon	RSAF 12-16
GZ-156-14 MURR 58	61944	9.657		3.0	0.324	Rockwell	
GZ-156-15 MURR 59	103240	16.095		5.0	0.540	MURR-800°C+S.C. Argon	Meese-26
GZ-156-16 MURR 60	103240	16.095		5.0	0.540	Rockwell	RSAF 12-16

78

TABLE 13 (Cont)

Sample No.	Counts	$\Phi \times 10^{-16}$ Integ.	$\Phi \times 10^{-16}$ Fluxwire	Φ_p/Φ_C	N_p/N_B	N_p Added (ppb)	Anneal/Exp.	Irrad. No /Position
GZ-156-17 MURR 61	8020	32.19		10.0		1.08	MURR-900°C+S.C.	Meese-27 1-2 50-75 cm 8019 ct/ppb
GZ-156-18 MURR 62	8020	32.19		10.0		1.08	Rockwell	
GZ-156-19 MURR 63	16040	64.38		20.0		2.16	MURR-900°C+S.C.	Meese-28 1-2 50-75 cm
GZ-156-20 MURR 64	16040	64.38		20.0		2.16	Rockwell	

79

TABLE 14. IDENTIFICATION DATA FOR CRYSTAL GZ 065.

Dew Corning Data Polysilicon	Rockwell Data of the Purified, Doped Crystal	
	Residual Impurities After one Vacuum Pass*	Gallium Concentration (cm^{-3})
N_A = 0.04 ppb $= 2 \times 10^{12}$ cm^{-3} N_D = 0.35 ppb $= 1.8 \times 10^{13}$ cm^{-3}	$N_A = 2 \times 10^{12}$ cm^{-3} $N_D = 1 \times 10^{13}$ cm^{-3}	5×10^{16} Wafer 21 of crystal GZ065 was used for the detector fabrication.

*Measured with 4-point probe at RT

Crystal purified with one vacuum pass to reduce residual phosphorus to N_D/N_A = 5.

5. Cut into cubes 40 x 40 x 20 mils.

6. Mount on heatsink.

2.4.4 Detector Data Evaluation

Measurements were made of detector properties under various combinations of bias voltage, temperature and background radiation. Whenever possible groups of detector samples were measured in close succession and under comparable sets of conditions in order to provide the best comparison of data. This was not possible in all cases. For example, the current-voltage characteristics of similar detectors might differ, presumably because of non-identical contacting. In such cases, best conditions for data collection were used and the data could be reduced to an assumed common basis (e.g., a common voltage) by simple ratio. This procedure appears adequate for the present purposes.

Samples fall into three groups. The first group consists of detectors fabricated from a set of different crystals each containing a different compensating donor X (X = Sb, Mn, Mg, Li). Data relating to this group of samples are contained in Figure 45 and Table 15. A second group consists of detectors fabricated from a single crystal (GZ 156) which was compensated by neutron transmutation (Si → P) to various controlled compensation ratios. Data relating to the group are contained in Figure 46 and Tables 16 and 17. Finally a group of samples prepared from a single crystal (GZ 065) which was compensated by residual phosphorus. Data for this group are contained in Tables 14, 18 and 19.
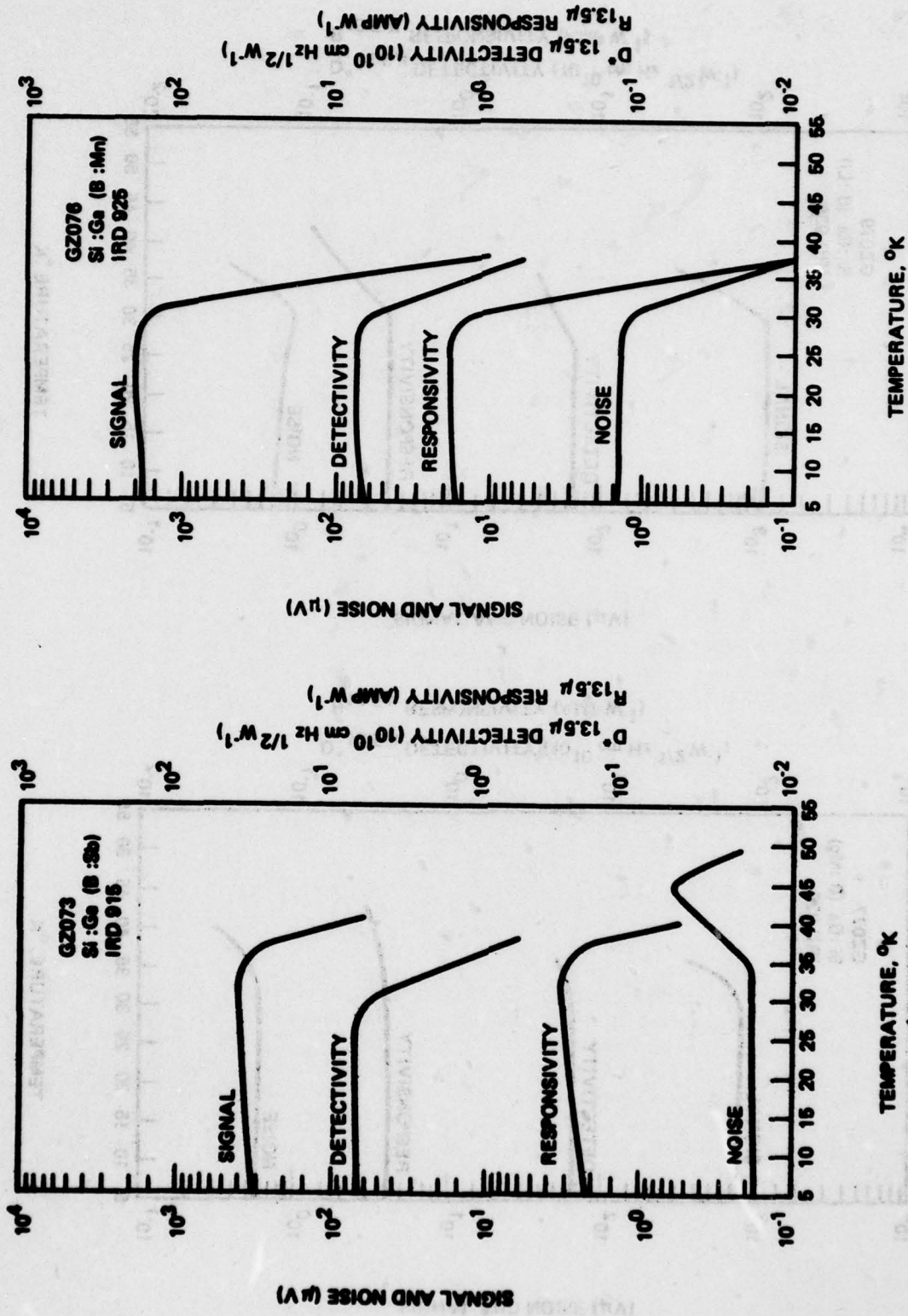
Figure 45.   Si:Ga Detector Performance vs Temperature
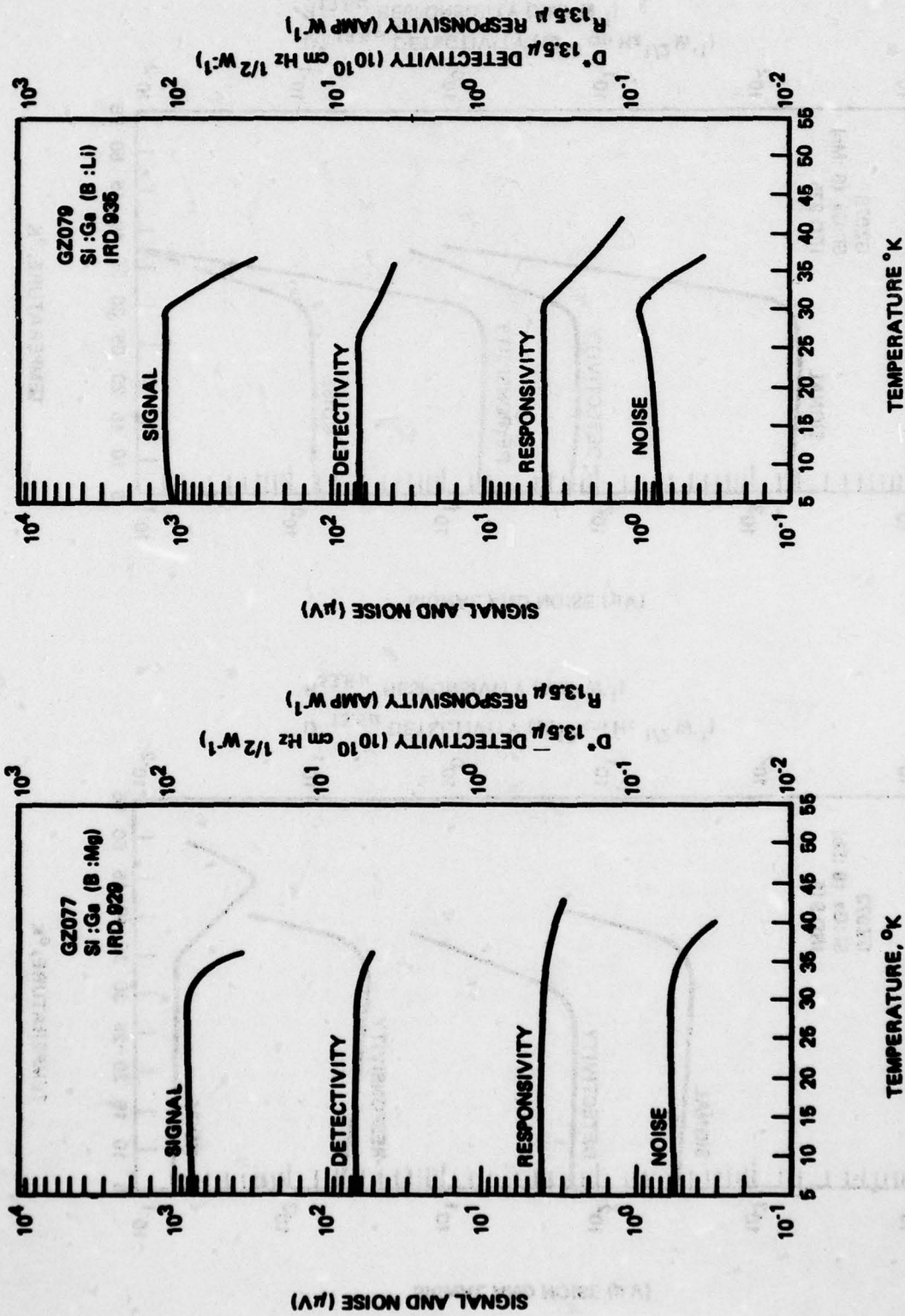
Figure 45. Si:Ga Detector Performance vs Temperature. (Concluded)

82

TABLE 15. LADIR MATERIAL DETECTOR TEST LOG, Si:Ga (B:X)

X = Sb, Mn, Mg, Li

T_{BB} 650°K Frequency 20 Hz; Aperture 0.032 inch
Background .52 x 10^5 ph/cm^2 sec

Detector Number	Wafer Number	Rockwell Crystal Number	Bias Voltage (V)	D*10°	D*16°	D*20°	D*22°	D*24°	D*26°	D* Roll Off	Temp (°k)	R Max	N_D/N_B
917	8	GZ 073	20	1.8	1.9	3.4	2.9	1.1	–	1.7	22	0.5	$N_{Sb}/NB \approx 0.28$
929	0	GZ 077	20	2.16	2.24	3.11	3.5	–	–	–	–	0.5	$N_{Mg}/NB < 1$
933	5	GZ 078	20	4.2	2.98	3.24	4.3	2.0	–	2.3	23	1.5	$N_{Li}/NB \approx 38$
925	3	GZ 076	20	3.0	2.1	1.7	1.5	–	–	–	–	0.9	$N_{Mn}/NB \sim 1$

83

TABLE 16. LADIR MATERIAL DETECTOR TEST LOG, Si:Ga (B:P), $N_{Ga} = 4.3 \times 10^{16}$, GZ 156.

T_{BB} 500°K; Frequency 20 Hz; Aperture 0.1 inch;
Background, 0.73 x 10^{17} ph/cm² sec

Boron Compensation by Nuclear Transmutation Doping

Detector Number	Crystal GZ 156 Wafer No.	NURR No.	Bias Voltage (V)	D*15°	D*20°	D*25°	D*30°	D*35°	D*40°	D* Roll Off	Temp (°K)	R 20°K	n (%)	N_P/N_B
1269	6	U 50	50	8.51	10.0	14.1	11.2	4.34	2.49	6.0	35	1.34	92	1
1268	9	A 51	50	8.24	8.24	5.80	9.88	5.0	2.1	4.0	35	1.2	46	1
1270	11	A 57	20	6.35	8.0	6.2	7.5	5.2	1.3	4.0	35	0.55	26	2
1270	14	U 58	50	9.3	10.0	10.0	9.5	8.0	1.0	5.0	37	0.85	26	3
1272	15	A 59	50	9.5	10.0	9.5	8.9	9.0	1.0	5.0	37	0.9	46	5
1273	16	U 60	50	12.9	12.9	12.9	12.2	9.0	1.6	6.0	36	1.0	77	5
1274	17	A 61	50	14.5	14.5	13.5	14.1	10.2	2.5	7.0	37	1.3	92	10
1275	18	U 62	50	9.0	10.2	10.2	9.5	6.2	1.3	5.0	35	0.95	48	10
1271	19	A 63	50	6.29	7.6	8.7	8.7	6.0	1.3	4.0	36	0.82	35	20
1276	20	U 64	50	11.5	11.2	10.0	9.5	8.0	1.3	5.5	36	0.85	61	20

U = Unannealed
A = Isochronal anneated Δ_T = 15 min. in argon

84

TABLE 17. LADIR MATERIAL DETECTOR TEST LOG, Si:Ga (B:P), N_{Ga} = 4.3 x 10^{16}, GZ 156.

Boron Compensation by Nuclear Transmutation Doping

T_{BB} 850°K, Frequency 20 Hz; Aperture 0.032 in.

Background 1.52 x 10^8 ph/cm² sec

Detector Number	Crystal GZ 156 Wafer No.	MURR No.	Bias Voltage (V)	D*10°	D*15°	D*20°	D*22°	D*24°	D*26°	D* Roll Off	D* Temp (°K)	R Max	Np/NB
1269	6	U 50	20	1.9	1.9	2.4	5.0	1.5	0.525	2.5	23	1.16	1
1268	9	A 51	20	1.7	1.37	3.04	6.35	1.09	-	3.0	23	1.12	1
1270	11	A 54	20	1.5	1.21	1.66	5.93	0.7	0.146	3.0	23	0.75	2
			80		3.95	7.82	4.48					4.08	
1278	14	U 58	20	1.3	0.8	1.99	5.25	1.9	0.263	2.5	23	0.8	3
			80		2.82	7.82	4.16					3.11	
1272	15	A 59	20	1.9	1.45	2.37	6.42	1.8	-	3.2	23	0.7	5
			80		3.9	5.5	3.8					4.5	
1273	16	U 60	20	1.75	1.8	1.9	5.5	1.7	-	2.8	22	0.8	5
			80		3.1	7.75	5.57					3.0	
1274	17	A 61	20	1.7	1.25	1.74	2.5	1.8	0.129	1.2	24	1.35	10
1275	18	U 62	20	0.9	0.8	2.1	5.8	8.0	0.18	4.0	25	0.74	10
1271	19	A 63	20	1.1	1.2	1.5	4.0	1.7	-	2.0	23	0.76	20
1276	20	U 64	20	1.28	0.856	1.75	5.0	1.32	-			0.826	20

U = Unannealed

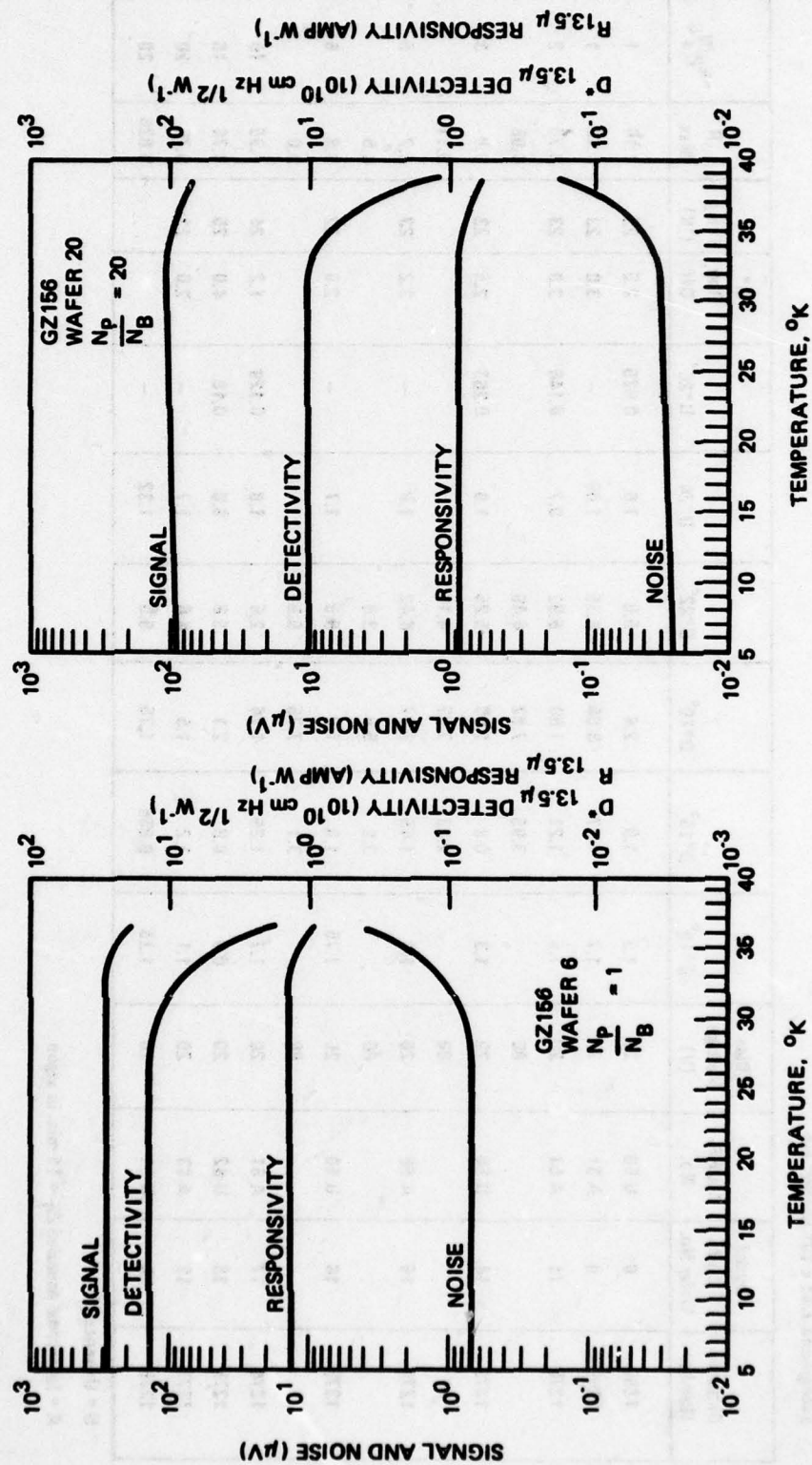A = Isochronal annealed Δ_T = 15 min. in argon

85

Figure 46a. Si:Ga Detector Performance vs Temperature; Boron Compensated by Neutron Transmutation Doping; High Background
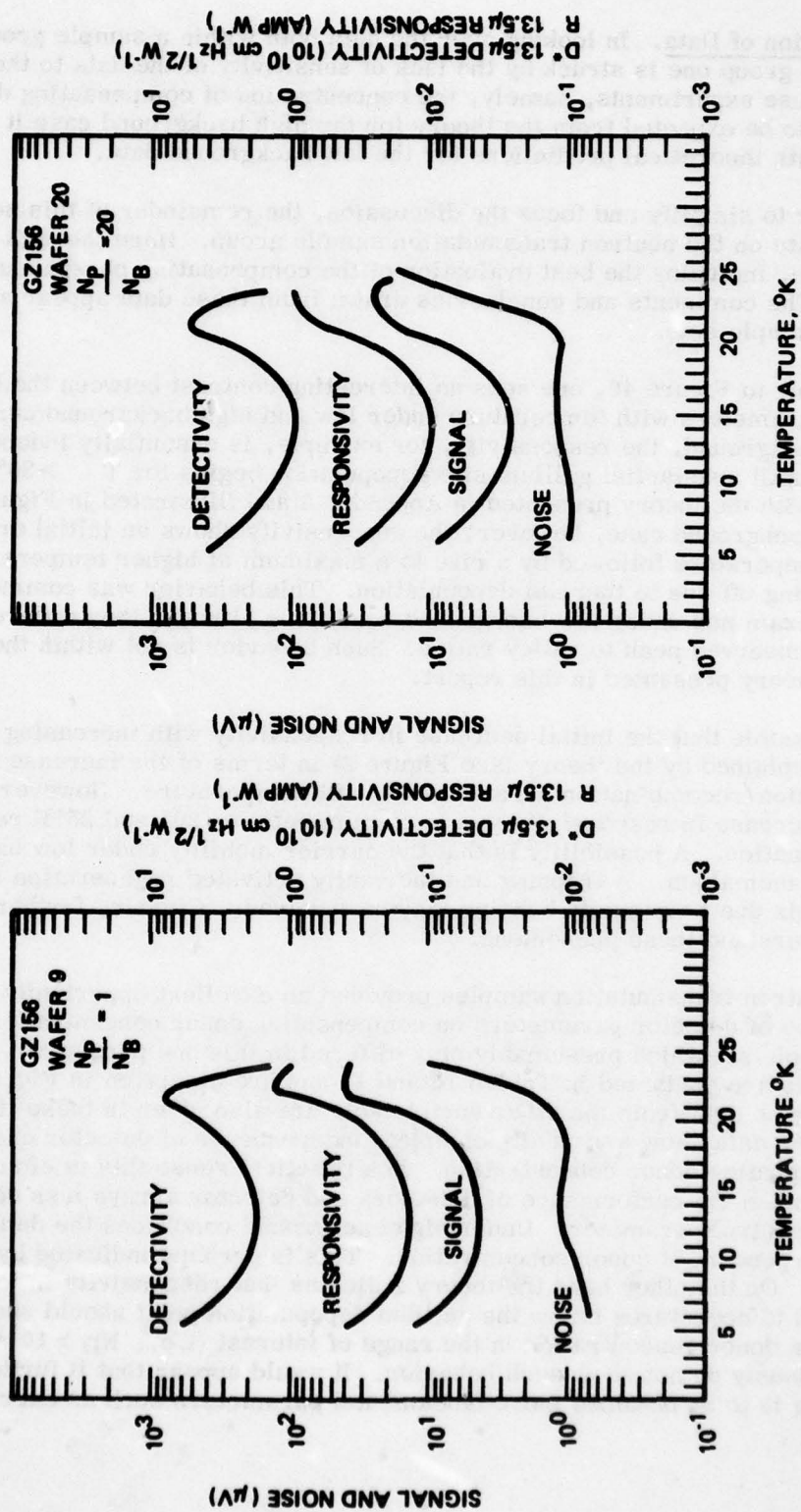
Figure 46b. Si:Ga Detector Performance vs Temperature; Boron Compensated by Neutron Transmutation Doping; Low Background.

MICROCOPY RESOLUTION TEST CHART

NATIONAL BUREAU OF
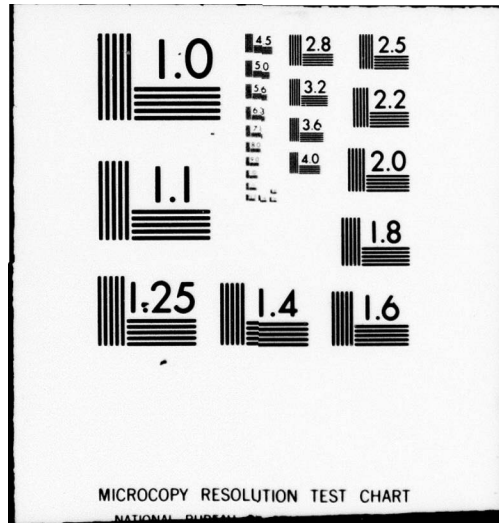
Discussion of Data. In looking over the data both within a sample group and from group to group one is struck by the lack of sensitivity of the data to the principal variable of these experiments, namely, the concentration of compensating donor. While this is to be expected from the theory for the high background case it stands at variance with theoretical predictions for the low background data.

In order to simplify and focus the discussion, the remainder of this section will concentrate on the neutron transmutation sample group. Here the data are most complete, including the best evaluation of the compensating phosphorus concentration. The comments and conclusions drawn from these data appear applicable to the other sample sets.

Referring to Figure 46, one sees an interesting contrast between the behavior of detector parameters with temperature under low and high background conditions. Under high background, the responsivity, for example, is essentially independent of temperature until substantial gallium site depopulation begins for T $> 30°$ K. This is in accord with the theory presented in Appendix A and illustrated in Figure 2. For the low background case, however, the responsivity shows an initial drop with increasing temperature followed by a rise to a maximum at higher temperatures prior to a final rolling off due to thermal depopulation. This behavior was common to all the samples examined under low background conditions although they differed to some extent in the observed peak to valley ratios. Such behavior is not within the framework of the theory presented in this report.

It is possible that the initial decrease in responsivity with increasing temperature can be explained by the theory (see Figure 2) in terms of the increase in the boron generation/recombination parameter α_B with temperature. However, the subsequent increase in responsivity to a maximum between $20°$ and $25°$ K requires another explanation. A possibility is that the carrier mobility under low background conditions is anomalous. A trapping and thermally activated regeneration mechanism or some effects due to impurity banding may be involved. Clearly, further study is needed to understand these phenomena.

The neutron transmutation samples provided an excellent opportunity to test the dependence of detector parameters on compensating donor concentration in a coherent sample set which presumably only differed in this one parameter. Data relative to this are contained in Tables 16 and 17 and are displayed in Figures 47, 48 and 49. Some data from the other sample sets are also given in these figures. In all cases the data show a virtually complete independence of detector characteristics to compensating donor concentration. In a practical sense this is of some value since it will make the performance of detectors and detector arrays less dependent on a difficult to control parameter. Under high background conditions the detectivity should be independent of donor concentration. This is perhaps indicated by the data of Figure 47. On the other hand the theory indicates that responsivity in low backgrounds at all temperatures below the gallium depopulation point should show a dependence on donor concentration in the range of interest (i.e., $N_D > 10^{12}$ cm^{-3}). The data obviously do not show such behavior. It would appear that if further understanding is to be obtained more fundamental parameters such as carrier density,

TABLE 18. LADIR MATERIAL DETECTOR TEST LOG, Si:Ga (B:P), GZ 065, WAFER 21

T_{BB} 500°K; Frequency 20 Hz; Aperture 0.025 inch;
Background, 1.3 x 10^17 ph/cm^2 sec

Detector Number	Opt. Bias	D*7°K	D*10	D*15	D*20	D*25	D*30	D* Roll Off	Temp (°K)	R 20°K	η (%)
1098	+42	3.67	5.64	8.61	8.51	3.88	8.58	3.78	34°	1.5	62
1099*	+60	3.29	4.95	5.30	4.84	4.50	3.16	1.17	33.6°	1.4	24
1100	+60	5.15	8.08	6.53	8.20	7.49	6.63	3.57	33.2°	1.5	57
1101*	+8	0.864	1.25	1.58	1.67	1.25	1.25	1.0	32°	0.18	3
1121*	+15	2.29	3.14	4.25	4.74	5.12	5.35	3.94	35°	0.32	24
1159	+42	2.85	4.16	4.74	5.19	5.99	5.76	1.87	33°	1.5	30
1160	+42	7.71	7.51	7.99	8.25	8.54	7.13	5.40	30.5°	1.3	62
1161	+42	3.78	4.98	5.98	7.27	7.46	7.22	2.58	33°	1.2	47
1162	+42	4.95	5.15	7.92	8.0	7.38	7.10	3.4	35°	1.0	54
1163	+42	7.61	7.08	7.28	7.44	7.68	7.75	4.44 (35°)	1.89 (36°)	0.6	51
1164	+36	7.26	8.20	8.46	7.78	7.74	7.74	3.65	35°	0.6	61
1165	+60	8.32	8.43	8.44	8.77	8.88	6.94	4.90	31°	1.1	67
1166	+42	7.23	8.26	9.67	10.8	9.12	8.24	3.39	35°	1.15	96

$D^* = D^*_{15.5\ \mu m}\ 10^{10}$ Detectivity (cm Hz$^{1/2}$ Watt^{-1})

R = Responsivity (Ampere Watt^{-1})

η = Quantum Efficiency

*These three detectors were scraped and cleaned and then retested with no significant change in results.

89

TABLE 19. LADIR MATERIAL DETECTOR TEST LOG, Si:Ga (B:P), GZ 065, WAFER 21

T_{BB}, 650°K; Frequency, 20 Hz; Aperture, 0.032 inch;
Background, 1.33×10^8 ph/cm^2 sec

Detector Number	Opt. Bias	D*7°	D*10°	D*15°	D*20°	D*22°	R 7°K	n (%)
1098	+40	48.2	31.5	14.9	3.73	0.149	2.6	2.0
1099	+50	57.1	49.8	39.4	10.8	7.37	4.2	3.1
1100	+40	55.53	45.6	17.4	6.85	0.768	3.8	2.9
1101	+40	66.82	35.79	19.05	5.60	0.597	4.5	4.2
1121	+35	46.38	36.5	16.66	4.67	0.332	3.8	2.0

Opt. Bias = Optimum Bias (Volts)

$D^* = D^*_{14.8 \mu m} \times F$ Detectivity (cm Hz$^{1/2}$ Watt^{-1})

R = Responsivity (Ampere Watt^{-1})

F = Multiplication Factor for Low Background D*

mobility and lifetime should be measured under detector-like conditions. Measurements of engineering quantities such as responsivity and detectivity do not afford sufficient visibility of the basic phenomena.

In summary, detectivity and responsivity measurements were made for a variety of crystals all of which had closely identical gallium and residual boron levels but which differed in the identity and concentration of the compensating donor. No effects were observed which indicated a dependence on the type or concentration of these donors, at variance with some aspects of theory. The temperature dependence of detector parameters showed a dependence on the background radiation level. At high background levels these parameters are temperature independent up to about 30° K. At low background levels they show a complex behavior which is not understood.

NOTE: BORON COMPENSATED BY NUCLEAR TRANSMUTATION DOPING

THEORETICAL D* T<30 °K

N_{BORON} = 1 × 10^{12}
Q_{BG} = 1 × 10^{17} ph/cm^2 sec

EXPERIMENTAL T = 25 °K

N_{BORON} ≅ 5 × 10^{12}
Q_{BG} = 0.7 × 10^{17} ph/cm^2 sec

N_D DONOR CONCENTRATION (cm^{-3})

D* DETECTIVITY (cm Hz 1/2 WATT^{-1})
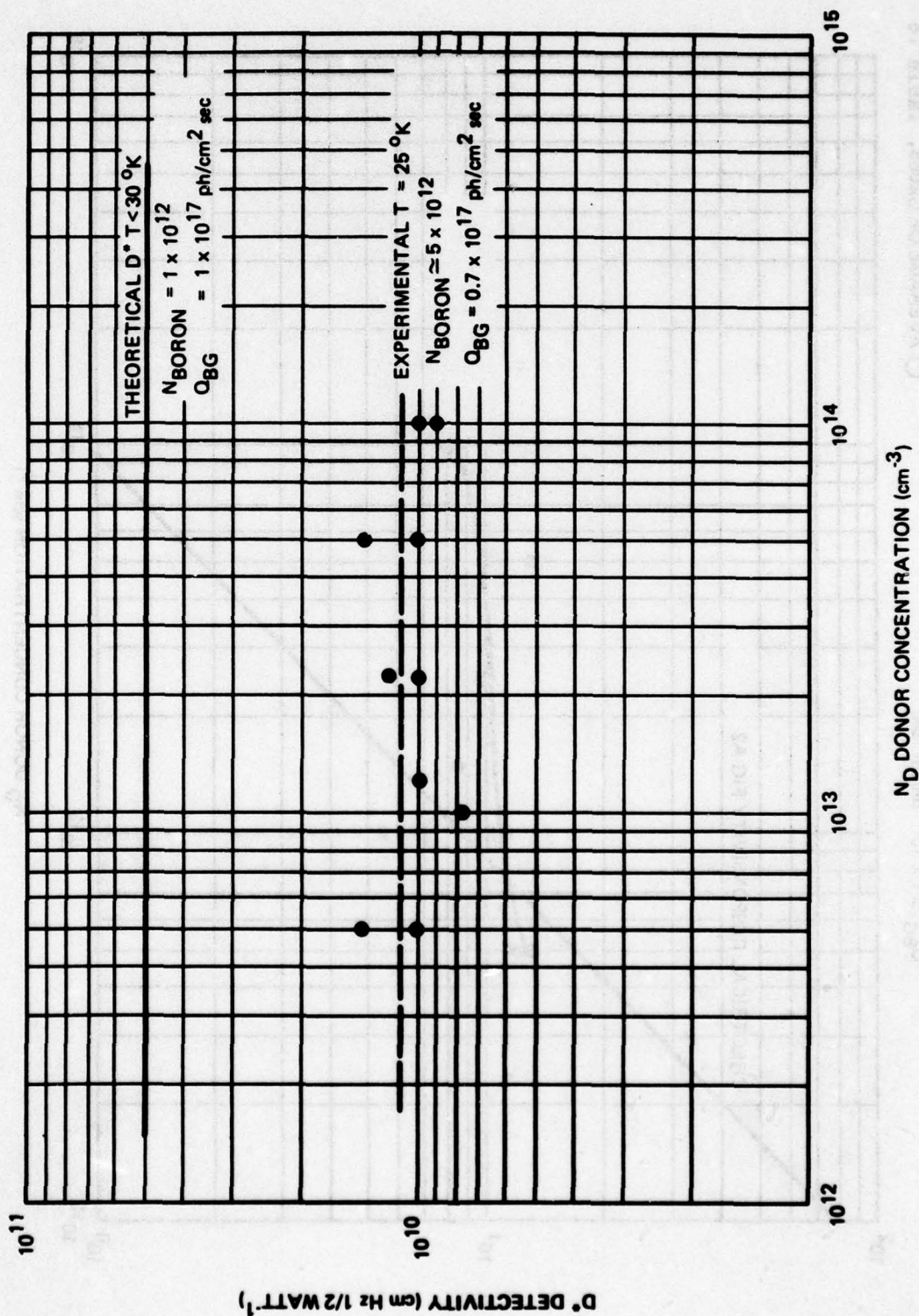
Figure 47. Detectivity D* at High Background, Crystal GZ 156.

91
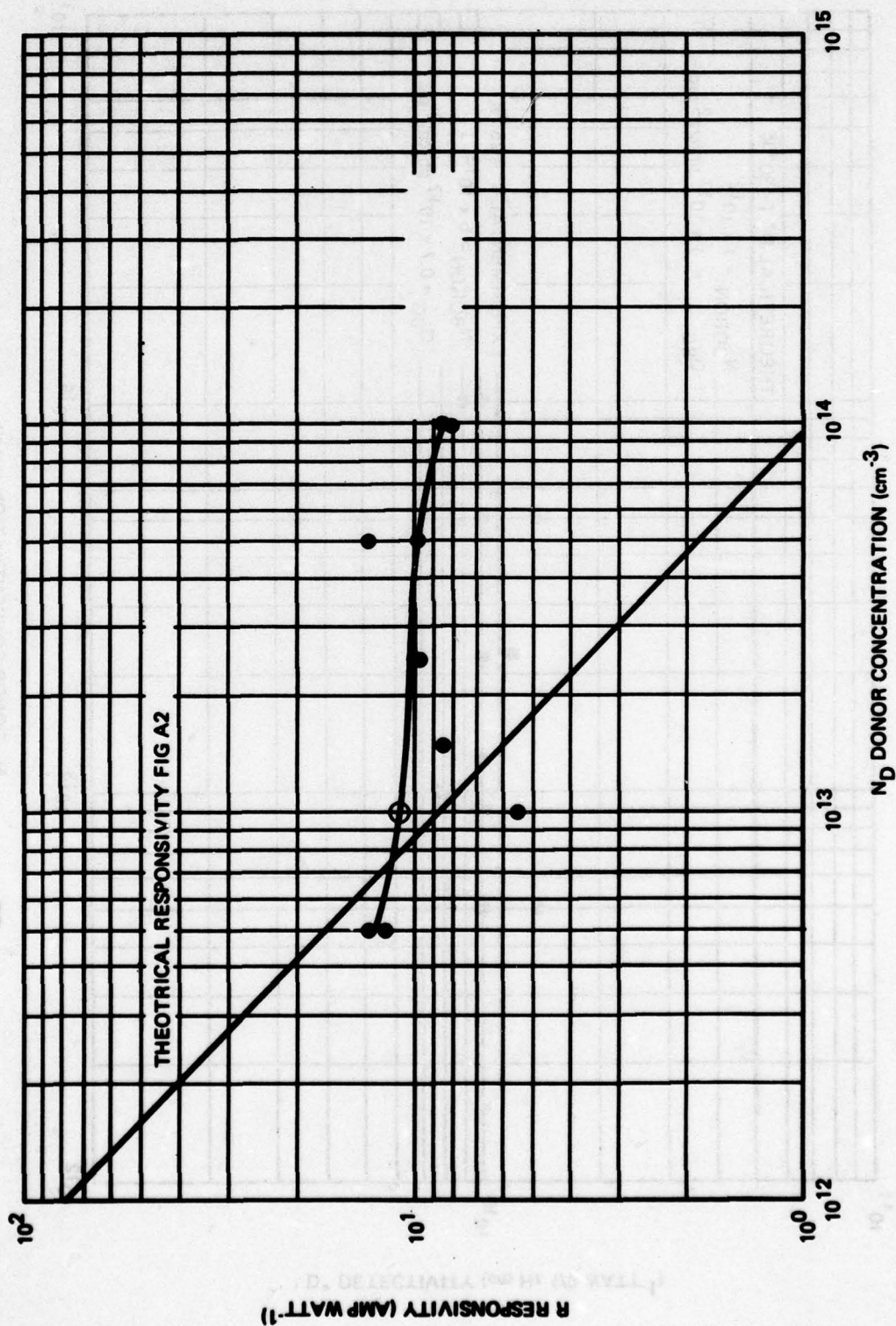
Figure 48. Responsivity at High Background.

Figure 49. Responsivity at Low Background

SECTION III

TASK IV DEFINITION OF THE GROWTH PROCESS

This section describes the growth process, equipment setup, and processing steps recommended to produce single crystal, boron compensated, gallium doped silicon.

3.1 GENERAL DISCUSSION OF EQUIPMENT AND ENVIRONMENT

Two float zoners, one a vacuum and the other gas, are required to grow highly purified, boron compensated, gallium doped single crystals. The initial purification of t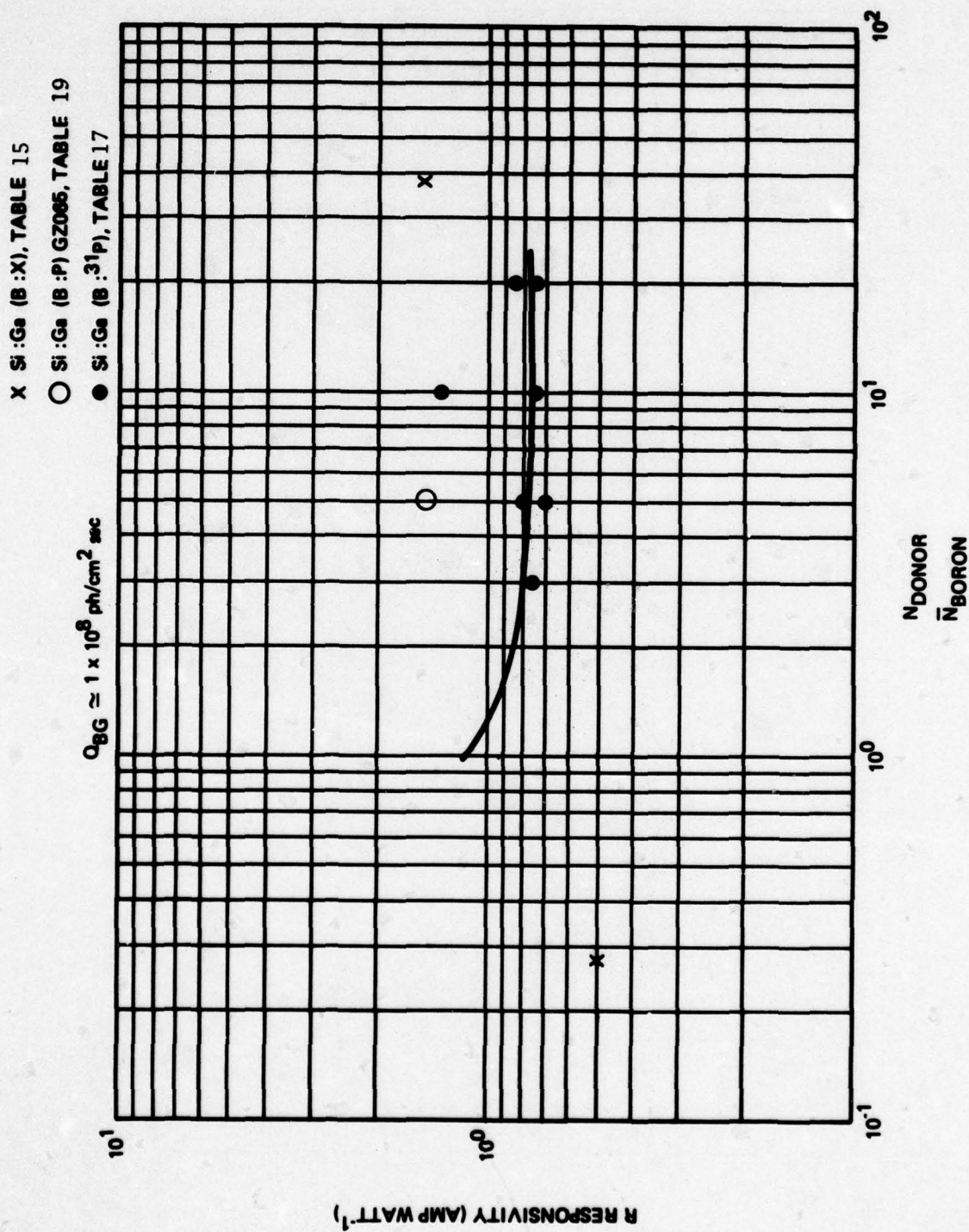he polysilicon is conducted in a vacuum float zoner which is assigned exclusively to this task to prevent contamination from doping runs. The gas zoner is used to grow single silicon crystals when chosen impurities are added during the final crystal growth. Preferably, the gas zoner is also used with only one kind of dopant.

Further, the achievement of uniform impurity distribution within a crystal with good crystallographic properties requires that

1. The entire float zoner be on a vibration free mount.

2. The construction of the float zoner provide smooth, vibration-free motion of all moving parts, thus achieving a vibration-free molten zone during the crystal growth process.

3. Precise power control over the entire range of growth be maintained.

Other requirements are clean facilities for etching, solvent cleaning and, if possible, cascade rinsing; a drying oven, used exclusively for silicon and parts used in this procedure; acids and solvents of semiconductor grade; DI water with greater than 18 MΩ resistance; and a laminar flow hood for cleaning and assembling the furnace parts.

The area immediately surrounding the float zoner should be dust free to prevent contamination while cleaning and setting up the equipment as well as processing the crystals.

3.2 FLOAT ZONER CONSIDERATIONS

The float zoner components of specific concern are discussed in this section.

3.2.1 Carbon Preheater

The carbon disk preheater must be fabricated from ultra pure carbon and should be outgassed by the manufacturer prior to delivery. A new carbon preheater is recommended for every run.

95

3.2.2 RF Coil

Each float zoner model requires a matched RF coil designed to optimize its operation. Some of the considerations in the design of an induction coil for float zoning are as follows:

1. A major consideration is the choice of a single or a multi-turn coil. This choice is a function of the power of the RF generator, the diameter of the silicon rod, the ability to couple between the silicon rod and coil, and the sensitivity of the power control system. A single turn heating coil results in less voltage across the connecting terminals and makes it possible to control heat application within a small rod (i.e., approximately 1/32 inch). The multi-turn coil is used where it is necessary to get maximum energy into a wider work piece such as a 7/8 inch silicon ingot. The spacing of the turns depends upon the applied voltage and the field concentration needed around the work piece.

2. The metallic fixture components must be non-magnetic to minimize heat and current losses.

3. The leads from the heating coil used to attach the induction heater terminals should be kept as close together as is compatible with the voltage being used.

A four-turn silver braised copper coil is typical for this application (see Figure 50). The coil tubing is slightly flattened to reduce the space between the turns, resulting in a higher concentration RF field around the ingot and the ability to more
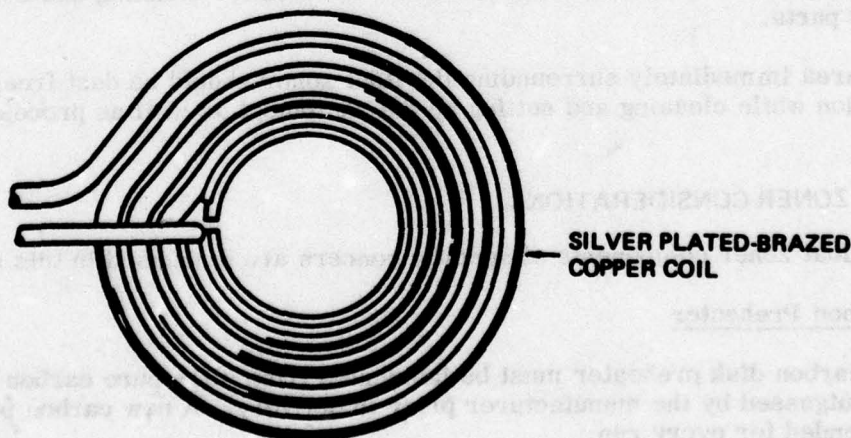

SILVER PLATED-BRAZED
COPPER COIL

Figure 50. Typical Four-turn Induction Coil.

96

accurately control crystal diameter. The more concentrated RF field of the closely spaced multiple turn coil also provides the desired slightly concave interface which minimizes super-cooling at the growth interface. However, sometimes the multi-turn coil causes difficulties in controlling the growth of the thin neck while starting the crystal for dislocation free growth.

An additional consideration is the surface texture of the coil, which must be rough (achieved by sandblasting) to allow the evaporated silicon to adhere to it. A completely smooth coil will allow the deposited silicon to flake off and contaminate the just solidified crystal area. The cleaning procedures are discussed in Section 3.4.

3.3 POLYSILICON MATERIAL

The basic polysilicon material can be purchased at different quality levels as defined by the residual boron content. For the LADIR program, a boron content of approximately 10^{12} cm^{-3} is required. It must be emphasized that procurement of material with this low impurity level is, in itself, not enough. The specific impurity level characterized by the supplier is an average and varies between the individual polyrods. Because of this, every precaution must be taken to avoid the inadvertent addition of contaminant during the entire procedure, beginning with the material supplier. At the supplier's, the rods are usually handled and packed without contact by bare hands, then sealed and shipped in plastic envelopes. Upon receipt at the crystal growing laboratory, they must be stored in a dry, clean enclosure and removed from the plastic envelopes only when inserted into the float zoner. If it is assumed that these precautions have been observed then no etching and cleaning of the polysilicon is necessary.

3.4 CLEANING PROCEDURES

Before the growth process is started, the float zoners, prezoned ingots, and seeds are cleaned. The cleaning procedures presented in the following subsections were developed for Rockwell equipment but, with modifications, can be applied to any equivalent equipment.

3.4.1 Float Zoner Cleaning Procedure

The float zoners* (vacuum and gas) are initially cleaned according to the manufacturer's specifications and instructions. After this initial cleaning, a purified silicon crystal should be grown in the zoner. The silicon evaporates from the liquid zone and deposits on the walls and door of the chamber. This deposit provides a wall cover of the most desirable material. For the time that this silicon coating covers the walls evenly, the following cleaning procedure is used.

1. Remove the work coil and etch it in a solution of approximately 3 to 4 gm NaOH in approximately 350 ml H$_2$O to remove evaporant coating, place in ultrasonic cleaner to hasten removal, etch until coil is clean (usually 15 to 20 min), and rinse in DI H$_2$O for about 1/2 hour and dry.

---

*VS A3 Model, Siemens, A.G., D-8000, Muenchen 1, Germany

2. Remove and discard the glass window. Remove carbon preheater, quartz support rod, and quartz panels from the shutter. Etch quartz pieces in 3 HNO_3 1 HF solution until deposit is removed (usually 1 to 3 min), rinse in DI H_2O for 1/4 hour. Wrap in lint free paper and dry in special, clean oven at 125°C for 1/2 hour min.

3. Wipe out chamber with "K-Dry."* Remove any coating that is not firmly attached to the wall.

4. Blow out chamber using pressurized nitrogen gas.

5. Replace coil and align.

6. Replace quartz support rod and install new carbon preheater.

7. Clean new window with DI H_2O and dry with K-Dry towel.

8. Install window and wipe door gasket and seal surface with K-Dry towel.

When blistering and peeling of the silicon coating are apparent, the following cleaning process is used. Again, this procedure was developed for use on the Rockwell float zoners but can be modified for use on any type zoner.

1. Remove the work coil and etch it in a solution of approximately 3 to 4 gm NaOH in approximately 350 ml H_2O to remove evaporant coating, place in ultrasonic cleaner to hasten removal, etch until coil is clean (usually 15 to 20 min), and rinse in DI H_2O for about 1/2 hour and dry.

2. Remove and discard the glass window. Remove carbon preheater, quartz support rod, and quartz panels from the shutter. Etch quartz pieces in 3 HNO_3 1 HF solution until deposit is removed (usually 1 to 3 min), rinse in DI H_2O for 1/4 hour. Wrap in lint free paper and dry in special, clean oven at 125°C for 1/2 hour min.

3. Using a stainless steel brush, scrub the chamber walls vigorously, removing all flaking and blistered material. Then thoroughly vacuum the chamber.

4. Using K-Dry and isopropyl alcohol, wash walls down until K-Dry appears clean.

5. Let chamber air dry and then wipe walls with dry K-Dry.

6. Blow out chamber using pressurized nitrogen gas.

7. Replace coil and align.

8. Replace quartz support rod and install new carbon preheater.

---

*Product of Nolex Paper Company, 6600 Valley View Ave, Buena Park, CA 90261

9. Clean new window with DI H_2O and dry with K-Dry towel.

10. Install window and wipe door gasket and seal surface with K-Dry towel.

3.4.2 Zoned Ingot and Seed Cleaning Procedure

The following etching procedure specifies the cleaning process for a zoned silicon ingot or a seed. At all times, the ingot or seed must be handled using clean plastic gloves.

1. Place ingot or seed in polyethylene etch sling.

2. Place in a plastic etch boat.

3. Put DI (deionized 18 M) H_2O into another large etch boat.

4. Pour etching solution 3 HNO_3-1 HF into etch boat containing the ingot or seed.

5. Agitate for approximately 3 min in the etch solution.

6. Quickly remove the ingot or seed and plunge it into DI H_2O rinse.

7. Rinse for 1/2 hour (minimum) in flowing DI water.

8. Remove the ingot or seed, dry with lint free paper, and wrap in clean lint free paper.

9. Place in the special dryer for 1/2 hour minimum, at ~100°C.

10. Cool in clean bench before installing in zoner.

3.5 FLOAT ZONER PREPARATION

The cleaned coil is installed and aligned. A new carbon preheater is installed and positioned above the coil. After the chamber is evacuated to approximately 10^{-5} torr, RF power is turned on and the carbon preheater temperature is elevated to a white color for outgassing. The vacuum level changes during this process and the outgassing of the carbon continues until the vacuum steadies again at approximately 10^{-5} torr. The power is turned off and the chamber stays under high vacuum for a minimum of four hours.

3.6 SINGLE CRYSTAL SEED CONSIDERATIONS

Crystal growth in the required orientation is initiated by a seed of the desired characteristics. This seed must be cut from a crystal of <100> growth orientation. The following considerations are applicable when using a single crystal as seed material:

1. The single crystal-seed crystal should have a minimum of six zone passes and a boron concentration of less than 3×10^{12} cm^{-3}. Its purity should be comparable to the desired quality of the crystal to be grown.

2. The crystal must be oriented to the desired orientation within ±0.5 deg. Any deviation can be measured by taking X-ray Laue photographs

3. The seed crystal should not have an extensive amount of lineage as it would create problems in connecting the crystal boule to start a single crystal.

Under proper conditions the dislocation density of the seed does not affect the dislocation density in the growing crystal, nor do the additional defects which occur from thermal shock when the silicon liquid drop connects with the solid seed. These conditions involve the growth of a long thin neck between the seed end and the crystal to eliminate the defect lines which grow out to the surface preventing their continuation into the crystal bulk.

3.7 VACUUM FLOAT ZONING PROCEDURE

After preparing the zoner and seed per Sections 3.4 and 3.5, the seed is inserted into the seed holder. The operator must wear plastic gloves and hold the seed by the sides with lint free paper. The seed end which will connect with the liquid zone must not be handled at all. Proper alignment and good rotation of the seed in the seed holder must be achieved. After the polysilicon rod is clamped into the holder, the seed, rod, and coil must be properly aligned. The chamber is evacuated to approximately 10^{-5} torr; an overnight pump down is recommended. Then, multiple zone passing is performed.

The acceptor and donor concentration of the polysilicon were specified by the supplier. The donor concentration, which is mainly phosphorus, generally exceeds the boron concentration by an order of magnitude. Figures 51 and 52 provide the data for the reduction rate of phosphorus at a given growth rate (coil speed). For example, a six-pass purification of Dow Corning silicon (see Figure 52) would reduce the donor concentration to approximately 3×10^{11} cm^{-3}. The silicon crystal will show a conductivity or resistivity corresponding to $N_A - N_D$. After six vacuum passes, the donor concentration, N_D, will be more than one order of magnitude smaller than the acceptor concentration, N_A; therefore, the resistivity evaluation will basically reflect the boron level only. This boron concentration should be the same as the acceptor concentration given by the polysilicon supplier. In the case of a drastic increase in acceptor concentration, the growing of a test crystal is recommended. This procedure will verify the type of impurity and the amount added with each pass.

A diagram of a suggested test crystal is shown in Figure 4. This crystal is called the 1-2-3-7 pass crystal, which permits evaluation of the donor in the 1-2 pass section and the acceptor concentration in the crystal as the material is exposed to the multiple-zone process. The amount of impurities remaining in different parts of the crystal are determined by resistivity and conductivity type measurements. The measurements have to be taken, as indicated, in the center of the rod area with constant diameter. The undercuts on the ingot are the last frozen liquid zones and contain the impurities which have been removed. This test crystal will verify the amount of impurity added with every pass. If heavy contamination is detected, corrective measures must be taken.
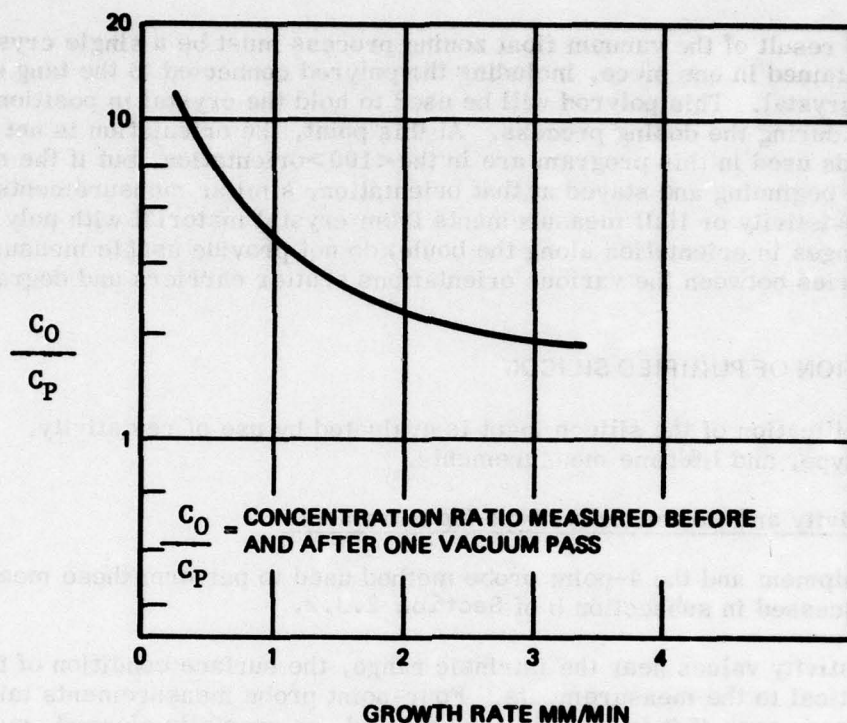
The end result of the vacuum float zoning process must be a single crystal which is maintained in one piece, including the polycrystal remnant at the long end of the single crystal. This solved will be used to hold the crystal in position in the gas zone during the zoning process. At some point, the impurities in the crystal test. All seeds used in this program are in the <100> orientation, and if the crystal thinned in the beginning and salvaged at the orientation. Structural breakdowns can be achieved. The latticle or if it measurements along the crystal boule with only characteristic lattice defects in orientation along the boule does not provide useful measurements as the boundaries between the various orientations tend to enter and degrade the data.

3.5 EVALUATION OF PURIFIED SILICON

The purification of the silicon boule is verified by resistivity, chemical analysis, and lifetime measurements.

3.5.1 Resistivity

The equipment and the 4-point-probe method used to make the resistivity measurements are discussed in subsection 3 of Section 3.3.1.2.

At resistivity values near the intrinsic range, the surface condition of the crystal is critical to the measurement. Measurement probe measurements taken at the input surface, even if it is a freshly cleaved surface, or specially cleaned, may not reflect the true resistivity of the bulk crystal. Techniques developed to achieve reliable data is shown in Figure 29. A 0.8 to 1 cm thin strip is lapped along the crystal. The final cut seed should be cut. After lapping, the crystal should be given a surface cleaning solution and rinsed in DI water. The ASTM standards book, Volume 43, F43 and F42, was consulted for guidance on surface preparation. The bulk concentration, the 4-point-probe of the center of the crystal will return along the boule.

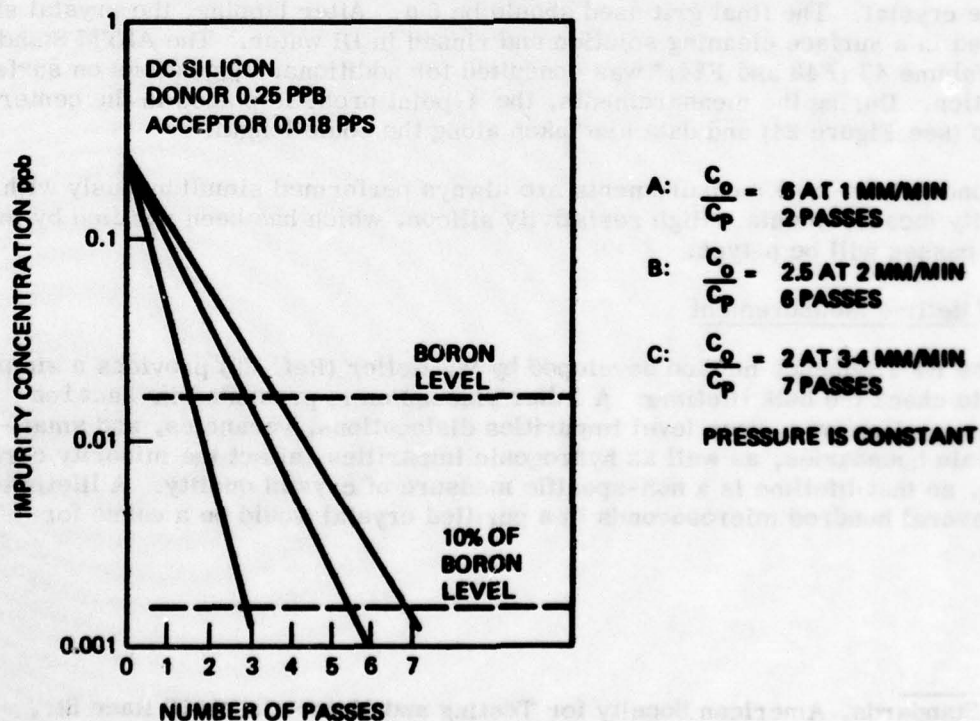Figure 51. Phosphorus Reduction During Silicon Purification.

Figure 52. Donor Reduction by Vacuum Float Zoning.

101

The end result of the vacuum float zoning process must be a single crystal which is maintained in one piece, including the polyrod connected to the tang end of the single crystal. This polyrod will be used to hold the crystal in position in the gas zoner during the doping process. At this point, the orientation is not important. All seeds used in this program are in the <100> orientation, but if the crystal twinned in the beginning and stayed at that orientation, similar measurements can be achieved. Resistivity or Hall measurements from crystal material with poly characteristics (changes in orientation along the boule) do not provide usable measurements as the boundaries between the various orientations scatter carriers and degrade the data.

3.8 EVALUATION OF PURIFIED SILICON

The purification of the silicon ingot is evaluated by use of resistivity, conductivity-type, and lifetime measurements.

3.8.1 Resistivity and Conductivity-Type Measurements

The equipment and the 4-point probe method used to perform these measurements are discussed in subsection b of Section 2.3.2.

At resistivity values near the intrinsic range, the surface condition of the crystal is critical to the measurements. Four-point probe measurements taken at the ingot surface, even if it is etched, sand blasted, or specially cleaned, may not reflect the impurity characteristics of the bulk silicon crystal. The method developed to achieve reliable tests is shown in Figure 24. A 0.8 to 1 cm wide strip is lapped along the crystal. The final grit used should be 5 μ. After lapping, the crystal should be washed in a surface cleaning solution and rinsed in DI water. The ASTM Standards Book, Volume 43 (F43 and F84)* was consulted for additional suggestions on surface preparation. During the measurements, the 4-point probe is placed in the center of the strip (see Figure 24) and data are taken along the boule length.

Conductivity-type measurements are always performed simultaneously with the resistivity measurements. High resistivity silicon, which has been purified by multi-vacuum passes will be p-type.

3.8.2 Lifetime Measurement

The RF frequency method developed by W. Keller (Ref. 32) provides a simple method to check the bulk lifetime. A fuller discussion is presented in Section 2.3.3. However, deep level impurities dislocations, vacancies, and small-angle grain boundaries, as well as hydrogenic impurities, affect the minority carrier lifetime, so that lifetime is a non-specific measure of crystal quality. A lifetime below several hundred microseconds in a purified crystal would be a cause for concern.

---

*ASTM Standards, American Soceity for Testing and Materials, 1916 Race St., Philadelphia, PA.

3.9 DOPANT CONSIDERATIONS

The results obtained in this program do not conclusively indicate that counter-doping of residual boron is effective in controlling detector performance. However, of the various counter dopants employed only antimony provides the necessary convenience and control.

The amount of either dopant, antimony or gallium, is calculated according to Eq (16). However, in calculating the amount of antimony, a safety factor of between 1.2 X and 1.5 X should be included to assure complete compensation because resistivity measurements of high purity silicon are subject to considerable uncertainty. Excess n-type donors at a concentration of approximately 3×10^{12} cm^{-3} will negligibly compensate the gallium impurity which is added at a much larger concentration of 10^{16} to 10^{17} cm^{-3}. Under operating conditions such that the steady state number of ionized gallium counters is of the order of 10^{12} cm^{-3} the Ga compensation is of no importance.

3.10 SILICON CRYSTAL PREPARATION

The chosen dopants can be introduced into the purified crystal in two different ways. As illustrated in Figure 53, the material may be placed into a slot, which has been cut into the boule, or in a cup, which is formed by cutting the boule in two, machining out a cup, and subsequently welding the boule back together. Depending upon which method is chosen, the following additional handling precautions must be observed.
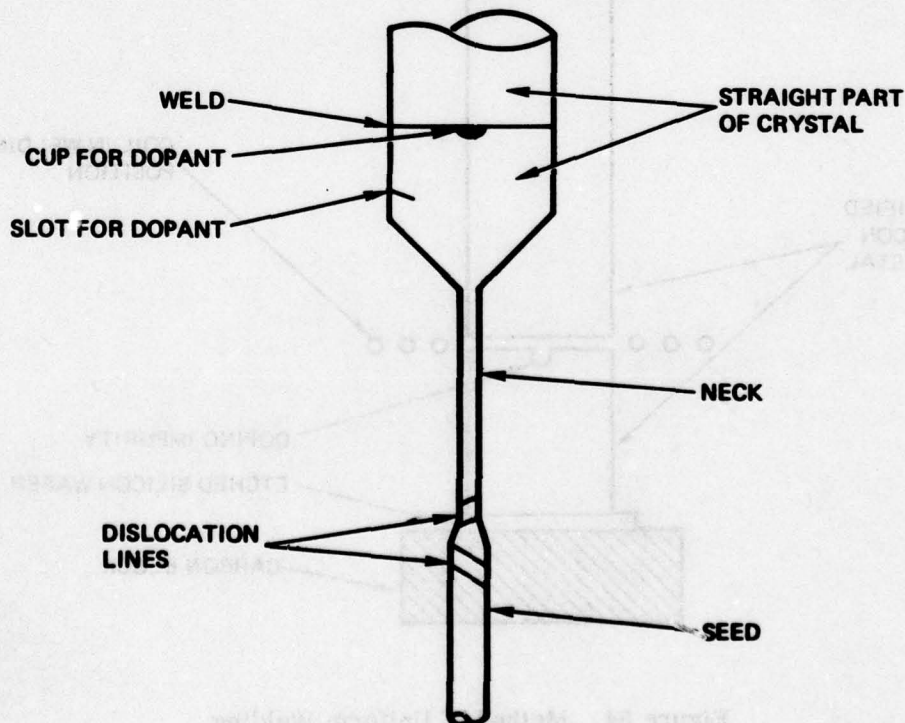
Figure 53. Method for Dislocation-free Crystal Growth.

103

3.10.1 <u>Slot</u>

The cut is easy to make, but when etching and rinsing the rod prior to crystal growth, great care must be taken to insure that the cut does not hold residual acid or moisture. Also, when adding the impurities into the slot, they must be protected from sudden air motion and shock. When placing the ingot into the chamber, the cut must be located so that it does not point in the direction of the vacuum port or inert gas inlet; and, finally, the closing of the chamber door must be performed slowly.

3.10.2 <u>Welded Cup</u>

In this method, care must be taken to insure that the weld is sealed uniformly (see Figure 54). During the sealing process, a carbon block is used as the support. To prevent contact between the crystal and the carbon, an etched silicon slice is placed between them. The crystal prepared for doping must be etched and cleaned according to the procedure in Section 3.4.

3.11 GROWTH OF DOPED CRYSTAL IN GAS FLOAT ZONER

The cleaning procedures for the zoner, ingot, and seed are presented in Section 3.4. The zoner setup is the same as for the vacuum float zoner except for the addition of the dopant into the ingot.

PURIFIED
SILICON
CRYSTAL

COIL IN WELDING
POSITION

DOPING IMPURITY

ETCHED SILICON WAFER

CARBON BLOCK
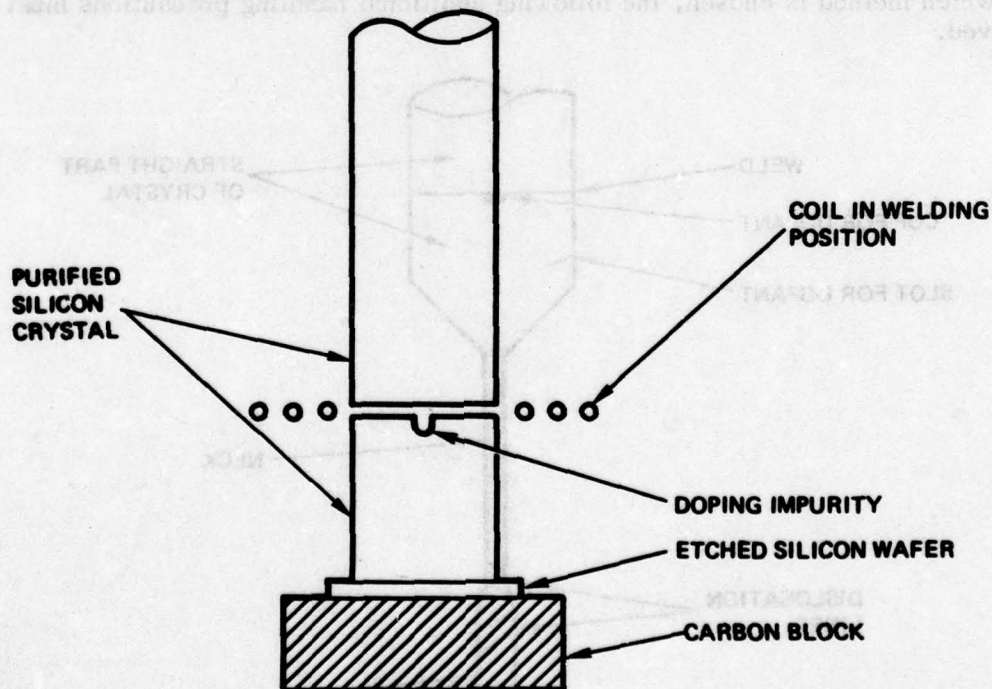
Figure 54. Method of Uniform Welding.

104

The gas float zoning process achieves the final growth and provides the silicon with the intentionally added dopant while solidifying it into a single crystal of desired perfection. The desired perfection includes freedom from dislocations, a minimum of vacancy clusters, and a uniform impurity (compensation and gallium dopant) distribution.

3.11.1 Dislocation-Free Growth

The Dash method (Ref. 47) is based on the idea that dislocation originate from the seed bulk and from thermal shock propagated by the seeding process. A reduction of the dislocations is achieved by growing a very thin neck on the seed. This extended seed growth is controlled by a large increase in growth rate, two to three times the growth rate used for the crystal growth on the straight part of the boule. After this initial growth of a very thin seed extension, the dislocations in the seed and those generated by the thermal shock propagate to the surface and disappear (see Figure 53). The crystal diameter can now be increased to grow a dislocation free crystal of the desired diameter.

3.11.2 Vacancy Clusters

As the dislocation-free crystal solidifies, the vacancies, which otherwise absorb defects, collect and build vacancy cluster formations. These vacancy clusters will associate with impurity atoms such as copper, lithium and oxygen during wafer processing at elevated temperature. These undesirable effects make it necessary to eliminate the buildup of vacancy clusters during the crystal growth. It was established that these defects form during the cooling period of the crystal; therefore, a crystal growth rate of 3.5 to 4.5 mm/min is recommended for the straight part of the crystal.[48]

3.12 EVALUATION OF DOPED CRYSTALS

The evaluation of the doped crystals is performed the same way as the evaluation of the purified silicon ingot, i.e., through the use of resistivity, conductivity-type and lifetime measurements. Therefore, the procedure presented in Section 3.8, is applicable.

3.13 TEST FAILURE

If instrumentation failure should occur or if the operator is unable to hold the liquid zone, the two ingot parts will separate, spilling silicon into the growth chamber. In such a case, the process should be discontinued. It is recommended that the ingot parts be discarded unless this occurs late in the process.

---

47. Dash, W.C., "Method of Growing Dislocation-Free Semiconductor Crystals", June 2, 1964, Patent No. 3,135,585, filed March 1, 1960.
48. Huff, H.R. and Burgess R.R., "Semiconductor Silicon 1973", Electro-Chem. Soc., pp 83-93, 1973.

3.14 BORON COMPENSATION BY NEUTRON TRANSMUTATION DOPING

In this technique, the compensation of the residual boron is accomplished after the crystal growth is completed. The detailed description of this process is published in the final report, "Silicon Detector Compensation by Nuclear Transmutation," by the University of Missouri, AFML-TR-77-178, February, 1978, DDC Access No. ADA057786.

THEORETICAL ANALYSIS OF THE THREE-IMPURITY SILICON SYSTEM

This appendix contains a detailed analysis of the three-impurity (Ga, B, Donor) silicon system, showing the interaction between detector temperature, flux level, and compensating (donor) impurity concentration. Figures 1 and 2 in the body of the report summarize the results obtained from this analysis.

The band gap diagram for the three impurity material under consideration is shown in Figure A-1.

The steady-state current through a detector with ohmic contacts is

$$I = q\,p\,\mu E \tag{A-1}$$

E is assumed to be a constant in the region between the electrodes. $E = V_B/d$, where V_B is the bias voltage and d is the interelectrode distance.

We shall calculate p as a function of photon flux ϕ, where ϕ consists of a constant background ϕ_B and signal flux ϕ_S.

$$\phi = \phi_B + \phi_S \tag{A-2}$$

The following equations relate the densities of the impurity states and the free hole density:

(1) The charge state equilibrium requires

$$\frac{\partial N_{Ga}^-}{\partial t} = \beta_{Ga}\,N_{Ga}^O - p\,B_{Ga}\,N_{Ga}^- = 0 \tag{A-3}$$

$$\frac{\partial N_B^-}{\partial t} = \beta_B\,N_B^O - p\,B_B\,N_B^- = 0 \tag{A-4}$$

where

$\beta_{Ga}\,N_{Ga}^O$ and $\beta_B\,N_B^O$ give the generation rates of the free holes from neutral gallium and boron impurities due to both absorption of photons and thermal excitation

107

$N_D = N_D^+$ (VARIABLE 0 TO 10^{13} cm^{-3})

ΔE_{Ga} ΔE_B

$N_{Ga} \sim 5 \times 10^{16}$ cm^{-3}

$N_B \sim 10^{12}$ cm^{-3}
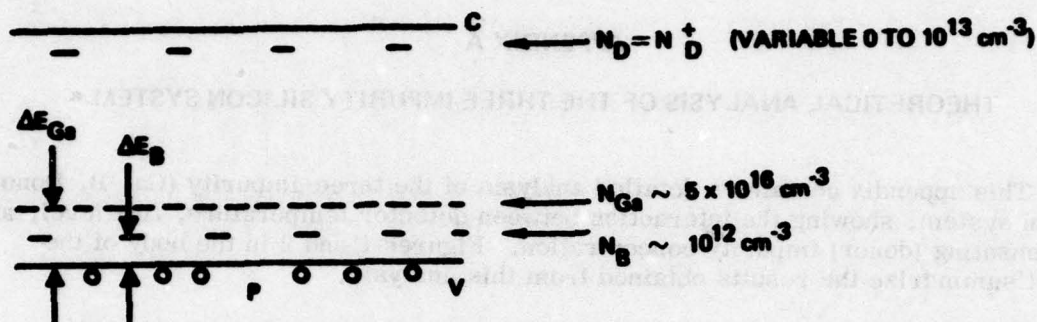
WHERE

N_{Ga} IS THE DENSITY OF GALLIUM IMPURITIES, OF WHICH N_{Ga} ARE NEUTRAL AND N_{Ga}^- ARE IONIZED

N_B IS THE DENSITY OF BORON IMPURITIES, OF WHICH N_B ARE NEUTRAL AND N_B^- IONIZED

N_D IS THE DENSITY OF DONOR COMPENSATING IMPURITIES WHICH ARE ALL IONIZED $N_D^+ = N_D$ AT THE TEMPERATURES OF INTEREST (4 TO 40°K)

p   IS THE FREE HOLE DENSITY

Figure A-1.   Bandgap Diagram of the Three Impurity System

B_{GA} and B_B are the coefficients for recombination of holes with ionized gallium and boron impurities, respectively.

$$B_{Ga} = <v_p> \sigma_{Ga}^- , \quad B_B = <v_p> \sigma_B^-$$

where

$<v_p>$ is the average velocity of holes

and

σ_{Ga}^-, σ_B^- are the cross sections for capture of holes by ionized gallium and boron, respectively.

(2) The conservation of the number of impurities requires

$$N_{Ga} = N_{Ga}^O + N_{Ga}^- \tag{A-5}$$

$$N_B = N_B^O + N_B^- \tag{A-6}$$

108

(3) The charge neutrality condition (with $N_D^+ = N_D$) requires

$$N_{Ga}^- + N_B^- = p + N_D \tag{A-7}$$

Assuming the detector is thin enough so that the photon flux can be taken as constant throughout the volume of the detector (Ref. 4, pages 49 through 55),

$$\beta_{Ga} = \phi S_{Ga} + B_{Ga} N_V g_{Ga}^{-1} \exp\left(-\frac{\Delta E_{Ga}}{kT}\right) \tag{A-8}$$

$$\beta_B = \phi S_B + B_{Ga} N_V g_B^{-1} \exp\left(-\frac{\Delta E_B}{kT}\right) \tag{A-9}$$

where

S_{Ga} and S_B are the photon absorption cross-sections for gallium and boron, respectively

g is the degeneracy of the ground state and equals 4 for both gallium and boron

N_V is the effective density of states in the valence band and is defined as

$$N_V = \frac{4\sqrt{2}}{h^3} (\pi m_p^* kT)^{3/2} \tag{A-10}$$

$$= 4.82 \times 10^{15} \left(\frac{m_p^* kT}{m}\right)^{3/2} cm^{-3}$$

where

m_p^* is the effective mass of holes

m is the electron mass

T is the temperature.

Defining

$$\alpha_{Ga} = \frac{\beta_{Ga}}{B_{Ga}} = \phi \frac{S_{Ga}}{B_{Ga}} + g_{Ga}^{-1} N_V \exp \left(-\frac{\Delta E_{Ga}}{kT}\right) \tag{A-11}$$

$$\alpha_B = \frac{\beta_B}{B_B} = \phi \frac{S_B}{B_B} + g_B^{-1} N_V \exp \left(-\frac{\Delta E_B}{kT}\right) \tag{A-12}$$

Eq (A-3) through (A-6) lead to the following expressions for N_{Ga}^- and N_B^-.

$$N_{Ga}^- = \frac{\alpha_{Ga}}{p + \alpha_{Ga}} N_{Ga} \tag{A-13}$$

$$N_B^- = \frac{\alpha_B}{p + \alpha_B} N_B \tag{A-14}$$

Substituting Eq (A-13) and (A-14) in Eq (A-7) p is found to satisfy the cubic equation,

$$p^3 + (N_D + \alpha_{Ga} + \alpha_B) p^2 + \left[\alpha_{Ga}\alpha_B - \alpha_{Ga}(N_{Ga} - N_D) - \alpha_B(N_B - N_D)\right] p$$

$$- \alpha_{Ga}\alpha_B (N_{Ga} + N_B - N_D) = 0 \tag{A-15}$$

We shall not attempt here to give an explicit solution for p. However, it is clear that knowing B_{Ga}^-, B_B^-, S_{Ga}, and S_B, the roots of this equation, completely describe p as a function of ϕ, T, and N_D. Assuming $\phi_S \ll \phi$, the responsivity is then obtained as follows

$$\Delta P_S = \frac{\partial p}{\partial \phi} \phi_S = \frac{W_S \lambda_S}{hc} \frac{\partial p}{\partial \phi} \tag{A-16}$$

where

W_S is the signal intensity at the detector in watts/cm^2.

For a detector of IR active area A_d equal to ℓw and the interelectrode distance ℓ, the steady-state current is

$$I = \ell w \, q\mu \, (p_o + \Delta p_S) \, E \qquad\qquad (A-17)$$

$$I_S = q\mu \, \ell w \, W_S \frac{\lambda_S}{hc} \frac{\partial p}{\partial \phi} E \qquad\qquad (A-18)$$

$$R = \frac{I_S}{\ell w \, W_S} = \frac{q\lambda_S}{hc} \frac{\partial p}{\partial \phi} E \qquad\qquad (A-19)$$

The above responsivity applies to a thin detector ($\alpha d \ll 1$) with no reflection loss at the front surface. For the 0.1 cm path for absorption of IR in the detectors evaluated in this program, the value of αd is 2.75 since $\alpha = S_{Ga} N^0_{Ga} = 27.5$. Therefore, we have to account for reflection loss and attenuation of ϕ in Eq (A-19).

$$\overline{R} = (1 - R) \frac{q\lambda_S}{hc} \frac{E}{d} \int_0^d \mu\frac{\partial p}{\partial \phi} e^{-\alpha x} dx \qquad\qquad (A-20)$$

If μ and $\partial p/\partial \phi$ are independent of ϕ, then

$$\overline{R} = (1 - R)(1 - e^{-\alpha d}) \frac{q\lambda_S}{hc} \frac{\mu E}{\alpha d} \frac{\partial p}{\partial \phi} \qquad\qquad (A-21)$$

Recognizing that $(1 - R)\left[1 - \exp(-\alpha d) \right] \approx \eta$, we can write Eq (A-21) as

$$\overline{R} = \frac{\eta q \, \lambda_S \, \mu_o \, \tau_o \, E}{hc} \frac{E}{d} \left[\frac{\mu}{\mu_o \, \tau_o \, \alpha} \frac{\partial p}{\partial \phi} \right] \qquad\qquad (A-22)$$

where

$\tau_o = \dfrac{1}{B_{Ga} N_D}$ and is the carrier lifetime at low background for a detector with compensating impurity density N_D.

μ_o is the mobility at low background.

111

For low background $\mu = \mu_o$, the steady-state condition for hole density is

$$\frac{\partial p}{\partial t} = \alpha \phi - \frac{p}{\tau_o} = 0 \qquad \text{(A-23)}$$

Therefore, the term in the brackets in Eq (A-22) is equal to unity and Eq (A-22) is then identical to Eq (A-24).

$$R_\lambda = \frac{q}{hc} \eta G \lambda$$

$$= 0.806 \, \eta G \lambda \text{ amp/watt} \qquad \text{(A-24)}$$

where

q is the electron charge

hc is the product of Planck's constant and the velocity of light

η is the detector quantum efficiency

λ is the wavelength in micrometers

G is the photoconductive gain.[1]

We shall discuss two special cases pertaining to the conditions under which the detectors in this program were tested.

1. **T < 15° K**

For the case of temperature below thermal ionization of boron impurities, T < 15° K, we rewrite Eq (A-13) and (A-14) as follows:

$$N_{Ga}^- = \frac{\alpha_{Ga}}{p} \frac{N_{Ga}}{\left(1 + \frac{\alpha_{Ga}}{p}\right)} \simeq \frac{\alpha_{Ga} N_{Ga}}{p} (1 - \delta_{Ga}) \qquad \text{(A-25)}$$

if

$$\delta_{Ga} = \frac{\alpha_{Ga}}{p} \ll 1$$

112

$$N_B^- = \frac{\alpha_B}{p} \frac{N_B}{\left(1 + \frac{\alpha_B}{p}\right)} \simeq \frac{\alpha_B N_B}{p} (1 - \delta_B) \qquad (A-26)$$

if

$$\delta_B = \frac{\alpha_B}{p} \ll 1 \qquad (A-32)$$

The above approximations can be made for $T \ll 15°K$ and $N_B \ll N_{Ga}$ since

$$\frac{\alpha_{Ga}}{p} \simeq \left(\frac{\phi S_{Ga}}{B_{Ga}}\right)\left(\frac{1}{\phi S_{Ga} N_{Ga}^o \tau_p}\right) \qquad (A-27)$$

and

$$\tau_p \simeq \frac{1}{B_{Ga} N_{Ga}^-} \qquad (A-28)$$

so that

$$\delta_{Ga} = \frac{\alpha_{Ga}}{p} \simeq \frac{N_{Ga}^-}{N_{Ga}} \ll 1 \qquad (A-29)$$

Similarly,

$$\delta_B = \frac{\alpha_B}{p} \simeq \frac{S_B}{B_B} \frac{B_{Ga}}{S_{Ga}} \frac{N_{Ga}^-}{N_{Ga}} \ll 1 \qquad (A-30)$$

when the term involving the photon absorption and recombination coefficients is of the order of unity.

A quadratic equation is obtained with Eq (A-25) and (A-26) in Eq (A-7).

$$\alpha_{Ga} (1 - \delta_{Ga}) N_{Ga} + \alpha_B (1 - \delta_B) N_B = p^2 + p N_D \qquad \text{(A-31)}$$

Equation (A-31) has the solution

$$p = \frac{N_D}{2} \left\{ \left[1 + \frac{4\alpha_{Ga} (1 - \delta_{Ga}) N_{Ga} + \alpha_B (1 - \delta_B) N_B}{N_D^2} \right]^{1/2} - 1 \right\} \qquad \text{(A-32)}$$

Since $N_B \ll N_{Ga}$ and $\delta_{Ga} \ll 1$, Eq (A-32) simplifies to

$$p \simeq \frac{N_D}{2} \left\{ \left[1 + \frac{4\alpha_{Ga} N_{Ga}}{N_D^2} \right]^{1/2} - 1 \right\} \qquad \text{(A-33)}$$

For an absorption coefficient for 28/cm and $N_{Ga}^0 = 5 \times 10^{16}/cm^3$
$S_{Ga} = 5.4 \times 10^{-16} \, cm^2$.

From Eq (A-11),

$$\alpha_{Ga} \simeq \frac{S_{Ga}}{B_{Ga}} \phi \simeq \frac{5.6 \times 10^{-16}}{B_{Ga}} \phi \qquad \text{(A-34)}$$

Upon examining Eq (A-33), the following limiting cases are evident,

For

$$\frac{4\alpha_{Ga} N_{Ga}}{N_D^2} \ll 1 \qquad \text{(A-35)}$$

114

which represents the low background condition,

$$p = \frac{\alpha_{Ga} N_{Ga}}{N_D} = 5.6 \times 10^{-16} \frac{N_{Ga}\phi}{N_D B_{Ga}} \tag{A-36}$$

and for

$$\frac{4\alpha_{Ga} N_{Ga}}{N_D^2} \gg 1 \tag{A-37}$$

representing the high background condition

$$p = \left(\alpha_{Ga} N_{Ga}\right)^{1/2} = \left(5.6 \times 10^{-16} \frac{\phi N_{Ga}}{B_{Ga}}\right)^{1/2} \tag{A-38}$$

In the detector material tested, $N_{Ga} \simeq 5 \times 10^{16}$, so that for the low background case where $\phi \ll 10^{-2} N_D^2 B_{Ga}$

$$p = \frac{28 \; \phi}{B_{Ga} N_D} \tag{A-39}$$

And for the high background case where $\phi \gg 8.9 \times 10^{-3} N_D^2 B_{Ga}$

$$p = \left[28\phi/B_{Ga} \right]^{1/2} \tag{A-40}$$

Applying these results to evaluating the responsivity as a function of N_D and ϕ, we obtain the behavior shown in Figure A-2. Responsivity data of about one amp/watt for low background ($\phi = 10^8$ ph/cm^2 sec) and high background ($\phi = 10^{17}$ ph/cm^2 sec) may be interpreted as indicating a density of compensating impurities N_D in these detectors of about 10^{13} cm^{-3} if a B_{Ga} value of 10^{-5} cm^3/sec is assumed.
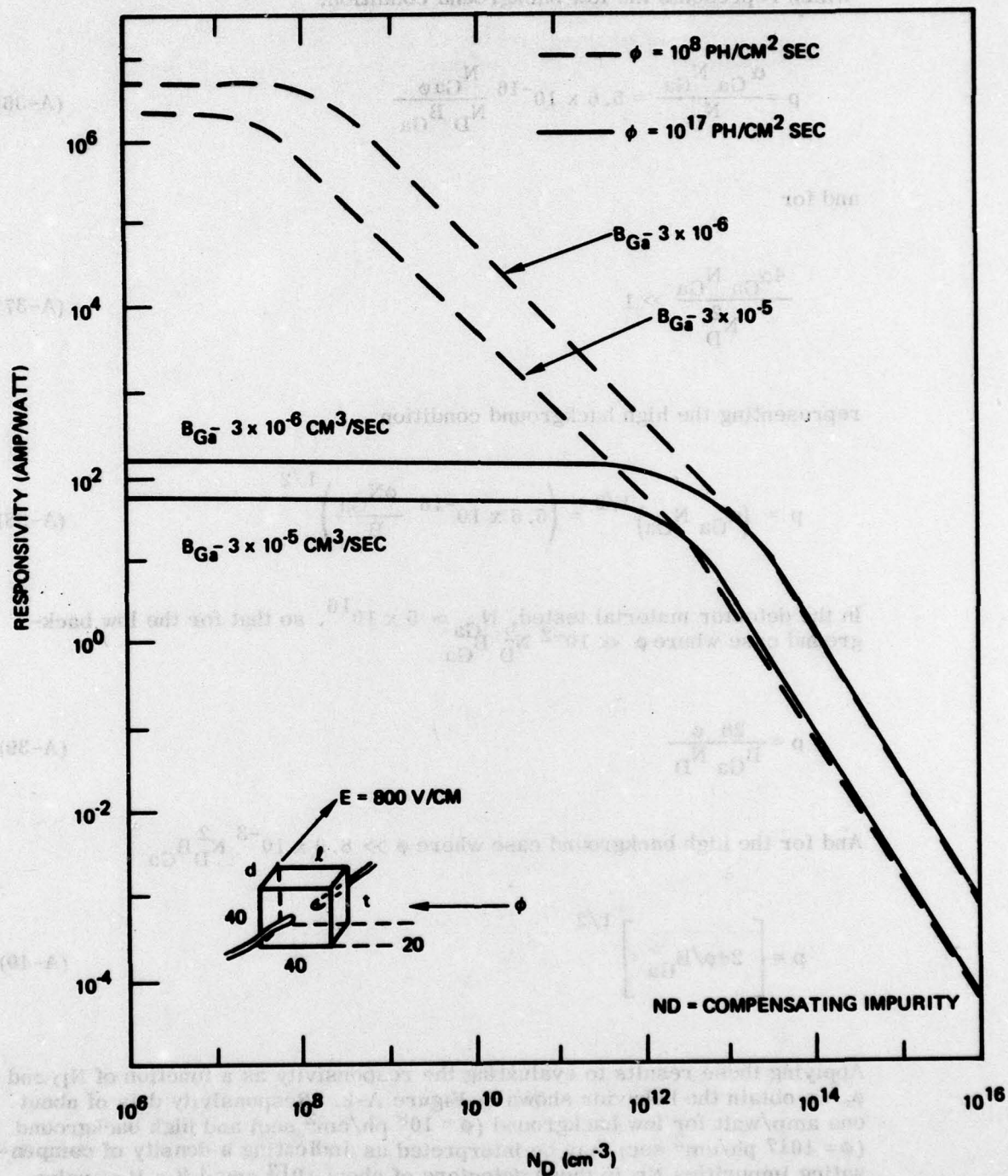
Figure A-2. Responsivity of 40 x 20 x 40 mil Si:Ga Detectors
at 40 Volt Bias for < 15° K

116

2. $T > 15° K$

For the case of temperature greater than 15° K but less than the thermal ionization temperature for gallium impurities ($\approx 30°$ K), as before, $\alpha_{Ga}/p \ll 1$ but $\alpha_B/p \gg 1$. For example, if we take $T = 25°$ K and $\phi = 10^8$ ph/cm^2 sec,

$$\alpha_B \simeq g_B^{-1} N_V \exp \; -\left(\frac{\Delta E_B}{kT}\right) \simeq 10^9 \qquad (A-41)$$

and

$$\alpha_{Ga} \simeq \phi \frac{S_{Ga}}{B_{Ga}} \simeq 5 \times 10^{-3} \qquad (A-42)$$

We can, therefore, use the following approximations for the region $N_D \leq N_B$.

$$N_{Ga}^- = \frac{\alpha_{Ga}}{p + \alpha_{Ga}} N_{Ga} \simeq \frac{\alpha_{Ga}}{p} N_{Ga}, \qquad (A-43)$$

$$N_B^- = \left(\frac{\alpha_B}{p + \alpha_B}\right) N_B \simeq N_B \left(1 - \frac{p}{\alpha_B}\right) \qquad (A-44)$$

$$\frac{\alpha_{Ga} N_{Ga}}{p} + N_B \left(1 - \frac{p}{\alpha_B}\right) = p + N_B \qquad (A-45)$$

$$p^2 + \frac{(N_D - N_B)\alpha_B p}{\alpha \, (\alpha_B + N_B)} - \frac{\alpha_{Ga} \, \alpha_B \, N_{Ga}}{(\alpha_B + N_B)} = 0 \qquad (A-46)$$

$$p = \frac{-(N_D - N_B)\alpha_B}{2 \, (\alpha_B + N_B)} \left[1 \pm \sqrt{1 + \frac{4\alpha_{Ga} N_{Ga} \, (\alpha_B + N_B)}{\alpha_B (N_D - N_B)^2}} \right] \qquad (A-47)$$

117

Since the second term inside the radical is less than unity for the case of interest except at $N_D \simeq N_B$, the following solutions are obtained.

For $N_D > N_B$,

$$p = \frac{\alpha_{Ga} N_{Ga}}{N_D - N_B} \qquad\qquad (A-48)$$

For $N_B \simeq N_D$, the second term in the radical is much greater than 1 so that

$$p = \sqrt{\frac{\alpha_B \alpha_{Ga} N_{Ga}}{\alpha_B + N_B}} \qquad\qquad (A-49)$$

For the undercompensated case where $N_D \ll N_B$, the approximation in Eq (A-44) is not applicable since p is expected to be larger than α_B. In this case, Eq (A-32) gives an approximate solution for p.

For $N_D < (\alpha_B N_B)^{1/2} < N_B$,

$$p = \frac{\alpha_{Ga} N_{Ga}}{N_B - N_D} + \frac{(N_B - N_D) \alpha_B}{\alpha_B + N_B} \qquad\qquad (A-50)$$

Using these results in Eq (A-22) with $N_B = 10^{12}$ cm^{-3}, we obtain the behavior of R with N_D shown in Figure A-3.

We derive the detectivity, D^*, from the general expression

$$D^* = \frac{\lambda}{hc} \frac{I_S}{\Phi_S I_N} \sqrt{\frac{\Delta f}{A_d}} \qquad\qquad (A-51)$$
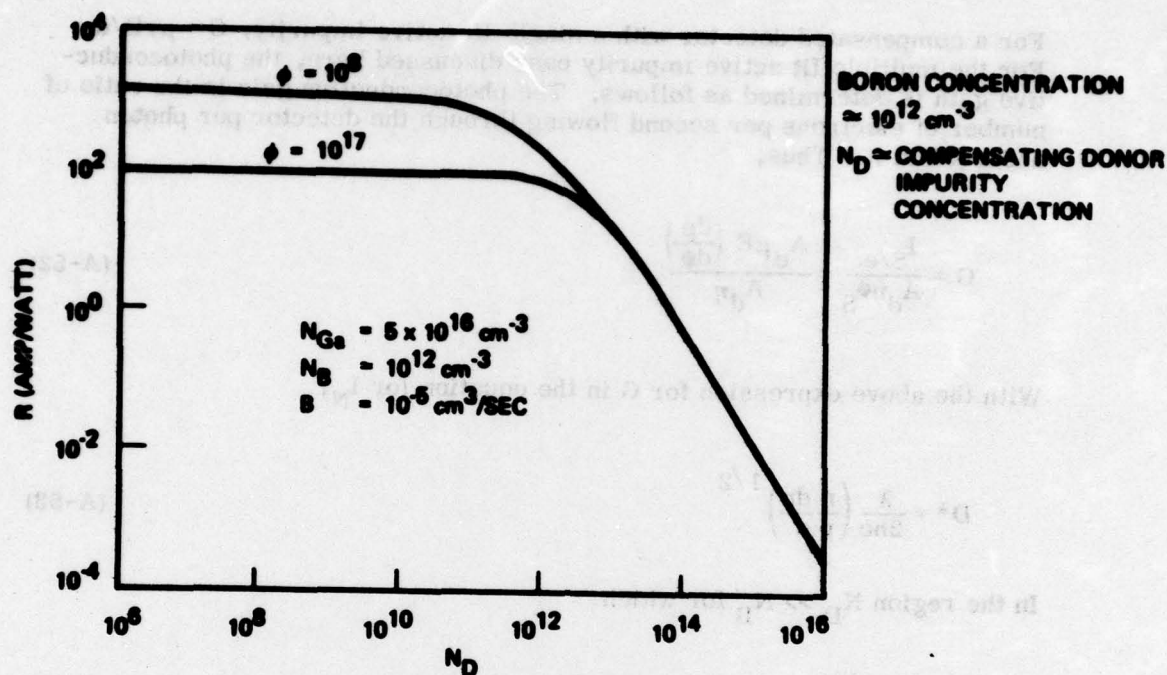
118

Figure A-3. Responsivity of 40 x 20 x 40 mil Si:Ga detectors with 40 volt bias operating at about 25° K.

The detector signal current I_S, noise current I_N, and background current I_B are

$$I_S = A_c\, \mu q\, E\, \frac{dp}{d\phi}\, \phi_S$$

$$I_N = \sqrt{4\, I_B\, qG\, \Delta f}$$

$$I_B = A_c\, \mu q\, E\, p$$

where G is the photoconductive gain.

119

For a compensated detector with a single IR active impurity, $G = \mu \tau E/d$.
For the multiple IR active impurity case discussed here, the photoconductive gain is determined as follows. The photoconductive gain is the ratio of number of electrons per second flowing through the detector per photon absorbed in it. Thus,

$$G = \frac{I_{S}/e}{A_d \eta \phi_S} = \frac{A_c \mu E \left(\frac{dp}{d\phi}\right)}{A_d \eta} \tag{A-52}$$

With the above expression for G in the equation for I_N,

$$D^* = \frac{\lambda}{2hc} \left(\frac{\eta}{p} \frac{dp}{d}\right)^{1/2} \tag{A-53}$$

In the region $N_D \gg N_B$ for which

$$p \simeq \frac{\alpha_{Ga} N_{Ga}}{N_D} \phi_B \tag{A-54}$$

so that

$$\frac{1}{p} \frac{dp}{d\phi} = \frac{1}{\phi_B} \tag{A-55}$$

We obtain the normal background limited detectivity

$$D^* = \frac{\lambda}{2hc} \left(\frac{\eta}{\phi}\right)^{1/2} \tag{A-56}$$

The effect of spectrophotometer background radiation upon spectral response measurements may be derived by rearrangement of equations (A-13) and (A-14).

$$\frac{N_{Ga}^-}{N_{Ga}} = \frac{\alpha_{Ga}}{p + \alpha_{Ga}} \tag{A-57}$$

$$\frac{N_B^-}{N_B} = \frac{\alpha_B}{p + \alpha_B} \tag{A-58}$$

$$\alpha_{Ga} = \frac{\beta_{Ga}}{\sigma_{Ga}^- \langle v_p \rangle} = \frac{S_{Ga}}{\sigma_{Ga}^- \langle v_p \rangle} + g_{Ga}^{-1} N_V \exp\left(-\frac{\Delta E_{Ga}}{kT}\right) \tag{A-59}$$

$$\alpha_B = \frac{\beta_B}{\sigma_B^- \langle v_p \rangle} = \phi \frac{S_B}{\sigma_B^- \langle v_p \rangle} + g_B^{-1} N_V \exp\left(-\frac{\Delta E_B}{kT}\right) \tag{A-60}$$

In low temperature ranges, the second term of Eq. (A-59) and (A-60) are comparable to the first terms as long as ϕ is large enough. With comparable photon absorption cross-sections S_B and S_{Ga} and capture cross-sections σ_B^- and σ_{Ga}^-, α_B and α_{Ga} will be of the same magnitude.

The minimum ϕ required for the above situation is

$$\phi_{min} = \frac{\sigma_B^- \langle v_p \rangle}{S_B} g_B^{-1} N_V \exp(-\Delta E_B/kT) \tag{A-61}$$

$$= \frac{10^{-5}}{1.8 \times 10^{-15}} \, 1/4 \times 4.8 \times 2 \times 10^{15} \, T^{3/2} \exp\left(\frac{-0.045}{0.86 \times 10^{-4} T}\right)$$

121

For $T = 10°K$, $\phi_{min} \approx 10^4$ photons/cm^2 sec. And for $T = 15°K$, $\phi_{min} \approx 10^{12}$ photons/cm^2 sec. At 4°K, the required flux is many orders of magnitude smaller than that for 10°K.

For the conditions under which the spectral response data were taken ($10^8 < \phi < 10^{15}$ photons/cm^2), p can be deduced from Eq (A33), i.e.,

$$p \approx \frac{\alpha_{Ga} N_{Ga}}{N_D} \tag{A-62}$$

so that

$$N_{Ga}^- \approx N_D \tag{A-63}$$

and

$$\frac{N_B^-}{N_B} \approx \frac{\alpha_B}{\alpha_{Ga}} \frac{N_D}{N_{Ga}} \tag{A-64}$$

Thus, both the boron and gallium impurities are only slightly ionized. The detector under these conditions will show a response peak proportional to the boron concentration.

REFERENCES

1. Breckenridge, R.G., Russell, B.R., and Hahn, E.E., <u>Photoconductivity Conference</u>, (John Wiley & Sons, Inc., N.Y., N.Y., 1956).

2. Burstein, E., Picus, G., and Sclar, N., "Optical Photoconductivity Properties of Silicon and Germanium", Ref. 1, pp 353-413.

3. Hudson, R.D., Jr., and Hudson, J.W., <u>Infrared Detectors</u>, (John Wiley & Sons, Inc., N.Y., N.Y., 1975).

4. Bube, B.M., <u>Photoconductivity in Solids</u>, (John Wiley & Sons, Inc., N.Y., N.Y., 1960).

5. Moss, G.S., Burrell, G.J., Ellis, B., <u>Semiconductor Opto-Electronics</u>, (John Wiley & Sons, Inc., N.Y., N.Y., 1973).

6. Trumbore, F.A., "Solid Solubility of Impurity Elements in Germanium and Silicon", Bell Sys. Tech. J., Vol. 39, pp 205-232, 1960.

7. Grove, A.S., Leistiko, O., Sah, C.T., "Redistribution of Acceptor and Donor Impurities During Thermal Oxidation of Silicon," Journal of Applied Physics, Vol. 35, No. 9, p 2695, 1964.

8. Ar-Ron, M., Shatzkes, M., Burkhardt, P.T., "Distribution of Dopant in S_iO_2-Si," Journal of Applied Physics, Vol. 34, No. 7, p 3159, 1976.

9. Kato, T., Nishi, Y., "Redistribution of Diffused Boron in Silicon by Thermal Oxidation," Japanese Journal of Applied Physics, Vol. 3, p 377, 1964.

10. Franks, R.K. and Robertson, J.B., "Magnesium as a Donor Impurity in Silicon", Solid State Communications, Vol. 5, p 479, 1967.

11. Fuller, G.S. and Ditzenberger, J.A., "Diffusion of Lithium Into Ge and Si", Physical Review, Vol. 91/1, p 193, 1953.

12. Reiss, H. and Fuller, C.S., "Influence of Holes and Electrons on the Solubility of Lithium in Boron-Doped Silicon", Journal of Metals, p 276, February 1956.

13. Reiss, H., Fuller, C.S., and Peitruszkiewicz, J., "Solubility of Lithium in Doped and Undoped Silicon, Evidence for Compound Formation, J. Chem. Phys., Vol. 25/4, p 650, 1956.

14. Reiss, H., Fuller, C.S., and Morin, F.J., "Chemical Interactions Among Defects in Germanium and Silicon", Bell Sys. Tech. J., p 535, May 1956.

15. Weiser, K., "Theory of Diffusion and Equilibrium Position of Interstitial Impurities in the Diamond Lattice", Physical Review, Vol. 126/4, p 1427, 1962.

16. Aggarwal, R. L., and Fisher, P., et al., "Excitation Spectra of Lithium in Silicon and Germanium", Physical Review, Vol. 138/3A, p A882, 1965.

17. Ho, L. T., "A Spectroscopic Study of Helium-Like Donors in Silicon", Purdue University, 1971.

18. Pratt, B. and Freidman, F., "Diffusion of Lithium Into Ge and Si", J. Appl. Phys., Vol. 37/4, p. 1893, 1966.

19. Seeger, A., and Chik, K. P., "Diffusion Mechanism and Point Defects in Silicon and Germanium", Phys. Stat. Solids, Vol. 29, p 455, 1968.

20. Pell, E. M., "Diffusion Rate of Li in Si at Low Temperatures", Physical Review, Vol. 119, p 1222, 1960.

21. Pell, E. M., "Diffusion of Li in Si at High Temperatures and the Isotope Effect", Physical Review, Vol. 119, p 1014, 1960.

22. Mott, N. F. and Twose, W. D., "Theory of Impurity Conduction", Advances in Physics, Vol. 10, p 107, 1961.

23. Matare, H. F., "Electronic Measurements of Semiconductor Material Parameters", North American Aviation, Anaheim, CA, 1967.

24. Logan, R. A. and Peters, A. J., "Impurity Effects Upon Mobility in Silicon", J. Appl. Phys., Vol. 31/1. p 122, 1960.

25. Debye, P. P., "Electrical Properties of N-Type Germanium", Physical Review, Vol. 93/4, p 693, 1954.

26. Morin, F. J. and Maita, J. P., "Electrical Properties of Silicon Containing Arsenic and Boron", Physical Review, Vol. 96/1, 1954.

27. Conwell, E. M., "Properties of Silicon and Germanium: II", Proceedings of IRE, p 1281, June 1958.

28. Messier, J. and Flores, J. M., "Temperature Dependence of Hall Mobility and μ_H/μ_D for Si", J. Phys. Chem. Solids, Vol. 24, p 1539, 1963.

29. Rideout, V. L., "A Review of the Theory and Technology for Ohmic Contacts to Group III-V Compound Semiconductors", Solid State Electronics, Vol. 18, pp 541-550, 1975.

30. Gibbons, James F., "Ion Implantation in Semiconductors", Proceedings of the IEEE, Vol. 60, p 1062, 1972.

31. ASTM Standards, F 28-66, Electronics, Measuring the Minority-Carrier Lifetime in Bulk Germanium and Silicon, Part 43.

32. Keller, Wolfgang, "Messung der Traegerlebensdauer in Siliziumkristallen mit Hochfrequenz", Zeitschrift fur Angewandte Physik, Vol. II, September 1959.

33. Noack, T., "Measurement of Minority Carrier Lifetime in Silicon of Low Dislocation Density", Phys. Stat., Vol. 32, K17, 1969.

34. Kolbesen, B.O., "Simultaneous Determination of the Total Content of Boron and Phosphorus in High Resistivity Silicon by I.R. Spectroscopy at Low Temperatures", Appl. Phys. Letters, Vol. 27/6, p 353, 1975.

35. Pajot, B., "Impurity Lines of Boron and Phosphorus in Silicon", J. Phys. Chem. Solids, Vol. 25, p 613, 1964.

36. Hrostowski, H.J. and Kaiser, R.H., "Infrared Spectra of Group III Acceptors in Silicon", J. Phys. Chem. Solids, Vol. 4, p 148, 1958.

37. Burstein, E., Picus, G., Henvis, B. and Wallis, R., "Absorption Spectra of Impurities in Silicon I", J. Phys. Chem. Solids, Vol. 1, p 65, 1956.

38. Runyan, W.R., Silicon Semiconductor Technology, T.I. McGraw-Hill, N.Y., 1965.

39. Kaiser, W., Keck, P.H., and Lange, C.F., "Infrared Absorption and Oxygen Content in Silicon and Germanium", Physical Review, Vol. 101/4, p 1264, 1956.

40. Gross, C. and Gaetano, G., "Comparison of Infrared and Activation Analysis Results in Determining the Oxygen and Carbon Content in Silicon", J. Electro-Chem. Soc., Vol. 119, p 926, 1972.

41. Baker, J.A. and Tucker, T.N., "Effect of Carbon on the Lattice Parameter of Silicon", J. of Appl. Phys., Vol. 39/9, p 4365, 1968.

42. Schink, N., "Concerning the Carbon Content in Semiconductor Silicon", Solid State Electronics, Vol. 8, p 767, 1965.

43. Ducret, L. and Cornet C., "A New Method for the Determination of Microquantities of Carbon in Semiconductors: Application to Silicon and Germanium", Centre National d'Etudes Des Telecommunications Issy Les Moulineaux, Seine, France, p 461.

44. Secco d'Aragona, "Dislocation Etch for (100) Planes in Silicon", J. Electrodium. Soc., Vol. 119, p 948, 1972.

45. Lang, A.R., "Studies of Individual Dislocations in Crystals by X-Ray Diffraction Microscope", J. of Appl. Phys. 30, p 1748, 1959.

46. Schibli, E. and Milnes, A.G., Deep Impurities in Silicon, Mater Sci Eng, Vol. 2, p 173, 1967.

47. Dash, W.C., "Method of Growing Dislocation-Free Semiconductor Crystals", June 2, 1964, Patent No. 3,135,585, filed March 1, 1960.

48. Huff, H.R. and Burgess, R.R., "Semiconductor Silicon 1973", Electro-Chem. Soc., pp 83-93, 1973.